# Forebody Shock Control Devices for Drag and Aero-heating Reduction: A Comprehensive Survey with a Practical Perspective

*Mahmoud Y. M. Ahmed[1] and Ning Qin[2]*

*1. Associate Professor, Aerospace Engineering Department, Military Technical College, Cairo, Egypt,*

*2. Professor, Department of Mechanical Engineering, University of Sheffield, Sheffield, S1 3JD, UK.*

**Abstract:**

One key feature that distinguishes the flowfield around vehicles flying in supersonic and hypersonic regimes is the bow shock wave ahead of forebody. The severe drag and aeroheating impacting these vehicles can be significantly reduced if the bow shock wave ahead of the vehicles forebodies is controlled to yield weaker system of oblique shocks. Benefits of forebody shock control include increasing flight ranges, economizing fuel consumption, reducing dead weights, and thermally protecting forebody structure and onboard equipment. Forebody shock control that has been widely studied since the early 1900s is achievable in numerous techniques that vary according to the mechanism of control. While some of these techniques have already been implemented in real systems, other techniques involve serious complications and tough trade-offs. The present paper is intended to serve as the first comprehensive survey on the field of forebody shock control devices. The objectives of the present paper are multifold. The paper categorizes the various forebody shock control devices in a physics-based manner, explains the underlying physics for each device, and surveys the key studies and state-of-the-art knowledge. The paper also addresses the existing gaps in knowledge, highlights the existing systems implementing these devices, and discusses the associated practical implementation issues and design-tradeoffs.

## 1. Introduction

Hypersonic vehicles are classified into three categories namely, cruise and acceleration vehicles, winged reentry vehicles, and un-winged reentry vehicles[1]. Cruise and accelerating vehicles include hypersonic cruise missiles and hypersonic planes. Typical winged reentry vehicles are space shuttles and inter-planetary vehicles while commercial reusable missiles and ballistic missiles are un-winged reentry hypersonic vehicles. Examples of these categories are shown in Fig. 1. In contrast to the former category, the latter two have exiting in-operation examples and are characterized by blunt forebody configurations. In fact, blunting the forebody of these hypersonic vehicles is viewed as the primary design alternative [2]. Blunting yields lower peak (stagnation) aeroheating flux levels[3], offers better accommodation and operation of crew or on—board seeker devices with a higher volumetric efficiency [4],[5]. It also enables a more cost-effective use of existing launch facilities for longer missiles[6]. Extreme drag and significant aero-thermodynamic impact on vehicles surfaces come as penalties for blunt forebodies.

(a) Cruise and acceleration vehicles [7]


(b) Winged reentry vehicles [8]

(c) Un-winged reentry vehicles [9]

**Figure 1 Typical hypersonic vehicles of different categories**

Needless to say, reducing *both* drag and aeroheating on the hypersonic vehicle forebody is a crucial design requirement. A lower drag yields longer ranges, less demands on propulsion system design, more payload capacity[3], and more economic fuel consumption. In addition, reducing the aeroheating on the forebody means better protection of forebody structure [10] and on-board equipment[4], less demands on TPS, and alleviating the communication blackout problem. Fortunately, the high drag and aeroheating impacting the forebodies in supersonic/ hypersonic flight regime stem from the same origin, namely, the generation of strong bow shock wave ahead of the forebody, the fore shock wave. Downstream of the fore shock, the flow attains extreme pressure and temperature levels that are responsible for the extreme drag and aeroheating on the forebody. Hence, both drag and aeroheating can be, simultaneously, reduced by reconstructing the flowfield ahead of the forebody to weaken the bow shock.

The focus of the present survey is on shock control devices for drag and aeroheating reduction. By these devices, we mean the techniques that handle the causes of high drag and aeroheating, i.e., bow fore shock, rather than those acting to alleviate the consequences of these causes. In this respect, thermal protection systems, energy release technique in the vicinity (i.e., in the shock layer) ahead of the forebody, and devices such as forward facing cavities are not considered. Drag and aeroheating reduction devices surveyed in this paper perform in the same concept. This concept is to reconstruct the flowfield structure ahead of the forebody via eliminating the strong bow fore shock wave ahead of the hypersonic vehicle forebody or replacing it with a much weaker shock system. Depending on the mechanism by which the flowfield structure is modified, these devices are classified here into three basic categories: structural (mechanical), fluidic, and energetic (thermal) devices. Structural devices act by attaching a physical body that protrudes ahead of the forebody into the incoming freestream. In contrast, fluidic devices act by pushing fluid jets into the incoming freestream. Energetic devices act by introducing an energy spot into the freestream ahead of the forebody. Apart from these basic devices, other existing devices are treated here as hybrid in the sense that their mechanism of operation can be viewed as a combination of more than one basic mechanism. One common classification of these devices is into passive (exclusively, mechanical spikes) and active techniques. However, as well be shown in the survey, mechanical spikes have been used as active devices. Figure 2 illustrates the categorization of forebody shock control devices adopted in the present survey.

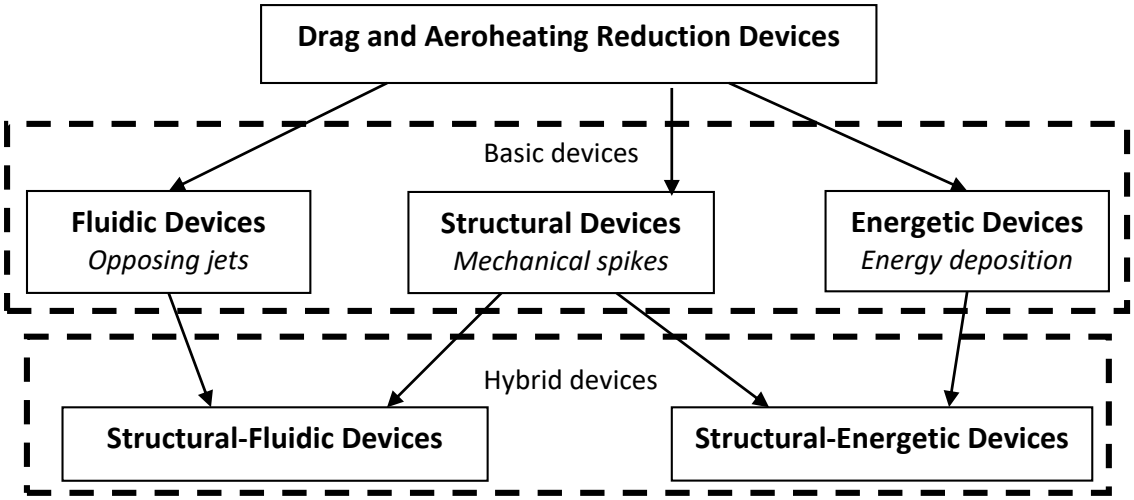


**Figure 2 Physics-based classification of drag and aeroheating reduction devices**

Since the early 1900s, huge efforts have been put in developing these devices by many researchers over the world; related aspects still attract the attention of more researchers. A number of recent publications were devoted to survey the progress of knowledge in this field. In[11], Ahmed and Qin presented a comprehensive survey on previous studies and latest contributions (up to 2010) for mechanical spike devices. The research group of Huang contributed with four review articles [12-15]. In [12], focus was made on opposing jet technique and its combinations with forward-facing cavity, energy deposition, and spikes. Survey on experimental and numerical simulation studies on these techniques and their combinations was presented separately in [13] and [14], respectively. In [15], a concise survey on spikes and their combinations was presented. Karimi and Oboodi [16] conducted a survey on drag and aeroheating reduction techniques and their combinations. Different techniques were categorized based on the authors' perspective of techniques evolution as they developed from geometric devices. However, the physics-based categorization proposed above (Fig. 2) is believed to more systematic and coherent. The objectives of the present survey are multifold. It is intended to:

- categorize the different devices in a physics-based systematic way,
- conduct a comparative analysis for the underlying physical principles and mechanisms of operation for each device
- provide a comprehensive and critical review for the previous studies in the field and to demonstrate the current knowledge,
- address areas of debate and knowledge gaps for future studies rather than revisiting already established knowledge,
- highlight the issues of practical implementation and design tradeoffs related to each of these devises in real systems, and finally
- list the available real hypersonic vehicles that already implement these devices.

The paper is organized as follows. Basic devices are presented starting with structural devices, followed by fluidic devices, and ended with energetic ones. For each of the basic devices, the mechanism of operation, impact on the flowfield, and factors influencing this impact are illustrated. Next, survey on benchmark researches, key research groups, as well as nonconventional studies is presented. Then, gaps of knowledge in the literature are highlighted. Finally, aspects of real implementation and design trade-offs are discussed. Following the basic devices, a survey on hybrid devices along with comments are presented. The paper finalizes with illustrating the existing real systems that implement the surveyed devices for drag and aeroheating reduction.

## 2. Structural devices, the mechanical spikes:

### 2.1. Principle of operation of mechanical spikes

The spike is simply a thin cylindrical rod mounted normal to the stagnation point of the forebody. A spike can have a fixed length, a variable length [6], or even erected only when needed [17]. It was introduced to the field of high-speed aerodynamics by Alexander in 1947 at Langley Pilotless Aircraft Research Division [18] as a light-weight means of drag reduction. The term "spike" was first used by Piland and Putland [19] and has been used since then. It is interesting to note that mechanical spike also found different applications such as acting as a Pitot tube, as probes for collecting planetary gas samples [20], as an escape rocket for space launch vehicles [6], at inlets of supersonic/hypersonic engines, to reduce sonic boom for supersonic aircraft [21], or to improve weapon lethality [22, 23].

If it is sufficiently long, the spike introduces two modifications to the flowfield structure around the hypersonic forebody. On the one hand, the strong bow fore shock ahead of the forebody is replaced by a system of weaker oblique shocks. On the other hand, the flow downstream of the oblique shock separates due to adverse pressure as it approaches the forebody at the spike root. The generated shear layer propagates downstream, reattaches on the forebody surface engulfing a dead air zone that screens a considerable portion of the forebody. Overall, a significant drop in drag and aeroheating to the body is achieved despite the local pressure and heat flux peaks at the reattachment zone. As the spike length increases, its favorable impact is enhanced since the reattachment point moves further away from the spike root [24]. Adding a relatively larger tip, the aerodisk, further enhances the device effectiveness [25] over a wider range of Mach numbers [10] and incidence angles [26] or to compensate short spike length [5] despite the added drag on the aerodisk [27]. The Intermediate disks along the spike stem have shown a favorable role as well [28]. An aerodisk commonly has a circular projection however, it performs the best if its projection is similar in shape to that of the forebody [29]. Figure 3 shows the typical flowfield features for a mechanical spike device mounted at the stagnation point of a hemispherical forebody.

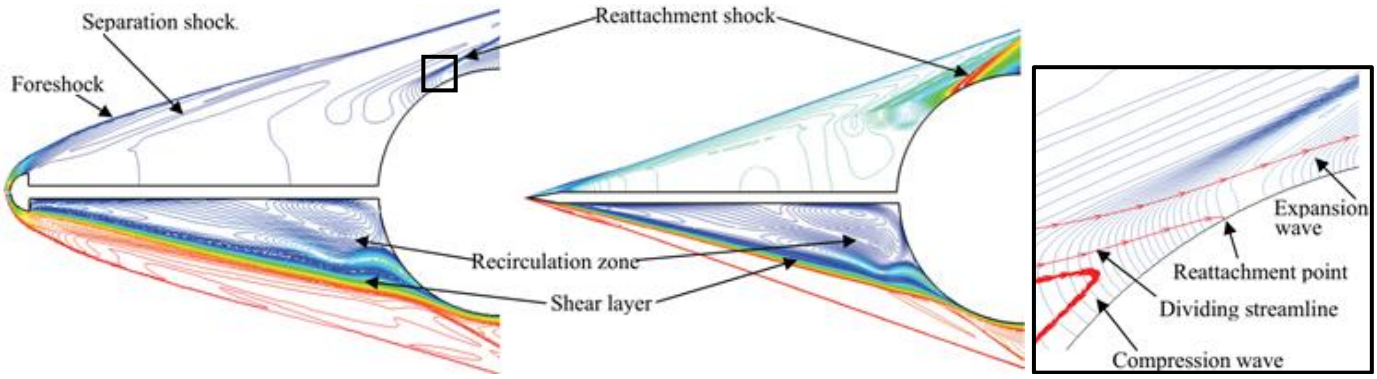


**Figure 3 Macroscopic features of the flowfield around of a spiked forebody in hypersonic speeds [30]**

The spiked forebody is transformed into a more slender effective body outlined by the spike/aerodisk tip, the dividing streamline of shear layer, and the forebody surface downstream of reattachment, Fig. 1. In effect, the overall fineness ratio of the forebody is increased with a marginal weight penalty. The fore shock ahead of the new body is modified accordingly. The mechanism of drag reduction by the mechanical spike is explained by the form of the effective body [31] as well as the creation of a low-pressure recirculation zone [32]. The mechanism of aeroheating to the forebody is explained by the geometry of flow at reattachment (impingement angle of the dividing streamline) [33], the energy level of the shear layer, and vortex structure inside the recirculation zone [30]. At the spike/ aerodisk tip, excessive thermal loads are witnessed that have remarkable impact on the flowfield structure and device effectiveness [34].

In terms of flow stability, the flow around spiked forebodies is generally steady. A sufficient condition for flow stability is that one single streamline within the shear layer should stagnate on the forebody [35]; the dividing streamline [36]. However, for some cases depending on spike length, freestream Mach number, and forebody configuration, the flow can be unsteady. There are two distinct modes of flow instability associated with mechanical spike device namely, violent and mild oscillations both appearing as self-sustained periodic variations in the flowfield

pattern, Fig. 4. The violent mode is termed the "pulsation mode" and the mild mode is termed the "oscillation mode" [37] and are commonly related to flat or highly blunt conical forebodies. For hemispherical and spherically blunted forebodies with mechanical spikes, the flow is generally steady. Signs of mild oscillation mode were recorded on such forebodies [32, 38, 39]. Adding an aerodisk at the tip of the spike was found to stabilize the flow for some spike lengths [31].

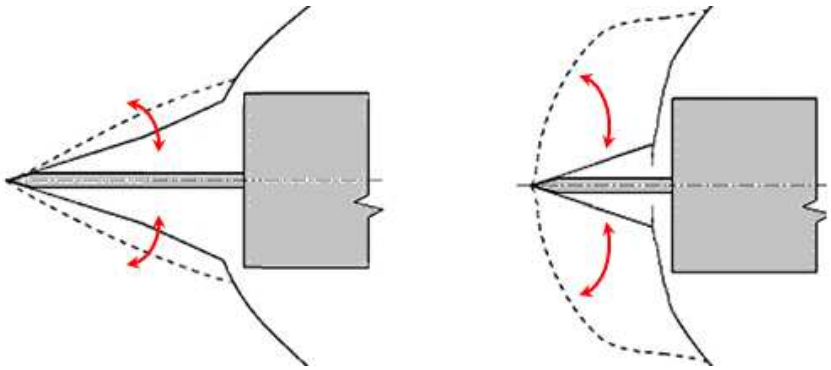

Oscillation mode Pulsation mode

**Figure 4. Evolution of flow pattern ahead of mechanical spike in unsteady modes**

In the pulsation mode, a continuous inflation and collapse of the recirculation zone takes place and forces the fore shock to continuously change its form from conical to bow. This low-frequency high amplitude oscillation is explained by the feeding of air from outside into the recirculation zone causing its inflation. At some point, the shear layer can not reattach on the forebody surface and the flow inside the recirculation zone escapes past the forebody shoulder causing the former to collapse. In contrast, oscillation mode is characterized by small amplitude, high frequency oscillation of the shear layer. The fore shock maintains its overall conical form with lateral flapping-like motion. Oscillation of the shear layer takes place due to the continuous mass imbalance between air scavenged out of the recirculation zone and reversed into it [40]. This is explained based on the level of energy of the dividing streamline [31]. In addition to lateral axisymmetric periodic motion in both modes, asymmetric circulatory periodic motion of the flow inside the shear layer was also reported [32, 41-43]. Pulsation mode is commonly associated with relatively short spikes (in the order of forebody diameter); the frequency of pulsating flow monotonically decreases by increasing the spike length [44]. As the spike length increases, the flow unsteadiness switches to the oscillation mode [45]. Further increasing the spike length restores the flow stability around the spike.

The mechanical spike device operates with its maximum effectiveness in terms of drag and aeroheating reduction at zero incidence and its effectiveness diminishes at elevated incidence [10, 46]. At angles of attack, the spike has the impact of increasing the lift [4, 17, 47, 48] and reducing the stability margin of the vehicle [49-52]. Adding a mechanical spike to forebodies with non-circular cross-sections does not degrade the favorable benefits of such lifting forebodies [53].

### 2.2. Factors controlling the mechanical spike effectiveness and flow stability

The effectiveness of the mechanical spike device is dependent on the freestream conditions. For instance, for turbulent freestream conditions, adding the spike was found to increase the aeroheating to the forebody [38, 54]. Aeroheating to the spiked forebody is significantly reduced for laminar freestream conditions [38, 55] or if the shear layer remains laminar until reattachment [2]. Under certain flight conditions and for a give forebody configuration, the performance of spikes varies depending on primarily its length and the aerodisk geometry while the spike diameter has a negligible role [20, 56]. However, a spike's effectiveness does not improve monotonically by increasing its length [54, 57, 58] or the aerodisk size [27, 59]. An optimum combination for both parameters can be devised for specific forebody configuration and freestream conditions [60-62]. Adding an aerodisk was proved to enhance flow stability associated with mechanical spike devices [63]. Even without using an aerodisk, modifying the tip of a plain spike was proved to have a strong impact on its performance [64] and can reduce flow instability [65, 66]. It is also

confirmed that the forebody configuration impacts the device effectiveness [33, 55, 67, 68]. In the context of a design optimization study [69], spike length is found to be responsible for about 50%, 20%, and 30% of drag, aeroheating, and flow stability, respectively. The aerodisk design contributes with about 30% of aeroheating impact. The forebody design is responsible for about 35%, 50%, and 56% of drag, aeroheating, and flow stability, respectively.

### 2.3. Survey on key studies on mechanical spikes

Following the proof-of-concept by Alexander [18], Moeckel [70] measured the surface pressure on a spiked parabolic forebody with a hemispherical nose in a laminar, low-supersonic freestream. Mair's experimental work [71] is the first milestone in the field in which he examined flat cylindrical and hemispherical models equipped with conically pointed spike of different lengths. Clear description of the flowfield, the role of spike length on the flowfield, and pressure and drag measurements were included. Stalder and Nielsen [54] conducted the first experimental study on spike's aeroheating effects on a hemispherical model. They concluded a significant increase in aeroheating to the spiked body regardless to spike length and tip geometry. This was owed to the high turbulence levels in the recirculation zone as well as turbulent shear layer impingement.

Another milestone is the comprehensive experimental work by Crawford [38] on a spiked hemispherical model equipped with a pointed spike of different lengths in Mach 6.8 flow. The role of Reynolds number and spike length was the focus of this study. The rich database in [38] were used by many researchers to validate their numerical studies on spiked forebodies. Wood [36] was the first to investigate the impact of changing both the conical forebody shape and spike length on the flowfield structure in Mach 10 laminar freestream. Five different flowfield patterns were distinguished depending on spike and forebody shapes. These patterns were refined and extended for higher Mach Reynolds numbers in the important study by Holden [33]. He also showed that the peak local heat transfer rate at the reattachment point is directly proportional to reattachment angle that is governed by both spike length and surface local inclination.

The pioneering numerical simulation studies in the field are [4, 72, 73]. Myshenkov [72] conduted the first numerical simulation study in the field of mechanical spike device by solving the full steady Navier-Stokes equations. The first implementation of unsteady N-S equations was attempted by Paskonov and Cheraneva [73], Karlovskii and Sakharov [56] solved the unsteady Euler equations, whereas Shoemaker [4] used the two-dimensional unsteady Navier-Stokes equations.

Finally, the active research group in the field of mechanical spike device are addressed. Antonov et al. focused in their experiments on flow unsteadiness related to mechanical spikes [67, 74-76]. The group of Reddy conducted a set of experimental and simulation studies in the field of mechanical spikes [3, 46, 77, 78]. Focus was on highly blunt forebodies in a Mach 5.75 and 8.0 laminar freestream conditions. Spikes with different lengths and aerodisk designs were examined and drag and aeroheating to the forebody at different incidence angles were measured. Mehta and his co-researchers conducted a number of experimental and numerical studies [26, 39, 48, 79-86]. They examined drag and aeroheating to a hemispherical forebody model equipped with various spike and aerodisk designs at Mach 6 and different incidence angles. The research group of Qin contributed with a number of numerical simulation studies on spiked bodies [30, 31, 42, 52, 60, 69, 87]. Drag and aeroheating reduction capabilities of a spike-aerodisk of different designs attached to a hemispherical model in a Mach 6 laminar freestream were investigated in [30, 31]. The focus of [60, 69] was to optimize the design of a spiked forebody for given freestream conditions. The work of Ahmed and Qin [69] was the first optimization study in the field and the only study to consider the design of the forebody, spike, and aerodisk in the optimization that involved six design parameters. Drag and aeroheating reduction objectives were found competing and the features of Pareto designs were addressed. In [42], Ahmed and Qin revisited and assessed the axisymmetry of the flow around a symmetric spiked forebody exposed to zero-incidence freestream. They concluded that a stable flow around a spiked forebody conveys a degree of asymmetry. In the recirculation zone and the inner part of the shear layer, flow asymmetry in the form of a weak rotating pressure wave was recorded that yields an undistinguishable variation in drag. For cases where the flow is unsteady, flow asymmetry is more significant in the lateral oscillation of the shear layer along with the rotational wave inside the

recirculation zone; a conclusion that is consistent with the experimental observation in [41]. They also concluded that axisymmetric solution overestimates the level of flow unsteadiness. In their survey paper on mechanical spike devices [11], Ahmed and Qin addressed the state-of-art (up to 2010) and their recent contributions. In [87], the benefits of fitting a double-disk aerospike to a winged lifting-body vehicle for different mounting and vehicle incidence angles were investigated.

### 2.4. Key studies on flow unsteadiness associated with mechanical spikes

The first record of flow instability for mechanical spikes was made by Mair [71] on flat cylindrical forebodies. For a critical spike length, the fore shock changes its shape in a self-sustained manner. This was explained based on pressure difference on the sides of the shear layer at reattachment.

Hermach et al. [44] captured pulsation mode of oscillation on a flat cylindrical model equipped with a mechanical spike whereas Bogdonoff and Vas [2] recorded both modes on unsteadiness. Maull [88] refined the mechanism of flow instability based on the equilibrium between the flows scavenged by the shear layer and reversed into the dead air zone dictated mainly by the flow turning angle at reattachment. Antonov et al. [67, 76] specified the ranges of spike length for both modes of unsteadiness and presented the first definition of pulsation cycle and mechanism. Their findings were independently supported by Kenworthy [40] and Panaras [45, 89] and confirmed by Zapryagaev et al. [90, 91]. Hankey and his co-researchers conducted experimental and numerical investigation of pulsation of flow around spiked truncated cone [41, 92] whereas Morgenstern [34] extended their simulations at higher incidence (up to 10 degrees). Feszty et al. [93, 94] confirmed using the numerical simulations the findings of Kenworthy. A high quality flow visualization for pulsation mode can be found in [95]. Sahoo et al. [66] confirmed experimentally that rounding the spike tip can change pulsation mode into oscillation one.

Beastall and Turner [96] recorded oscillation mode and linked it to small shear layer lateral oscillations. Kenworthy [40] was the first to explain the mechanism of oscillation mode. Feszty et al. [97] reproduced numerically the experimental investigation of Kenworthy [40] on oscillation mode and confirmed his conclusions. Based on [40, 97], the cause and cycle of oscillation mode can be explained for flat forebodies. In [31], the oscillation cause and mechanism were improved and extended to hemispherical forebodies. Oscillating flow can be significantly stabilized by rounding the spike tip [66].

In addition to these two modes of flow unsteadiness, a hysteresis phenomenon was also discovered to occur associated with extensible spikes. For a given spike length, the drag and aeroheating to the forebody depend on whether the spike is extended or retracted. Hysteresis was first reported and explained by Kenworthy [40] in his experimental work and was later investigated by Calarese and Hankey [41]. The experiments on hysteresis [40] were reproduced numerically by Feszty et al. [98]. The comprehensive numerical study by Panaras and Drikakis [99] focused on the initial development of flow in both modes of unsteadiness. It also included numerical reproduction for a variety of previous experiments on flow unsteadiness and hysteresis [40, 41, 89].

### 2.5. Non-conventional studies on mechanical spikes

The literature on mechanical spike device includes a number of studies on different non-conventional techniques that are intended to enhance the device effectiveness. An aerodisk attached at a distance from the forebody using a strut was proposed by Guy et al. [100] to satisfy practical implications while rotating the spike about its axis was proposed by Khlebnikov [101-103]. Adding four more spikes to the central one was argued by Gilinsky et al. [104] to improve the flow stability with an added drag penalty.

Three concepts in mechanical spike that worth highlighting are porous spikes, inclined spikes, and multi-disk spike devices. Li et al. [105] proposed using a porous material for fabricating the spike. Based on their numerical simulations, a porous spike was argued to reduce the reattachment heat flux and the overall drag. The porous spike effectiveness was found to vary with the spike size and to settle after a transient period of time. Experimental validation of the porous spike concept is needed. A spike that is fitted inclined to the forebody symmetry axis was proposed by Thurman [106] and was found to add more lift to the vehicle. The concept was implemented recently

by Deng et al. [87] for lifting body configuration. A more advanced implementation of the concept, the "pivoting spike", that is maintained aligned with the freestream regardless to the vehicle incidence was proposed by Schülein [107, 108]. Different techniques for implementing this concept were proposed [109] and validated experimentally for static conditions [110] and dynamic (pitching) conditions [111] by Schülein's workgroup.

Finally, a spike device with one or more intermediate aerodisks along its stem was examined independently by a two research groups. Kobayashi et al. [23, 112] referred to this concept as the "multi-row-disk" in which (up to 12) disks of increasing sizes towards the spike root are added to its stem. The concept was found to add more drag reduction to the spike device at a wider range of incidence angles and was also argued to attenuate the flow hysteresis associated with extending and retracting the spike. However, an aeroheating penalty upon using such device was reported in [113]. The group of Yadav [28, 114, 115] used the term "multiple-disk" spike to refer to the same concept in which one or two more hemispherical aerodisks are added to locations along the spike stem. Monotonic drop in drag and aeroheating was reported by adding more disks with marginal benefits as the number of disks increases. The findings of Yadav et al. require experimental validation. Gopalakrishna and Saravanan used the term "double spike" to refer to the same concept in their experimental-computational study [116] and confirmed further aeroheating reduction capabilities of this device. The same concept was utilized with application on a lifting vehicle configuration [87] and was found to improve the aerodynamic efficiency of the vehicle as well as reducing the drag. A concise summary for all spike-related literature is listed in Table A1 in the Appendix.

### 2.6. Prospective gaps in the field of mechanical spikes

The previous studies on mechanical spike devices have already covered almost all aspects. For instance, a wide range of freestream Mach number (up to Mach 20 [117]) and Reynolds number (ranging from 100 [73] to 2e7 [118]) was considered. Real flight altitudes of supersonic and hypersonic vehicles were also addressed in the literature [119]. Various forebody configurations were examined including models for reentry vehicles [51, 55], lifting bodies [29, 52, 87, 120], and complete projectile configurations [121, 122]. Design optimization of complete spiked forebody was also performed at different freestream conditions [62, 69]. Nevertheless, some aspects related to mechanical spike devices that invoke further studies can be identified:

- The laminar assumption based on the relatively low Reynolds number for the hypersonic flow cases in numerical simulation studies should be revisited. Flow transition can occur in the free shear layer and the boundary layer for the spike flow. In fact, based on the findings of Chapman et al. [123], the flow around the spiked body may transit into turbulent as the spike length increases. The flow along separated shear layer and within the recirculation zone is likely to be transitional or turbulent rather than laminar.
- Numerically simulating the flow unsteadiness associated with extensible spikes is a challenging topic.
- The transients associated with accelerating and decelerating vehicles during flight were briefly investigated by Qin et al. [34] and can invoke more studies. Inclusion of the variation in flight altitude as well as speed to account for real accelerating ascent/ descent of the vehicle is recommended.
- Another attractive topic is coupling aerodynamic simulation and flight mechanics models to predict the real trajectory of spiked vehicles.
- The structural features of this mechanical device such as bending and vibration coupled with the aerodynamic flow problem was only briefly highlighted in [6]. This topic poses another challenging research using FSI simulation capabilities. The impact of excessive thermal loads on the spike/ aerodisk can be considered.
- Finally, a multi-disciplinary design optimization of spiked bodies at different flight regimes can be conducted to account for volumetric, structural, as well as aerodynamic demands.

### 2.7. Design tradeoffs and issues of practical implementation of mechanical spikes in real systems

Adding the mechanical spike to the hypersonic forebody is subject to some limitations. A spike has insignificant impact if it is very short [20], if the forebody is not blunt enough [33], at low Mach numbers [4, 19], or in rarefied conditions [124]. In addition to degrading the vehicle flight stability [6], a spike's effectiveness at high

incidence unless sophistical devices are used [109] on the expense of design simplicity. In addition, under certain conditions, excessive (even doubled) aeroheating can impact the forebody [17, 54]. Clearly, pulsation, oscillation, and hysteresis should be avoided in real applications due to their apparent drawbacks [17, 41, 47]. Structural rigidity of a spike should be considered and measures should be taken to alleviate the intensive heating to its tip [118]. Whether the attached spike will impact the operation of onboard optical seekers should also be considered; local heating at the spike tip is sought to impact infrared seekers. Overall, a mechanical spike as a forebody shock control device is case-sensitive and should be carefully tailored for the mission in concern.

## 3. Fluidic devices, counterflow (opposing) jets:

### 3.1. Principle of operation of counterflow jets

The counterflow jet is simply a jet emanating from an orifice at the stagnation point of a blunt supersonic/hypersonic vehicle. If the orifice is the port of a convergent nozzle, a sonic jet is generated while a supersonic jet is created if the orifice is the port of a convergent-divergent nozzle. If it has the sufficient strength, the jet pushes the bow shock wave ahead of the blunt vehicle. Thus, the flowfield about the vehicle is modified such that both drag and aeroheating are reduced. Counterflow jets were introduced to the supersonic flight regime by Eugene S. Love in Langley Aeronautical Laboratory of NACA in 1952 [125] and were found superior in supersonic regime compared to lower speed ones [126]. It is interesting to note here that counterflow jets were originally implemented to generate reverse thrust for planetary landing, e.g. retrorockets [127]. Despite acting as decelerators (i.e., drag generators), the benefit of retrorockets in reducing the overall drag on the vehicle forebody was confirmed [128]. As far as aeroheating is concerned, an opposing jet at the stagnation point was introduced to replace the porous structures due to their lack of rigidity and the multi-holes systems due to their low efficiency [129]. Apart from controlling the pressure and heat flux distribution over high speed vehicles' forebodies, opposing jets were found useful in different fields; as fuel injectors in supersonic combustion J30 and as vertical landing devices for planetary vehicles [130].

Counterflow jet can have two operation modes namely, the long penetration mode (LPM) and short (blunt) penetration mode (SPM); the terms were first used by Jarvinen and Adams [127]. Whether the jet will have either of the modes depends on the design of the nozzle upstream of the jet. Sonic jets generated by convergent nozzles maintain the SPM. If a convergent-divergent nozzle is used, the generated supersonic jet can be in LPM or SPM if it is under-expanded or highly under-expanded, respectively, depending strongly on the nozzle design [131, 132]. The jet is said to be under-expanded if its pressure as it exits the orifice is higher than that of the surrounding air, i.e., downstream of the fore shock ahead of the vehicle. If the jet exit pressure exceeds twice that of the surrounding air, the jet is said to be highly under-expanded [131, 133]. So, for a given nozzle and orifice, the jet mode depends primarily on the ratio of total pressures of jet to that of the freestream. Some researchers use the total pressure of the freestream downstream of a normal shock wave; the freestream Pitot pressure. Hence, in the literature, the two following definitions of the jet pressure ratio are adopted; the two expressions are inter-related through the freestream Mach number:

$$PR = P_{jo}/P_{\infty o} \qquad\qquad PR = P_{jo}/\acute{P}_{\infty o}$$

With very low values of $PR$, the jet is incapable of causing any changes in the flowfield structure, mainly the forward bow shock wave (the fore shock). In this case, the jet acts as a transpiration cooling [134] or film cooling [135] devices. For higher $PR$ values, the jet protrudes ahead of the forebody forming the LPM in which the jet has the regular diamond configuration witnessed with under-expanded jets. As $PR$ increases, the length of the jet increases pushing the fore shock further away from the body and maintaining the same diamond pattern. The LPM sustains until the pressure ratio reaches a critical value, $PR_{cr}$, at which the jet attains its maximum length [136]. By slightly increasing the pressure ratio, the jet changes abruptly to the SPM in which the fore shock gets almost immediately more curved and closer to the forebody. By contrast, the jet in the SPM has the single cell (Mach cell)

configuration witnessed with highly under-expanded jets. By further increasing the pressure ratio in the SPM, the Mach cell gets larger pushing the fore shock further upstream away from the body.

The flowfield associated with opposing jets can be described as follows. In SPM, the high value of PR implies that the jet is highly under-expanded such that the jet boundary acts as a fictitious extension of the nozzle [133]. Through this extension, the jet flow expands in the axial direction while its pressure is reduced. To come to a stop, a normal shock wave is created, the Mach disk, downstream of which the jet becomes subsonic. The jet eventually comes into stagnation at the surface of contact with the freestream; the interface. Thus, the jet is formed of one cell engulfed by barrel shocks and ending upstream by a Mach disk ahead of which the jet flow becomes subsonic and hence, no more cells are formed [137]. Thus, a subsonic pocket is formed bounded by the fore shock and the Mach disk. Downstream of the interface, the jet flow is turned back towards the vehicle in the form of a shear layer. Part of the jet flow manages to pass along the vehicle while the rest of the jet forms a recirculation zone that covers the region engulfing the nozzle. The two parts of the jet are divided by one streamline that comes to stagnation on the vehicle; the dividing streamline. Upstream of the interface, the freestream creates a fore shock such that its total pressure equals that of the jet exactly at the interface [138, 139]. To follow the interface, the flow downstream of the fore shock is turned away from the vehicle through an oblique shock wave; the reattachment shock. The flow pressure and temperature on the vehicle surface attain peak values immediately downstream of reattachment. Figure 5a illustrates the macroscopic features of the SPM.

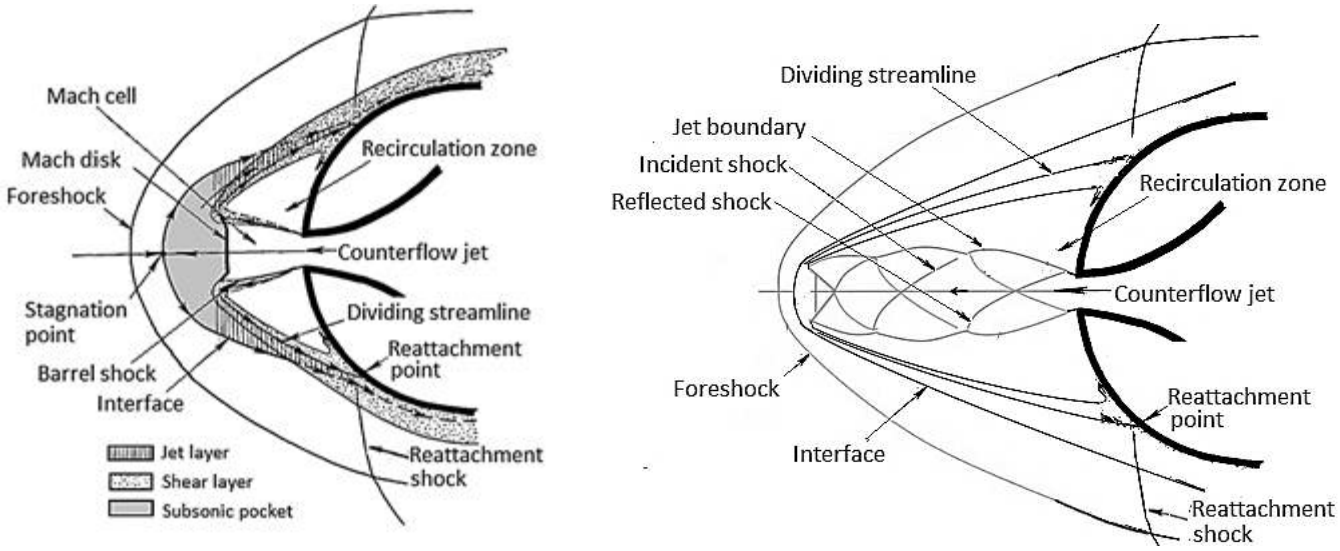


**(a) short penetration mode, adapted from [140]** **(b) long penetration mode**

**Figure 5 Macroscopic features of opposing jet flow into a supersonic freestream**

As both $PR$ and orifice area increase in the SPM, the size of the Mach cell increases in axial and lateral directions [139, 141-143]. This pushes the interface and the fore shock further away from the vehicle. In addition, the location of reattachment is pushed outwards which weakens the reattachment shock and causes the reattachment pressure and heat flux peaks to drop. Meyers et al. [144] showed that both skin friction drag and aeroheating reduction were correlated to larger jet size. Eventually, the overall drag and aeroheating on the vehicle are reduced [145, 146].

In LPM, the flowfield shows similar details to those in SPM. The key difference is that in LPM, the jet acts similar to the under-expanded jets. This is generally associated with supersonic jets rather than the sonic ones [132]. The jet is composed of a series of incident and reflected oblique shock waves that yield the conventional diamond form. The jet total pressure drops gradually as it passes this shock system terminating in a small normal shock wave downstream of which the jet flow becomes subsonic. The impact of increasing the pressure ratio in LPM is also

similar; the jet gets longer pushing the fore shock further upstream. In addition, the interface becomes more slender, the recirculation zone size increases in axial and lateral directions. In effect, the pressure on the forebody surface becomes lower, the reattachment becomes less severe at a point further away from the orifice.

Overall, the jet in LPM produces a thinner and longer penetration for the flow ahead of the orifice than that in SPM. Hence, the generated recirculation zone is more elongated in the axial direction. Figure 5b illustrates a schematic for the flowfield features in the LPM of opposing jet. In terms of flow stability, it is confirmed that the LPM encounters flow instability whereas the SPM is generally stable [140, 147, 148].

The interaction between the jet and freestream flows creates an effective body outlined by the surface of contact between the two flows, the interface [138]. A recirculation zone of low pressure and temperature is entrained between the jet and the interface. Thus, the mechanisms of drag and aeroheating reduction of opposing jets are twofold. On one hand, the new fore shock is pushed further away from the vehicle forebody and has a more slender and less blunt form [136]. Downstream of the new fore shock, air pressure and temperature attain lower values compared with those downstream of the original fore shock ahead of the body alone. On the other hand, the recirculation zone (characterized by low air pressure) covers a significant part of the forebody. Eventually, drag and aeroheating on the vehicle forebody are reduced. As a shock control device, opposing jets are more beneficial with blunter bodies than with more slender ones [149]. Compared with mechanical spikes, opposing jets are confirmed to yield more drag reduction especially with more slender forebodies [150] even with shorter effective body [52].

As the pressure ratio increase in both modes, the overall drag and aeroheating on the forebody decrease. At the critical pressure ratio, the jet length and the drag reduction reach their maximum values. The value of the critical pressure ratio is dependent on the forebody configuration, jet Mach value, and orifice area [140, 151]. As the Mach number and orifice area increase, both the critical pressure ratio and the associated maximum drag reduction decrease [152]. More importantly, slightly beyond the critical value of pressure ratio, a bifurcation phenomenon where transition from one mode to the other and back takes place [136, 147]. This is associated with an abrupt rise in drag that continues to fall with a lower slope afterwards [136, 140, 151]. This drag jump becomes more severe if the jet exit Mach number of orifice are increase [152]. Using small orifice areas, bifurcation phenomenon can be avoided on the expense of drag reduction capabilities of the opposing jet [152].

At incidence, it is agreed that the opposing jet loses its effectiveness as a drag and aeroheating reduction device [153-156]. Nevertheless, compared with mechanical spikes, opposing jets provide slightly more drag reduction at moderate incidence angles [52]. At very high incidence, drag and aeroheating to the forebody can exceed those with no jet [126, 128, 157]. When applied to vehicles with lifting design at incidence, opposing jets yield negative impact on lift [158]. For non-lifting vehicles, opposing jets increase the lift and the lift-to-drag ratio of the vehicles at incidence [153, 154]. It has also been shown that at incidence, the jump between LPM and SMP becomes less severe [151].

### 3.2. Factors controlling the counterflow effectiveness

Guo et al. [159] demonstrated that the jet pressure ratio and both freestream and jet Mach numbers have the dominant impact on jet effectiveness. For given freestream conditions and pressure ratios, the impact of other factors was investigated by many researchers. The impact of gas type was examined by Warren [157]. He proved that Helium jet was superior to Nitrogen in reducing the pressure reattachment peak. This was also confirmed in [160, 161]. Helium was also found to yield a slightly better cooling compared with Hydrogen [162] and was found to over-perform air and carbon dioxide [163-165]. Finley [140] concluded no difference when comparing air and carbon dioxide. Using a mixture of gases, the mixture ingredients were found to have a slight impact on jet function [126]. The higher effectiveness of lighter gases in reducing aeroheating and drag was explained owed to their higher specific kinetic energy that yields longer penetration for a given pressure ratio [166]. In the vicinity of stagnation and reattachment zones of the vehicle, heavier gases were found more effective in reducing aeroheating [134, 164].

Barber [167] reported a strong dependence of the fore shock standoff distance and heat flux on the specific heat ratio of the jet gas. Finley [140] confirmed the impact of jet temperature and specific heat ratio on heat transfer to the vehicle rather than the pressure distribution on it. In contrast, it was shown that increasing the specific heat ratio pushes the fore shock further away from the body [141]. Jet temperature has a negative impact of the thermal protection capabilities of the jet as it increasing the peak heat transfer at the reattachment point [145, 168, 169]. Impact of jet temperature on drag reduction capabilities of opposing jet was a point of debate. The jet temperature was proved in some studies to have no impact on the fore shock standoff distance [169] nor on drag [168]. Other studies [166, 170] confirmed that increasing the jet total temperature yields more drag reduction which explains the relative superiority of plasma and high-temperature jets over conventional ones [166].

### 3.3. Measures of opposing jet strength

Different measures have been developed by researchers to address the strength of the jet as a shock control device. The first measure was the *thrust coefficient* of the jet defined as the jet thrust divided by the product of freestream dynamic pressure and reference area. It was introduced by Love [125] and later used by McGhee [128] and Meyers et al. [144]. Pamadi [135] used exactly the same measure under a different name; *the momentum coefficient*. He proposed a closed-form equation to estimate the total drag coefficient on the vehicle as a function of the jet thrust coefficient based on available measurements [140, 157].

Stalder and Inouye [129] introduced a new parameter to indicate the jet strength namely, the *injection parameter*, $F$, defined as the ratio between the jet mass flow rate and the product of freestream density, velocity, and reference area. Warren [157] used an identical measure with a different name, the *mass flow rate coefficient*, $C_{\dot{m}}$, and introduced a new measure termed the *momentum flow coefficient*, $C_{\dot{\mu}}$. It is simply defined as the mass flow rate coefficient multiplied by the ratio between jet and freestream velocities. The mass flow rate coefficient was found to decide the fore shock standoff distance [171]. A slightly different measure was introduced by Barber [167] namely, the *relative mass flow* parameter. It was defined as the ratio of the product of jet density and velocity to that of the freestream.

Hayman and McDearmon [172] introduced a rather different measure for the strength of the jet namely, the *jet pressure ratio* defined as the ratio between the jet total pressure and the freestream pressure. Romeo and Sterrett [138] were the first to modify the definition of jet pressure ratio to the one that has been adopted by all researchers since then. The jet pressure ratio was defined as the ratio between the total pressures of the jet and the freestream Pitot. A slight modification to the pressure ratio measure was later proposed by Rong and Liu [173] to better reflect the jet intensity. The new measure, $R_{PA}$ is simply the jet pressure ratio (based on freestream total pressure) multiplied by the ratio between the orifice and the reference areas. Yisheng [174] concluded a linear correlation between $R_{PA}$ and both the overall drag and fore shock standoff distance.

Recently, Shen et al. [168] introduced interesting parameters to assess the jet based on its final outcome rather than its design. The *jet efficiency parameter* is defined as the relative reduction in drag or heat flux to the forebody per unit mass flow rate of the jet. Such parameter can be implemented to compare different jets. It will be also of a great importance if the operation time of the jet is considered.

### 3.4. Survey of key previous studies on counterflow jets

Following the promising investigation in transonic regime [175], Love [125] conducted the first experimental study on counterflow jets from slender elliptical model into a low supersonic (Mach 1.62) laminar and turbulent freestream and total drag on the model was measured. The Schlieren images captured clearly the two modes of the jet with transition at thrust ratio value of about 0.005. Love argued that the jet was subsonic in the LPM and supersonic for SPM. The jet was found to reduce the pressure drag over the range of Reynolds number tested, however, Love did not find the forward jet superior compared with a similar backward jet. Stalder and Inouye [129] focused on measuring the heat flux to a hemispherical model with a counterflow jet exposed to Mach 2.7 laminar and turbulent freestream flows. For low values of injection parameter, $F$, the jet was found to have no impact on the

flow structure or heat transfer. By increasing the injection parameter, the heat transfer to the model was found to increase up to the double with both Reynolds number and the injection parameter. For all values of $F$, the generated jet belonged to the LPM form.

The work of Warren [157] is a milestone in the field. He measured the drag and heat transfer to a spherically blunted $10^0$ cone exposed to Mach 5.8 freestream. In contrast to previous studies, Warren confirmed that even subsonic jets (with sufficient momentum) could achieve drag reduction. Increasing the mass flow rate coefficient, the reattachment pressure would decrease wile peak heat flux would increase. This was owed to the increase in shear stress due to the jet. He addressed the impact on jet protrusion on the fore shock form. Baron and Alzner [171] confirmed the finding of Warren for higher mass flow rate coefficients of the jet on a hemispherical model exposed to Mach 4.8 freestream and included high quality flow visualization. The fore shock standoff distance was confirmed to be dependent on the jet mass flow rate coefficient. The dependence of the fore shock standoff distance on the jet flow rate was confirmed in another study [162] but was related in a more elaborate expression to the jet pressure ratio and diameter in [172]. Romeo and Sterrett [138, 176] explored the structure of a sonic jet emanating from a flat cylindrical model in Mach 6 and 8.5 freestream. They provided clear explanation of the jet structure in SPM. They proved that the distance to both the Mach disk and the fore shock are solely dependent on the jet pressure ratio regardless to the freestream Mach number. They also addressed that fact that a sonic jet would yield the farthest standoff distance for a given pressure ratio.

The comprehensive work by Finley [140] is another milestone in the field. He focused on understanding the flow physics and measuring the surface pressure on two models. Hemispherical and spheroidal cylindrical models with sonic and supersonic jets exposed to a Mach 2.5 freestream were examined. Finley confirmed the findings of [138, 176]. He also proved that the critical pressure ratio, $PR_{cr}$, increases by increasing the jet Mach number and orifice diameter and the body slenderness. Identical conclusions were highlighted by Cassanova and Wu [177] who conducted experiments and theoretical analysis of the sonic jet from a flat cylindrical model into a low-density Mach 3 freestream. Implementing retro-nozzles of planetary entry vehicles as a means to control drag and aeroheating on these vehicles was first discussed by Adams and Jarvinen [127]. McGhee [128] measured the pressure distribution and drag on a reentry vehicle model exposed to Mach 3, 4.5, and 6 freestream at up to $5^o$ incidence using Nitrogen jet. He highlighted that at high thrust coefficient, the recirculation zone could cover the entire vehicle forebody.

The first numerical simulation study of opposing jets was conducted in 1976 by Schiff [178]. Axisymmetric flow simulation based on the Euler equations was implemented and the objective was to assess the simulation capabilities and explore the numerical flowfield physics. Macaraeg [179] followed using the Navier-Stokes equations to simulate the pressure and heat flux to an ogive-cone model in Mach 6.7 freestream. Fox [180] conducted numerical simulation for opposing jet flow form a hemispherical model exposed to Mach 2.5 and 6 freestreams. The majority of researches that followed were mainly numerical simulation studies.

The work by Daso et al. [156, 158] is a comprehensive side-by-side experimental and numerical simulation contribution to the field. In addition to surveying some of the fundamental literature, they examined a reentry capsule model at different freestream Mach numbers and incidence angles. The work involved various jet parameters including jet Mach number, orifice size, and pressure ratio. Similarly, Chen et al. [181, 182] presented a detailed description of the flowfield structure and physics of unsteadiness in their numerical reproduction of the experiments in [183].

Aso and his coworkers contributed actively with a number of studies spanning from 1992 to 2011 [145, 184-189] using both experimental measurements and numerical simulations. They examined various forebody shapes including flat cylinders, hemispheres, and ogives at different freestream conditions covering Mach ranges from 3 to 8 as well as high enthalpy flows. Both drag and aeroheating reduction capabilities of opposing jets were explored. Similarly, the research group of Reddy conducted a number of experimental and simulation studies on sonic and supersonic opposing jets of air, Nitrogen, and Helium [160, 164, 190-192]. The vehicle forebody was $60^o$ blunt cone exposed to Mach 5.75 and 8 and their focus was on flowfield structure, drag, and aeroheating. The active research group of Cheng also contributed in the field with a number of high quality numerical simulation studies. In [156, 193,

194], they reproduced the experimental work on a reentry capsule model by Daso et al. [158] and examined more freestream conditions (Mach numbers and incidence angles). Detailed flow physics illustrations are also included. Later in [143, 195], they shifted to supersonic slender aircraft models with truncated conical and quartic nose configurations exposed to Mach 1.6 freestream. Parametric studies of nozzle geometry among other parameters were conducted. The unique finding of their study is the negative impact of opposing jet on the vehicle lift at non-zero incidence [156].

### 3.5. Studies on flow unsteadiness associated with counterflow jets

The first record of unsteadiness in opposing jet flows was made by Klich and Leyhe [162]. Unsteadiness had the form of axial (forward and backward) oscillation of the fore shock ahead of the body. No explanation was proposed but it can linked to oscillatory variation of the jet length. Finley [140] proved that unsteadiness is related to the multiple cell structure of the jet (the LPM jet structure) that occurs at low pressure ratios. Negligible unsteadiness was recorded by Finley in the single-cell jet pattern (the SPM jet structure) at high pressure ratios and the single-cell pattern was considered globally stable. McGhee [128], Karpman [147], and Nishida et al. [139] confirmed Finley's findings whereas an associated lateral asymmetric motion of the jet was also reported [144, 148, 155]. Debiève et al. [148] pointed out that instability could become less intense is the opposing jet was at an angle with respect to the freestream.

The first attempt to explain the cycle of unsteadiness was proposed by Fujita et al. [137, 182, 196] in his numerical reproduction of experiments by Karashima and Sato [183]. According to Fujita, the minor unsteadiness witnessed in the stable SPM is owed to negligible unsteadiness in the flow in the subsonic pocket ahead of the Mach deik, Fig. 2. In LPM, the pattern of periodic instability can be explained as follows. The jet pressure ratio is below some critical value such that the multi-cell pattern is established. The jet length changes periodically from a maximum to a minimum. At the minimum length, the jet attains the single-cell pattern hence, the surrounding recirculation zone has a minimum size and the flow pressure inside it is maximum. According to Love [125], this forces the jet to change its pattern to the regular reflection (diamond) pattern, to have more than one cell, and to extend upstream. As consequence of jet elongation, the recirculation zone expands and the flow pressure inside it decreases. At the maximum jet length, the pressure in the recirculation zone attains a minimum value at which the jet cannot maintain the multi-cell pattern. The second cell collapses, the single-cell pattern is restored, and the process is repeated again in a self-sustained manner.

Shang et al. [136] proposed a different mechanism for the opposing jet instability. At low jet pressure ratios, the jet injection rates are low such that the reflecting jet layer becomes subsonic. Hence, the domain that engulfs the freestream layer downstream of the Mach disk including the recirculation zone is subsonic. Any instability in the free shear layer can propagate upstream impacting directly the Mach disk forcing it to move axially. Some frequencies of the shear layer instability can cause resonance yielding the self-sustained unsteadiness of the Mach disk and fore shock. This mechanism seizes at higher pressure ratios (above the critical value) as the supersonic jet layer separates the subsonic pocket and the subsonic recirculation zone such that the Mach disk becomes insensitive to the shear layer instability.

The transition of opposing jet from the unstable LPM to the stable SPM at the critical pressure ratio was first recorded by Finley [140] then by Karpman [147] and was termed *transition* by Adams and Jarvinen [127]. According to Finley, transition takes place at the critical value when $P_{jo}/\acute{P}_{\infty o} = 1$; a condition that was confirmed by Fujita [137]. This phenomenon was termed "*bifurcation*" by Shang et al. [136] upon similarity with a phenomenon associated with changing the mechanical spike length. From a different perspective, Gerdroodbady et al. [165] were interested in the transients of evolution of opposing jet in both LPM and SPM. Using numerical techniques, they provide good illustrations of the physics of transients.

Finally, almost all opposing jet flow studies were considered axisymmetric at zero incidence. All numerical simulation studies adopted the 2D axisymmetric computational domains. Half 3D domains were used in case of non-zero incidences [151, 153, 155, 156] or in cases if the vehicle is not axisymmetric [154, 197, 198]. The three-

dimensionality of opposing jet flow from an axisymmetric body at zero incidence was first investigated by Chen et al. [181] in their high quality numerical study. Based on their analysis, it is confirmed that the stable SPM is dominantly axisymmetric whereas the unstable LPM is dominated by asymmetric off-axial motion. This asymmetry has the form of rotational vector that around the axis that generates a periodically varying side force. This helical form of instability in LPM was later confirmed by Farr et al. [199] in the context of understanding the aeroacoustics associated with this mode.

### 3.6. Non-conventional studies on counterflow jets

Warren [157] suggested swirling the jet instead of directing injecting in into the freestream. No marked impact on the jet effect was recorded. Sriram and Jagadeesh [134] examined experimentally using am array of microjets rather than a single central jet carrying the same momentum. It was found that microjet array provided better cooling for the vehicle. The provided images show no change in the fore shock ahead of the vehicle. Gerdroodbary et al. [161] also presented microjets as a remedy for the excessive aeroheating associated with the single jet at reattachment. Obviously, microjet provide film cooling that is expected to over-perform a single central jet. However, since no change in the shock system can be attained, the cause of aeroheating is not handled and no drag reduction can be expected from such devices. Similar devices were examined by the group of Huang as jet aperture and multiple orifices at the leading edges of a waverider [200, 201] and hypersonic vehicle [202] configurations. Multiple orifices over-performed the single aperture while especially with odd number of orifices since an orifice was placed at the vehicle's stagnation point. Augmenting opposing jet device with platelet transpiration passive cooling device was explored numerically by Yisheng et al. [203] and then by Shen et al. [204],[205] for different freestream and operating conditions. Adding the transpiration cooling capability further enhanced the opposing jet effectiveness (in terms of reattachment peak heat flux) with a small added mass flow rate penalty.

Berdyugin et al. [150] implemented liquid jets rather than gas jets in their experiments on various forebodies. LPM was reported with unsteadiness at high flow rates along with degradation in the drag reduction benefits of the opposing jet. Later, Ce et al. [206] found experimentally that water jets were longer and more stable compared with gas jets. Comparing both fluids in terms of drag and aeroheating capabilities was not presented while gravity was reported to have a negative impact on water flow axisymmetry. Storing such incompressible fluid in the limited space of real vehicles is troublesome.

Recently, the group of Wei Huang and his coworkers contributed with a number of interesting numerical studies concerning the orifice configuration and jetting style. Impact of orifice shape on jet effectiveness was the scope of their first set [154, 197, 198]. In [198], they compared different polygons, cirque as well as the conventional circular orifice of the same area. They argued that a pentacle orifice yielded lower drag and local heat flux compared with the other polygons. However, a pentacle yielded higher surface heat flux and pressure compared with the conventional circular one. They went further in [197] by addressing the impact of number of star points on a star orifice. It was shown that the star shape had no impact on drag while a 7-point star yielded the minimum local heat flux. In [154], they went further with the 7-star orifice. They showed that drag and lift on the vehicle were asymmetric with incidence angle. They also addressed the impact of jet angle with respect to the vehicle symmetry axis. Both lift and drag on the vehicle were found to increase monotonically with jet angle; a slight increase in heat flux with jet angle was reported as well. It should be noted however, that such asymmetric orifice configurations would yield asymmetric pressure and heat flux profiles on the vehicle. This would add to uncertainty of flight prediction of the vehicle since lift, drag, and side force will be asymmetric with respect to incidence and side-slip angles. Whether such orifice shapes be synergic to upstream convergent or convergent-divergent nozzles is questionable.

The other set of studies by Huang et al. were concerned with the temporal pattern of jet [207-209]. Instead of using a jet with a fixed pressure ratio, they proposed using jets with periodic variation; pulsed jets. In [207], a sinusoidal pulsed jet with different periods was examined. Longer pulsation periods were found to yield better results

especially in aeroheating reduction. Drag reduction was found to deteriorate with pulsed jet. Focus was then drawn in [208] towards the impact of pulsation on the jet structure. It was claimed that a pulsed jet would always maintain SPM features even at low instantaneous pressure ratios. Both drag and aeroheating levels were found to vary considerably. No comparisons were made with a steady jet performance. Finally, in [209], triangular and rectangular pulse shapes were compared with the sinusoidal one. Better aeroheating reduction and poorer drag reduction were claimed compared with the steady jet. A rectangular pulsed jet demonstrated the worst performance. These studies however, did not discuss the worthiness and practical implementation of such complexity.

### 3.7. Derivatives of opposing jet device

#### 3.7.1. Opposing plasma jets

An opposing plasma jet is simply a jet of gas at extreme temperatures (many thousand degrees) before exiting the vehicle through the orifice towards the incoming flow. At these extreme temperatures, the gas becomes ionized and electrically conductive (plasma state). This is attained by passing the gas through a high voltage electrode placed within the forebody. The pioneering proof-of-concept experimental work in this field was conducted by Gordeev and his research group [210-212]. The idea was based on augmenting the conventional opposing jet device with the favorable drag reduction features of electric discharge. This feature of plasma discharge (along with other energy discharge forms) will be discussed later in this survey. To date, the studies on opposing plasma jet have been exclusive to three research groups: Gordeev et al. [166, 170, 210, 213, 214], Shang et al. [152, 215, 216], and Fomin et al. [217, 218].

On fluid dynamics side, a plasma jet shows identical features to those of the conventional jets. Both LPM and SPM are evident, bifurcation at critical pressure ratio takes place, and dependence of drag reduction on design and operating conditions shows the same trends. The key aspects that characterize the plasma jets are that LPM of plasma shows a more stable pattern [152, 217]. In addition, for the same pressure ratio, a plasma jet yields thinner and shorter penetration into the incoming flow [152]. Finally, the critical pressure ratio of the plasma jet at the same other conditions is higher [218].

The role of elevated temperature of the jet is to reduce the density and mass flow rate of the jet. So, if the same mass flow rate is maintained, the plasma jet yields about 10% more drag reduction [152]. In addition, for a given impact to be achieved, plasma jets require less total amount of gas. However, for the same pressure ratio, a plasma jet yields less drag reduction compared with the conventional jet [152] despite that the reversed thrust is reduced. The argument that electric discharge features of plasma jet add to its drag reduction capability was criticized in the literature. It was concluded that the operation of opposing plasma jet is mainly due to fluid dynamics, i.e., flowfield structure modifications and in a small percentage due to thermal effects while discharge contribution is negligible [152, 218, 219]. Conventional opposing jets with very high total temperature values (e.g., combustion gas products) were found comparable to plasma jets [170].

Three issues related to plasma and very hot gas opposing jets can be raised. One is the negative impact of such devices on aeroheating to the forebody. In supersonic and hypersonic regimes, drag and aeroheating are equally important. On reducing drag, aeroheating can not be compromised. This issue was not addressed in the literature so far. The second issue is the ionized field associated with plasma jets. Such ionized field surrounding the vehicle forebody has a negative impact on quality of electromagnetic wave communications essential to the guidance, navigation, and control of the vehicle during flight. The third is the power, space, and weight requirements for such devices. These demands add to the design tradeoffs and degrade the overall efficiency [218, 219]. Alternatively, light gases have shown results that are comparable to plasma jets at significantly lower stagnation temperatures [166, 214] and can be considered as a proper solution.

#### 3.7.2. Combined jet-cavity device

A forward-facing cavity is simply a hole in the hypersonic vehicle forebody located at its stagnation point. The cavity can be deep or shallow. Deep cavities can be cylindrical, conical, or ogive while shallow cavities can have spherical or ellipsoidal shapes. Such cavities were found to have a favorable impact on the peak aeroheating (at the

stagnation zone) as well as on the overall and average aeroheating to the forebody. The mechanism of aeroheating reduction differs in deep cavities from that in shallow cavities. A deep cavity acts as an organ pipe along which the column of air downstream of the fore shock wave oscillates in its natural frequency [220-222]. This oscillation causes the fore shock wave to oscillate yielding a cooling effect. Eventually, the aeroheating to the forebody is alleviated. The deeper is the cavity the higher the amplitude of oscillation of the fore shock wave [223, 224]. In contrast, the mechanism of aeroheating reduction in shallow cavities is twofold. On the one hand, theoretically, the concave surface of the cavity acts similar to a flat surface that yields a minimum heat flux. On the other hand, air downstream of the fore shock creates an annular vortex structure around the inner lip of the cavity. This vortex acts to isolate the new stagnation zone (inside the cavity) from the high-enthalpy flow upstream [225]. For both deep and shallow cavities, a local excessive heat flux is attained at the lip of the cavity that may exceed that at the stagnation point of the forebody without the cavity. A cavity (alone) is not considered as a drag and aeroheating reduction device in the sense adopted in the present survey. This is because the cavity does not handle the cause of aeroheating namely, the strong fore shock ahead of the vehicle. More importantly, introducing the cavity increases the overall drag on the forebody. In fact, the drag penalty of forward facing cavity was not discussed by the previous studies in this field.

A few researches were conducted on the combination of jet and cavity as a hybrid (combinatorial) shock control device. In this device, rather than injecting the jet from an orifice located immediately at the forebody surface, it is injected from the orifice into a cavity (of the deep type) before exiting into the flow ahead of the forebody. Treating such combination as a hybrid device is not technically accurate for two reasons since the concept of hybridizing two devices is not satisfied here. The mechanism of operation of the deep cavity no longer exists once the jet passes through it towards the freestream. In fact, the cavity in this combination acts as a downstream divergent nozzle for orifice jet. The design of the divergent nozzle is found to significantly impact the jet operation. Bibi et al. J6 addressed this dependence through a comprehensive parametric study on the design of divergent nozzle. Based on this argument, the devices by Lu and Lui [226-229] and by the research group of Huang [230-234] are considered in this review as derivatives for the opposing jet rather than distinct hybrid devices. A summary for all opposing jet literature is listed in Table A2 in the Appendix.

### 3.8. Prospective gaps in the field of counterflow jets

Considering the huge body of studies on opposing jets, a small percentage focused on implementing the real flight conditions of supersonic and hypersonic regimes namely, high Mach numbers at high altitudes. Cassanova and Wu [177] examined experimentally and theoretically the low-density Mach 3 freestream. They found an increase in the fore shock standoff distance at low densities. Apart from [177], all studies using experimental facilities were concerned with satisfying the Mach number ranges up to Mach 8 [190]. Only recently, a few studies using numerical simulations implemented atmospheric conditions at 15 km [143, 195], 25 km [168, 201], 32.5 km [235], 40 km [155], and 60 km [161]. The thermal protection benefits of opposing jet in rarefied medium conditions were only theoretically investigated by Larina [236]. In terms of vehicle configurations, the majority of studies examined the typical “academic” model shapes including hemispheres, blunted cones, truncate cones, and even flat cylinders. Only a small percentage of studies focused on the impact of opposing jet on real shapes of supersonic and hypersonic vehicles. The real configurations that were examined included space capsules [158, 194, 206, 237], high speed aircraft [143, 155], and waverider [200, 201].

Three aspects appear to be overlooked by researchers on opposing jets so far. Firstly, all previous researches examined scaled models that are suited for experimental facilities. Numerical simulation studies were also limited to reproducing the experiments on the same models. The effect of full scale model was not investigated. This demands a systematic studies devoted solely to the impact of Reynolds number on the opposing jet operation. Even with laminar freestream conditions, transition to turbulent should be considered especially in areas of high viscous effects. Secondly, the performance of opposing jet in the real flight conditions of an accelerating vehicle while descent has not been explored. It should be noted that, as a hypersonic vehicle accelerates while descent, the pressure ratio would decrease monotonically for a given jet total pressure. The resulting jet structure will vary continuously and

may change from SPM to LPM during flight. Thirdly, the impact of jet transients on drag and aeroheating on the forebody has not been examined thoroughly. Special attention should be paid to the events of start, varying the operating pressure, and shutoff of opposing jet during flight. Gordeev et al. [210] briefly mentioned an overshoot in drag during jet shutoff.

Due to the complexity of jet flow interaction with shock waves, the flow is unlikely to be axisymmetric even as zero incidence. Asymmetry of opposing jet flow was only examined in [181, 199] and indeed requires further investigation. A number of new ideas proposed in the literature are assessed only numerically; experiments are needed to assess the validity and applicability of such ideas. Pulsed and periodic jets, polygonal orifices, micro-jets, and augmented transpiration cooling are examples of these new concepts. Whether pulsed jets would be beneficial in terms of power requirements requires further analysis. Finally, the field of opposing jet requires a multi-objective design optimization study that involves all design factors including the nozzle geometry, jet total pressure, jet total temperature, forebody geometry, etc. [131, 140, 151, 158]. Since the flight conditions impact the opposing jet function, a multi-point optimization may be also considered. Drag reduction and aeroheating reduction are expected to be competing; the jet efficiency factors by Shen et al. [168] are candidate objective functions for such study.

### 3.9. Design tradeoffs and issues of practical implementation of opposing jet in real systems:

Whether to use an opposing jet with high or low pressure ratio is a point of debate. On one hand, a low (below critical) pressure ratio yields more drag reduction. The opposing jet attains its maximum effectiveness exactly at the critical pressure [136, 137, 140, 192]. In addition, better boom signature of the flying vehicle is linked to longer jet penetration [195]. However, flow unsteadiness and hence, high surface pressure fluctuations, flight instability and uncertainty in flight prediction come as penalties of the associated LPM jets [136, 148]. Drag oscillation amplitude up to 130% of the nominal value was reported [155].

On the other hand, jet with pressure above the critical values ensure flow stability. In addition, the aeroheating reduction capabilities of the opposing sonic jet increase considerably at high jet pressures [157, 158, 181]. Kulkarni and Reddy [192] and Chang et al. [160] reported contradicting results with supersonic jets. However, opposing jets with higher pressures for longer periods of time seems to be less practically affordable [155]. More importantly, high pressure jets yield high retarding thrust (i.e., more drag). If sufficiently high, the drag reduction benefits can be overwhelmed by the retarding thrust and the opposing jet would act as a drag generator rather than reducer [128, 135, 144, 155, 160, 164, 193]. This was contradicted by the findings of Shang et al. [136]. Meyers et al. [144] suggested that the jet thrust of a sonic jet could be reduced if the jet was made supersonic of the same size (i.e., using a divergent nozzle). However, it should be noted that this comes on the expense of the mass flow rate of the jet for a given total pressure. If the total pressure is to be maintained by fixing the nozzle throat area, generating a supersonic jet implies larger jet size and hence, more thrust. In addition, Shang et al. [136] pointed out that the stable SPM is linked to sonic jet whereas supersonic jets would produce the unstable LPM. As the Mach number of the supersonic jet increases (for a given jet size), the length of jet increases giving higher drag reduction capabilities [132].

As far as practical implementation of opposing jets is concerned, the key issue is the associated space and power requirements. To serve for a considerable period of time, the jet must be continuously supplied with the adequate pressure according to the desired protection level. Although it is not clearly stated in the literature, normally, there are two sources of opposing jet gas; a compressed gas vessel and a gas generator. Compressed gas vessels have the advantages of supplying arbitrarily selected gas, better flow control as well as shut-down and restart capabilities. However, higher complexity and lower reliability of the system emerge as penalties. In addition, as the operation time and/or increase, the vessel size and weight can get so large that using a vessel becomes impractical. In this case, gas generators can be a reasonable alternative. The size and weight of gas generators (using solid, liquid, or gas propellants) increase slightly with operation time and flow rate of the jet. The main drawbacks of gas generators are the nature of generated gases as well as the associated hazard for the onboard payload of the vehicle. A solid propellant engine was used by Ganiev et al. [170] as a source for high temperature jet in their experiments. This

concept was recently revisited by Shen and Liu [169]. Instead of using the real combustion gas products in their numerical simulations, they used air with corresponding temperatures. Indeed, using plasma or high-temperature opposing jet adds to the complexity of the design and to the power demands.

In fact, the reverse thrust effect and the power demands pose the two main drawbacks of opposing jet devices as compared with mechanical spike devices. The source of jet, space and power demands for given operation time were not discussed in the open literature. The important study by Josyula et al. [238] discussed the worthiness of opposing jet drag reduction device in real supersonic and hypersonic vehicles including launch vehicles and rockets. They addressed the internal space and packaging constraints of such vehicles. They also estimated the overall improvement in performance of different systems for a given drag reduction offered by the opposing jet; a minor to limited improvement was achieved associated with a fuel loading penalty.

## 4. Energetic (thermal) devices, energy deposition devices:

### 4.1. Principle of operation of energetic devices

Energetic devices are based simply on creating a high-energy spot in the undisturbed incoming flow (deposition) in which the flow is locally extremely heated. The flow downstream of this source loses significant parts of its dynamic energy [239, 240] and total pressure [241, 242]. Thus, if a supersonic/hypersonic vehicle is made to fly in the "aerodynamics shadow" of this spot, the fore shock wave ahead of the vehicle will be much weaker or even totally eliminated since the vehicle is exposed to low-density subsonic flow (as a consequence of high local temperatures) [243]. This phenomenon was first addressed and analyzed theoretically by Krasnobaev and Syunyaev [244, 245] in the early 1980s. In other areas, energy deposition has found applications in reducing sonic boom [246] and improving intake conditions for supersonic/hypersonic propulsion engines [247]. The level of the energy deposition in the undisturbed upstream should be high enough that the local air reaches the thermal (homogeneous) plasma state in which it becomes extremely hot, fully ionized and electrically conductive [248]. The continuous feed of the freestream maintains the plasma cloud in the upstream. The common type of plasma is referred to as the thermal (or homogeneous) plasma. Some efforts were made to implement cold (non-thermal, non-homogeneous) plasma to reduce the fore shock wave strength [249, 250]. In cold plasma, that acquires less power demands [251, 252], air maintains a normal temperature and is weakly-ionized.

From the literature, plasma clouds are generated either optically or electrically. Optically, the energy source is created by focusing a laser beam (continuous or pulsed) at the desired deposition location ahead of the vehicle. Alternatively, an electric (DC or AC) discharge is applied to air ahead of the vehicle. Based on literatures included in the present survey, Figure 6 reflects the relative researchers' interest in each of the plasma generation techniques.

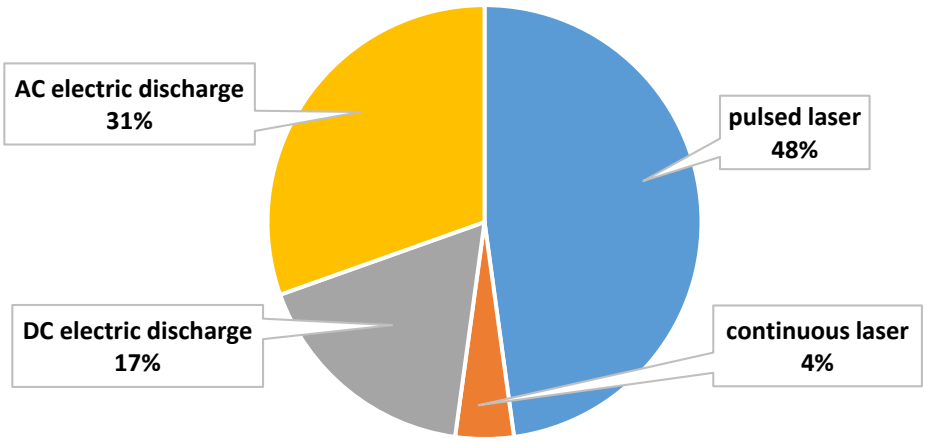


**Figure 6 Types of energy deposition devices discussed in the surveyed literature**

The preference of laser devices over electric discharge ones (as inferred from Fig. 6) is justified by being position-flexible, contactless, transmittable through hot shock layer around the forebody, independent of the carrier vehicle [253], and more synergic to flight applications [254]. With electric discharge devices, the forebody must be involved (as one of the electrodes) in the discharge process [255]. More importantly, part of the power spent in electric discharge devices is dissipated due melting of electrodes and radiation as well as electric circuits losses [256]; laser devices can be viewed as loss-free in this perspective. The ability to use laser in a pulsed mode adds to the advantages of these devices since it reduces the power demands for these devices [257]. Even if the continuous energy budget is split into multiple lower-energy pulsed ones, the overall energy efficiency is enhanced [258].

The impact of the energy source on the flowfield features depends on whether the energy source is created once or made continuously active. If this spot is created only once, the highly-pressurized, extremely-hot gases that are instantaneously generated in this spot expand abruptly pushing the surrounding medium away through a blast wave. The scavenging action of this localized "detonation-like" behavior in the medium creates a zone of very hot, low pressure, low density bubble that continues expanding as it is convected downstream of the incoming flow, Fig. 7a. As this wave interacts with the existing bow fore shock ahead of the hypersonic vehicle, the highly pressurized air downstream of the fore shock expands inside the low density bubble. In addition, the high temperatures inside this bubble have the role of reducing the local Mach number to subsonic values [259-261]. The combined effect of both aspects is that the fore shock is pushed away from the forebody [260, 262] and its strength is significantly reduced [262] or even totally eliminated [242, 255]. Eventually, the pressure field around the stagnation zone of the forebody attains low pressure levels that reduce drag. This is schematically illustrated in Fig. 7b. Pulsed repetition of energy deposition yields a more complicated flowfield structure that is dependent on the energy level, repetition frequency, pulse duration, and deposition location [248].

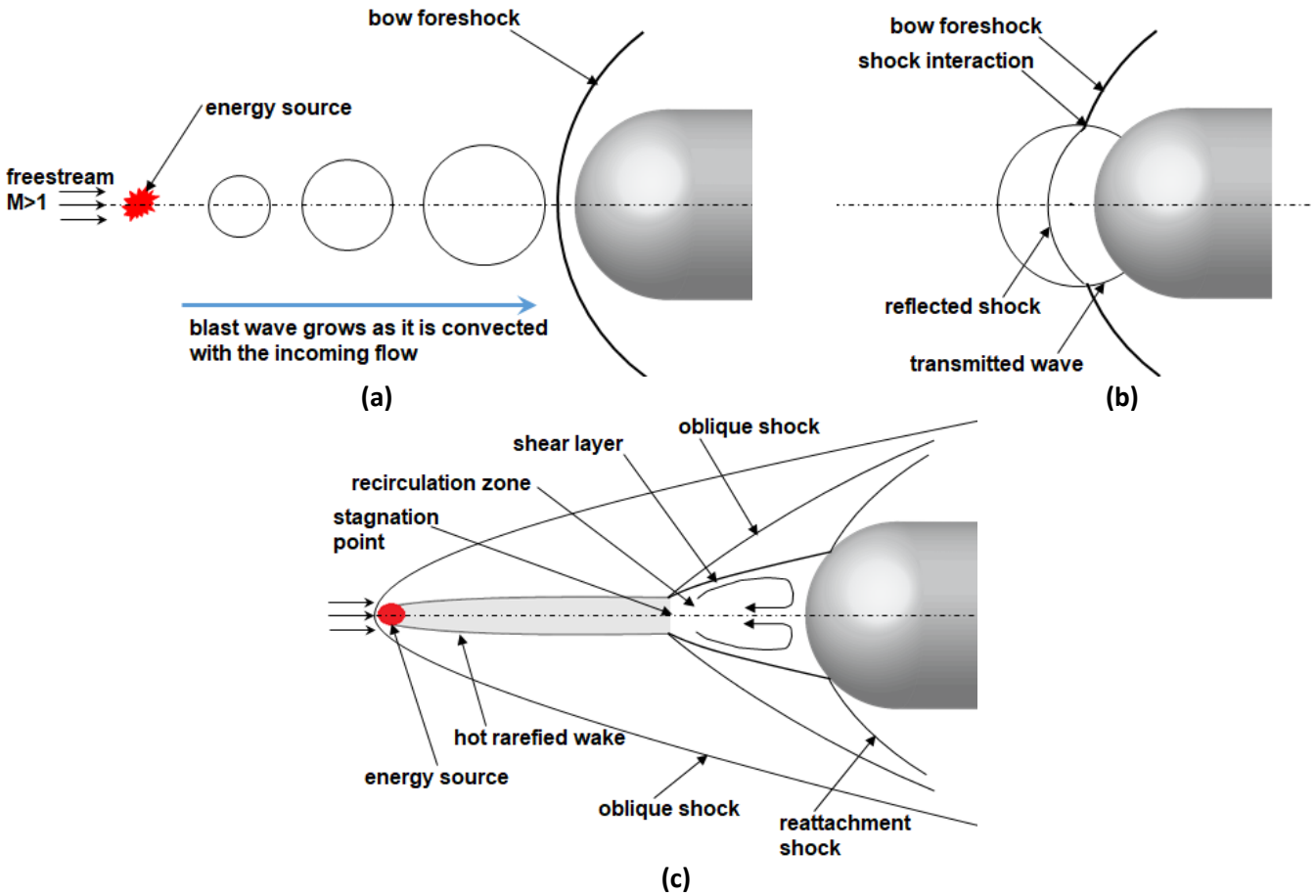

**Figure 7 Macroscopic flow features due to energy deposition into a supersonic freestream**

If the energy spot is made continuously active, the flowfield features are modified. A fore oblique shock wave is created ahead of the energy of energy spot location. In addition, a wake channel of very hot rarefied flow is created that propagates downstream of the high-energy spot. The form of this hot wake is dictated by the freestream Mach and total enthalpy [263]. Upon approaching the forebody, air in this low-density core stagnates easily (due to its low total pressure [264]) and evolves into a zone of low-pressure recirculating flow that partially masks the forebody. As the shear layer that engulfs the recirculation zone reattaches on the forebody, a reattachment shock is created at which the local pressure and heat flux attain peak values that are lower that their stagnation point counterparts in the "unprotected" forebody [239]. These features are schematically illustrated in Fig. 7~~8~~c. The replacement of the conventional bow fore shock with a system of weaker shock as well as the low-pressure recirculation zone downstream of a rarefied gas channel act to reduce the drag on the forebody [247, 248, 252]. Instability of the flowfield around the forebody can take place with both continuous [261, 265, 266] and pulsed energy deposition [267, 268] devices.

In contrast to mechanical and fluidic devices, the mechanism of drag reduction with energy deposition is widely agreed to be mainly (to entirely) thermodynamic [259, 261, 262, 269]. Kuo et al. [255, 270] added that with electric discharge devices, the free electrons in the plasma cloud act as spikes that deflect the incoming flow and disperse the fore shock wave. The mechanism of fore shock wave mitigation in case of cold plasma is different. It was explained due to rise in shock wave speed in the cold plasma region [250].

The ability of energetic devices to reduce drag is widely confirmed. In this regard, they are viewed as a remedy to a number of drawbacks of mechanical and fluidic devices namely, distance restrictions, the inability to control the effective region's position and shape, and performance degradation at high incidence [243]. Moreover, energy deposition devices save the friction drag and mass penalty associated with the addition of mechanical spike [262]. Similar to fluidic jet devices, a drag overshoot occurs at the event of power-off of energetic devices [271]. However, the aeroheating reduction of these devices is an issue of debate. On one hand, Takaki and Liou [239] confirmed that energy deposition can significantly reduce aeroheating. Satheesh and Jagadeesh [254] reported a remarkable reduction in stagnation point aeroheating. Similarly, Kremeyer [252] claimed that forebody surface temperature could be significantly reduced using cold plasma. On the other hand, Kandala and Candler [272] found it ineffective in this regard due to the increased temperature in the plasma region ahead of the forebody. A significant increase of the gas temperature confined in a thin layer ahead of the model was reported by Bivolaru and Kuo [273]. Similarly, Erdem et al. [274] reported increased stagnation zone aeroheating using DC discharge device while Ohnishi et al. [268] reported doubling the stagnation point heat flux values even with cold plasma devices. Based on simulations of Kulkarni et al. [275, 276] the flow becomes extremely hot ahead of the forebody regardless to the medium. Recently, Ganesh and John [263] predicted undesirable impact of energy devices as far as aeroheating to the forebody is concerned.

In addition to reducing drag and aeroheating, energy deposition has been confirmed to be an active flight control device. If focused at a location off the vehicle symmetry axis or its flight path, an energy spot yields lift and control moment on the vehicle [252, 260, 262, 277]. Flow stabilization using these devices was also reported [252].

### 4.2. Factors controlling the energy deposition devices effectiveness

Riggins and Nelson [278] introduced the *power effectiveness ratio* to express the impact of the energy deposition device. It is defined as the ratio between the propulsive power saved due to energy deposition and the power spent in creating the energy spot. This parameter was adopted in following studies (e.g., [261, 264]). Effectiveness mainly depends on level of energy, deposition location, size of the generated spot, freestream conditions, and forebody configuration. Configuration of the energy spot was also reported to impact its effectiveness [279, 280]. A concentrated energy spot yields more drag reduction than a distributed one with lower energy efficiency [243].

Increasing the energy level (or intensity) results in more drag reduction [278, 281] (with a significant aeroheating penalty, [239]) until a threshold beyond which further drag reduction can not be attained [241, 265, 282]. With laser-based energy devices, effectiveness is found sensitive to laser detailed parameters [268]. In addition, increasing the energy source size for a given distance yields more aeroheating reduction but less drag reduction [239, 275]. Device effectiveness can be maximized if the energy source size (relative to that of the forebody) is made as small as possible [264, 275, 283]. Closed-form expressions for energy devices' efficiency can be found in [284].

A source that is very close to the forebody would yield more aeroheating [239] with no drag reduction benefits [243, 261] or even more drag [263]. As the deposition distance increases, drag and aeroheating are reduced to minima at an optimum deposition location that is dependent on the freestream Mach value. With further increase of deposition distance, drag and aeroheating reduction hold plateau patterns [239, 240] while drag may even increase [241, 278]. In addition, for a given deposition location, increasing both Mach and Reynolds values yields more drag reduction [241, 278, 283, 285]. As the freestream Mach value increases beyond a given value, drag reduction degrades [241]. If the freestream Mach value is increased, the deposition distance should increase to yield the same effectiveness [253]. In addition, more drag reduction is achieved with the same energy intensity as the freestream pressure decreases [286] while higher freestream pressure enables using less intense energy deposition to achieve the same effectiveness [248]. The effectiveness of energy devices degrades with reducing both pressure [286] and density [254] of the freestream.

For pulsed energy deposition, longer pulse durations yield more drag reduction [248]. In addition, as the pulse frequency increases, more drag reduction is achieved [287] up to a certain limit beyond which no more reduction is achieved [288, 289]. More importantly, flow instability becomes more pronounced as the pulse frequency increases [287] nevertheless, further increasing the frequency is found to dampen unsteadiness [258]. Similarly, increasing the time between successive pulses yields an unsteady behavior due to fore shock wave recovery [267].

The effectiveness of energy deposition devices in reducing drag is also dependent on the forebody geometry. More significant drag reduction and higher efficiency of these devices are achieved if applied to blunt draggy forebodies compared with slender ones [258, 265, 266, 281, 290]. More importantly, in electric discharge devices where the forebody itself acts as one of the electrodes [291], the shape of the forebody has a significant impact on the intensity of the generated electric field [270, 292].

### 4.3. Survey on key studies on energy deposition devices

Arafailov [279] in 1987 was the first to address the impact of energy deposition on the aerodynamic characteristics of an aerodynamic body. In his theoretical study, he addressed the role of a generic energy source in changing the lift, drag, and moment acting on a blunt conical body in Mach 10 freestream. Following that pioneering work, various studies have been conducted starting with numerical studies [241, 243, 290]. Brozov et al. [248] conducted the first experimental study of pulsed laser energy device applied to a hemispherical model in Mach 1.95 freestream. The flowfield structure was the main focus of this pioneering work. Later, various studies were devoted to explore the structure of the flowfield due to pulsed energy deposition. Of these, the authors recommend the experiments of Oliviera et al. [267], Sasoh et al. [293], and Adelgren et al. [260], the numerical simulations of Joarder et al. [294], and the combined work of Schülein et al. [295]. As for flowfield structure associated with continuous energy deposition devices, the authors recommend the experimental work of Schülein et al. [296] and Satheesh, Jagadeesh [254].

Efforts have been made to develop mathematical models for accurate representation of energy deposition effect within numerical simulations. Of these, Ohnishi [268], Kandala and Candler [272], and Sangtabi et al. [258] are the most promising efforts. A concise survey for the key governing equations of steady and unsteady energy deposition in ideal gas conditions was presented by Knight [284]. In addition, the comprehensive numerical work of Takaki and Liou [239] includes a comprehensive parametric study on a drag and aeroheating reduction of a generic energy source in Mach 14 freestream. As for flow instability associated with energy deposition devices, the readers are encouraged to refer to the studies by Oliviera et al. [267], Schülein et al. [265], Erdem et al. [266], and Ohnishi et al. [268].

The most active research groups in the field of energy deposition devices are the following. The group of Myrabo conducted a set of experimental and combined experimental-simulation studies [247, 256, 267, 271, 282, 297] with AC electric discharge devices applied to blunted forebodies in Mach 3 and 10 conditions. Flowfield structure, wall pressure, and drag were concerned. In contrast, the research group of Schülein contributed with a set of combined experimental-simulation investigations of DC electric discharge and pulsed laser devices with hemispherical and conical forebodies in Mach 2 and 5 conditions [265, 295, 296, 298]. Based on their and others' results database, Schülein developed elaborate mathematical models for the drag reduction capabilities of energy deposition devices [264]. Kuo and his co-researchers conducted a set of experimental studies [255, 270, 273, 299] that focused on flow structure around a truncated conical forebody using AC electric discharge device in Mach 2.5 freestream. Finally, the group of Sasoh [283, 287, 293, 300] investigated experimentally and numerically the drag on a flat cylindrical forebody exposed to Mach 1.92 and 3.2 freestream using pulsed laser devices. Suchomel et al. developed expressions for overall system performance for energy shock control devices [301-303]. Table A3 (in the appendix) summarizes all energetic devices literature.

### 4.4. Prospective gaps in the field of energy deposition devices

Despite the huge body of studies on energy deposition devices, this field demands more studies in some areas with lack of understanding and knowledge gaps. As a consequence of the numerous parameters involved, a significant diversity in these devices effectiveness is found in the literature. For example, 96% reduction in drag was calculated numerically [277] while minor to no reduction was measured experimentally [274]. Indeed, more systematic parametric studies involving all parameters should be conducted to distinguish the key parameters from the less-dominant ones. More importantly, the debatable aeroheating reduction capabilities of energy devices invoke more systematic investigations. In this regard, cold plasma devices can be a promising track.

In addition, more than one-quarter (27%) of all literatures surveyed are theoretical and numerical studies that have dealt generically with the energy source. The vast majority of these included no validation with experimental database. This may be owed to the lack of mathematical models for the physical phenomena taking place in the flow upon applying energy sources of different origins (electrical, laser, .. ). More studies are required to cover this gap. Simulations of energy deposition accounting for real gas aspects are also required [284]. Moreover, in almost all previous experimental studies (especially on electric discharge devices), plasma was created using hardware that are external to the vehicle model. Apart from the inevitable influence of these facilities on the measured data [254], the impracticality of this approach is evident. Otherwise, the vehicle model becomes involved as one or both of the electrodes [255]. More efforts should be made to develop experimental facilities in which energy devices are fully contained onboard the test models. Finally, the aspects of flow instability associated with energetic devices invoke more analysis especially with pulsed or off-axis deposition scenarios.

### 4.5. Design tradeoffs and issues of practical implementation of energy deposition devices in real systems

The main concern with real implementation of energy deposition devices is the associated power budget and design complexities [304]. Using these devices, the design of a forebody should fully accommodate the devices without the forebody itself being involved in their operation. In this respect, contactless laser and microwave devices can be more promising [254]. In addition, some ideas proved to reduce power requirements of these devices such as pulsed deposition, multiple energy sources, and creating ring-shaped spots [253, 288]. However, the overall efficiency is still questionable [219]. The likelihood of excessive aeroheating to the forebody complicates the thermal protection demands of carrier vehicles [304]. Even with cold plasma devices, air ahead of the vehicle is inevitably ionized [259]. This complicates and prolongs the communication blackout problem commonly encountered by hypersonic reentry vehicles and brings this problem to hypersonic atmospheric vehicles. This may not be acceptable as far as guidance, navigation, and control of these vehicles are concerned.

## 5. Hybrid devices

### 5.1. Structural-Fluidic devices

A hybrid device composed of the mechanical spike and fluid spike is based on the idea of extending the mechanical spike effectiveness using fluid jet features. In effect, adding the jet to the spike emphasizes the modifications to the structure of the flowfield around the vehicle forebody due to spike. Adding the jet pushes the fore shock further upstream and the reattachment point of the shear layer further downstream along the forebody thus further weakening the reattachment shock. Eventually, the drag and aeroheating capabilities of the conventional spike are improved.

The underlying concept of this device is not new. In 1975, Chapman et al. [123] proved that injecting a flow inside a recirculation zone engulfed by a shear layer reduces the peak heat flux at shear layer reattachment. In 1961, Wood [36] expected that such injection in the recirculation zone around the mechanical spike would stabilize the flow. However, this hybrid device has gained attention only recently in a relatively small number of researches; out of all 30 previous published studies that were available to the authors, only one is more than a decade old. Due to immaturity of this field, some terminologies are not unified yet especially when referring to the location of the jet on the spiked forebody. The authors suggest the terminologies shown in Fig. 8 that are consistent with those of spike device; they will be used in the following survey. The figure also shows the relative researchers' interest in spike-jet combination alternatives based on this survey.

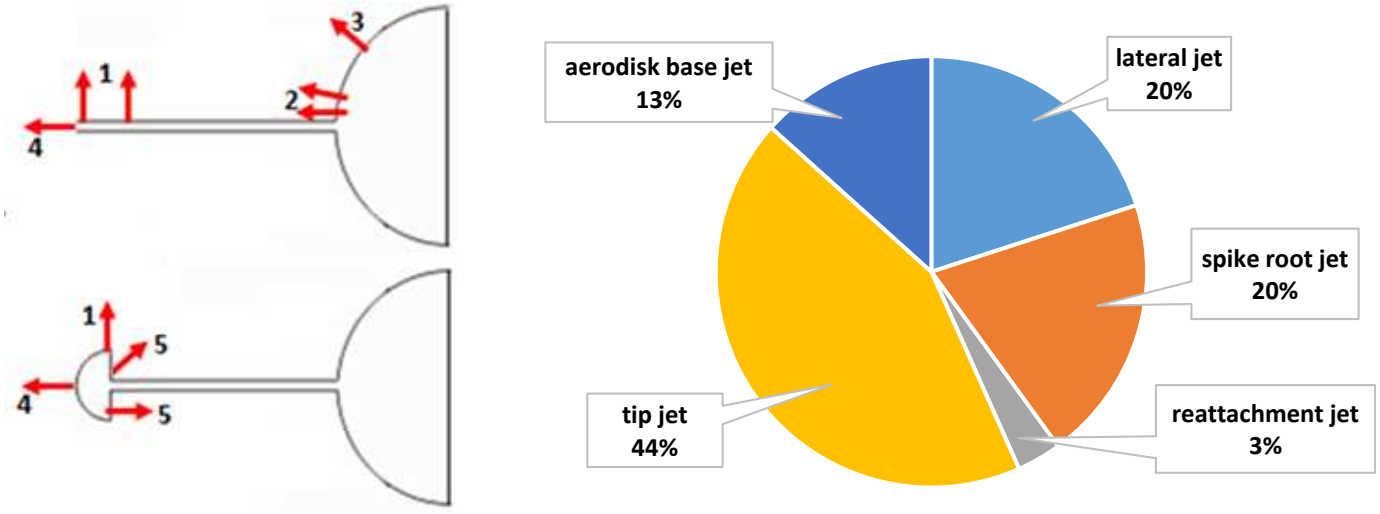


1: lateral jet, 2: spike root jet, 3: reattachment jet, 4: tip jet, 5: aerodisk base jet

**Figure 8 Different jet locations and proposed terminologies for hybrid spike-jet devices**

To assess Wood's intuition [36], Hahn conducted the first experimental study on this hybrid device [305]. Jets at three different locations of the spiked model were examined namely, lateral jet at the spike tip, root jet, and reattachment jet. Hahn concluded that root and reattachment jets of low flow rates would stabilize the flow. In contrast, lateral jet of all flow rates and root and reattachment jets of high rates destabilized the flow. Root jet at high flow rates shifted the reattachment point downstream and had the effect of reducing the peak aeroheating at this spot. For all other jets cases, aeroheating would rise due to increase in flow effective Reynolds number.

More than forty years later, the concept was revisited in the experimental work by Jiang et al. [118]. A lateral jet of air added at the spike tip was believed to broaden the range of incidence angles within which the spike will be effective in reducing the drag. By pushing the shear layer laterally away from the spike, the lateral jet significantly reduced the reattachment pressure yielding a better drag reduction. Jiang et al. confirmed their findings numerically and proved that lateral spike further enhanced the aeroheating reduction capabilities of the plain spike [304, 306]. They recently confirmed that the favorable role of adding the lateral jet diminishes for longer spikes and that freestream Mach number has insignificant impact on the hybrid device effectiveness [307]. Zhu et al. [308] extended the investigation on lateral jet; focus was on understanding the impact of lateral jet pressure and axial location on

the spike. They concluded that the closer is the lateral jet to the spike tip the more drag and aeroheating reduction is attained. In addition, increasing the jet pressure was found to enhance the device function regardless to the jet location. Maximum reduction is achieved at an optimum combination of spike length and lateral jet location.

Independent of Jiang et al., the research group of Aso [188] followed a different approach leading to a similar device. In their experiments on conventional opposing jet device, they found that extending the nozzle outside the forebody surface enhanced thermal protection capabilities of the opposing jet. Despite that it was not intended, their concept acts as a hybrid spike-jet device with the jet at the spike tip. They confirmed their findings numerically [309, 310] and concluded that a longer nozzle (spike) and higher jet pressure yield more drag and aeroheating reduction. In [311], they applied the same concept on a reentry capsule model. The same work was replicated numerically by Qu et al. [312] whereas Pish et al. [313] reported the same conclusions in their numerical study on different jet settings. Contradicting conclusions were reported by Huang et al. [314] in their numerical simulation studies. By varying the spike length and tip jet pressure ratio, a maximum drag reduction was not achieved by maximizing both spike length and jet pressure. Eghlima et al. [315, 316] supported the conclusions of [314]. By increasing the pressure ratio of the tip jet after an optimum value, asymptotic trends in drag and aeroheating reduction are attained. Drag and aeroheating to the forebody would even increase for higher jet pressures.

Adding a jet at the tip of an aerodisk rather than the tip of a plain spike was proposed by Ou et al. [317, 318]. Different jet pressures and radial locations on the base of forward and intermediate aerodisks along the spike were examined. The aerodisk tip jet was found to further enhance the aerodisk function. Jet pressure and size were confirmed to dominate the role of aerodisk in the conventional mechanical spike device. Similarly, Qin et al. [319] compared lateral, tip, and oblique base jets emanating from a hemispherical aerodisk at the tip of a spike attached to a hemispherical model. While a lateral jet was more beneficial for aeroheating reduction, oblique jet from the aerodisk base yielded more drag reduction. In contrast, Mosavat et al. [320] argued that a tip jet yielded more aeroheating reduction compared with lateral and base jets.

Spike root jet was examined by Gerdoorbary et al. [321-323]. They claimed that root jet enhanced the aeroheating reduction capabilities of a spike. Increasing the jet pressure was claimed to further reduce both reattachment pressure and heat flux. At high jet pressures, aeroheating reduction was argued to diminish. In addition to the apparent flow unsteadiness in the flow, the studies did not examine this key issue. Impact of root jet on drag was also overlooked in this studies. Huang et al. [324, 325] argued that increasing both spike length and root jet pressure enhanced the drag and aeroheating reduction capabilities; flow unsteadiness was not reported. Aerodisk base jet acts similar to the spike root jet is the sense that they both inject into the recirculation zone around the spike/aerodisk. Qin and Xu recently examined aerodisk base jet in a numerical study [326, 327] and concluded that a jet with higher pressure yielded more aeroheating reduction with a more drag penalty. An optimum radial location of the jet was addressed. Possible flow unsteadiness was overlooked in the reported findings. The studies on hybrid structural-fluidic devices are summarized in Table A4 in the Appendix.

***Comments on structural-fluidic devices:*** Previous research has shown that adding a jet to the mechanical spike is indeed beneficial. In addition to further modifying the flowfield in the favorable manner, tip and lateral jets can act to reduce thermal loads on the spike/aerodisk tip [306, 327]. By this augmentation, a jet can compensate short spikes while a spike can compensate low pressure jets [309]. Nonetheless, the benefits of the hybrid device diminish for longer spikes, higher jet pressures, and flow rate [307, 321, 328]. As for practical implementation of this hybrid device, the same concerns of the conventional opposing jet can be raised namely, space and power demands and source of jet. In addition, drop in total pressure of jet can be expected as it is pushed and redirected through the highly slender spike. This should be addressed in future studies. Indeed, using high temperature/plasma jets will have a negative impact on the mechanical and structural features of the mechanical spike. Lateral jet demands can be significantly lower than those of spike/aerodisk tip jets. This is because a lateral jet is directed towards zones with much lower pressure. Hence, for a given effect, lateral jets require much lower pressure and mass flow rates than tip jets with no thrust penalty [328]. It was even suggested that evaporating water (used as a spike coolant) can be

adequate as a source for lateral jet [306]. The main concern with lateral jets is their impact on vehicle flight stability at incidence. A lateral jet that is directed towards the windward side of a spiked vehicle at incidence is expected to generate a destabilizing moment that may impact vehicle stability. This topic invokes further investigation. Aerodisk base and spike root jets also require much lower pressure and flow rate demands. However, further assessment should be made to their capabilities in reducing both drag and aeroheating while maintaining a stable flight.

The studies on hybrid spike-jet device are too recent to properly assess its utility. In addition, concerns can be raised regarding the credibility of some reported conclusions in the numerical simulation studies so far. Due to the lack of experimental database, some simulation studies used experiments on isolated spikes, conventional opposing jets, or even plain blunt forebodies [314-317, 328] to validate simulation techniques. Other simulation studies did not include any validation with experiments at all [313, 314, 323, 324, 329]. Hence, more experiments on this hybrid device must be conducted. Studies with more profound flow physics analyses and their connection with device effectiveness are also needed.

### 5.2. Structural-Energetic devices

A hybrid device composed of a mechanical spike and an energy source is based on the idea of augmenting the mechanical spike capabilities with the benefits of heat addition. It is interesting to note here that such device was experimented well before the establishment of mechanical spike and energy devices. Fomin et al. [330] mentioned unpublished experiments back to 1914 in which drag on blunted projectiles was reduced due to head addition (by burning) at a mechanical spike tip. However, the first reported study on this approach was conducted by Maurer and Brungs [331] in 1968. Their idea was to gain more drag reduction by adding thermal energy (external burning of hydrogen) at the tip of a spike/ aerodisk fitted to a hemispherical forebody. The same approach was later revisited by Reding and Jecmen [332, 333]. They experimentally examined spiked hemispherical and blunt ogive forebodies in Mach 2.2 freestream. Burning hydrogen injected from lateral orifices in the aerodisk at the tip of the spike was found to totally eliminate the reattachment shock and to further enhance the effectiveness of the mechanical spike device. Their experiments were reproduced numerically by Srinivasan and Chamberlain [334]. Additional 10% reduction in drag was reported. Similar experiments were performed by Golovitchev et al. [335] and Iwakawa et al. [336].

In the researches above, energy is added to the mechanical spike in the form of thermal energy attained through burning. The set of experiments by Kuo et al. [255, 273] can be considered as another approach for structural-energetic devices in which electric discharge is the source of thermal energy. In these experiments, a pointed spike protruding from a flat truncated conical forebody was examined. The spike acted as one of the electrodes while the forebody acted as the other one. By involving both the spike and the forebody, the resulting self-contained hybrid device was argued to enhance the drag reduction capabilities of the spike.

***Comments on structural-energetic devices:*** The researches on this type of forebody shock control devices are clearly sparse and invoke more studies. In fact, this type of devices poses efficient implementation of energy sources compared with pure energetic devices. In addition, the use of energy, even with low amplitude, can compensate shorter spikes and add controllability feature to spike's operation. The negative impact on aeroheating capabilities of spikes due to heat addition and should be considered in future studies. Heating to the spike tip itself should also be addressed.

## 6. Existing practical applications for forebody shock control devices:

In this section of the survey, existing supersonic and hypersonic vehicles that utilize shock control devices in concern are explored. Most of the technical specifications data of these systems are classified. However, the authors did their best to confirm (and accurately predict) these data based on conference/ journal articles and governmental websites. Some of the practical applications are shown in Fig.9. To the authors' best knowledge in the open literature, mechanical spikes are the sole drag and aeroheating device that has been successfully implemented in real systems. Other devices included in the survey were not used in any real system.

Trident I (C-4) and Trident II (D-5) are submarine-launched ballistic missiles that can reach maximum ranges of about 7400 km and 12000 km, respectively, following a vertical launch ballistic trajectory. Their forebodies have the shape of blunt ogives and are both equipped with a telescopic aerodisk that is normally retracted fully inside the forebody before launch. After exiting water into air, the aerodisk is extended and locked under gas pressure from a solid propellant gas generator contained within the forebody. The fully extended aerospike is 2/3 and 1 caliber long in C-4 and D-5, respectively, whereas the diameter of the flat aerodisk at its tip is 0.15 caliber in both models. It is reported that the aerodisk yields a 50% drag reduction during the atmospheric boost phase of these multi-stage missiles by the end of which the flight Mach number is believed to reach up to Mach 25 [6, 25, 337, 338].

Igla (NATO: SA-18) and Igla-1 (NATO: SA-16) are man-portable, tube-launched short-range anti-aircraft missiles. They follow an atmospheric direct flight trajectory towards targets flying at altitudes up to 3.5 km. Forebodies of both missiles are highly blunt to accommodate infra-red seekers. To reduce drag, Igla missile is equipped with a fixed rounded-tip spike that is 1-calibre long. In contrast, Igla-1 is equipped with a tripod-mounted conical aerodisk; no spike stem is used to clear the forebody nose area. Igla and Igal-1 can reach speeds of Mach 2.4 and 1.7, respectively [339]. SB-735 is a small rocket that is used as a wrap-around booster for the Mu-3S-II space launch vehicle. Drag on booster rocket during ascent phase is reduced using a spike with blunt aerodisk that is about 1 caliber long. In the same domain, the escape rocket of Saturn launch vehicle family was reported to act as a spike for the main vehicle [6, 340]. The escape rocket is responsible for the emergency escape of the crew compartment located at the top of the launch vehicle. It represents a conical-tipped spike that is about 1 caliber long.

M490A1 is a spin-stabilized anti-tank projectile which muzzle (maximum) velocity can reach Mach 3.4. The projectile itself has a flat-ended cylinder equipped with a flat-tipped spike that is 1.5 caliber long. The spike contains an impact sensor at its tip to enhance the lethality of the round. A tripping ring placed behind the spike tip was found to enhance the drag reduction capabilities of the spike [22, 121]. A different application for mechanical spikes in real systems is the Quiet spike concept. It is an extensible spike that was successfully tested to minimize the sonic boom ground signature of supersonic civil aircraft [21, 341] . Figure 9 shows a gallery of real systems implementing mechanical spikes.

(a) D-5 (left) and C-4 [342]

(b) Saturn launch vehicle [343]

(c) M490A1 projectile [344]


(d) Igla missiles [339]

(e) Quiet spike [345]

**Figure 9 Gallery of real systems implementing mechanical spike devices (figures are not to scale)**

## 7. Conclusions and Recommendations

Developing forebody shock control devices to reduce drag and aeroheating to supersonic/ hypersonic vehicles has attracted researchers for more than a century. These devices are categorized into mechanical devices (spikes), fluidic devices (opposing jets), and energy deposition devices. Mechanical devices are structural spikes protruding upstream at the stagnation zone of the vehicle forebody. In fluidic devices, a high-speed jet is ejected upstream ahead of the carrier forebody while in energy deposition devices, energy (commonly, laser or electric) is focused at a distance upstream of the vehicle. Combinations of these devices (i.e., hybrid devices) were also developed. Despite their apparent diversity, these devices operate on the same fundamental principle, namely, creating an effective body that is more aero-thermal friendly than the carrier vehicle. The incoming high speed flow adapts to the new effective body and establishes a shock system that is much weaker than that encountered by the "unprotected" carrier vehicle. In addition to having a common principle, these devices are similar in being most beneficial for blunt forebodies flying in a dense atmosphere with hypersonic speeds. These various shock control devices however, differ according to design simplicity and efficiency, operation flexibility, and function stability.

In terms of design simplicity, mechanical spike devices are advantageous over fluidic and energy devices. Design simplicity implies ease of manufacture, operation, maintenance, and regulation as well as high reliability. Moreover, mechanical spikes involve the minimum number of parameters that control their operation namely, length of spike and size of aerodisk at its tip. In contrast, fluidic and energy systems are more complicated in design since. Storing, driving, and controlling the operating fluid in fluidic devices pose the main challenges in the real implementations. Similarly, securing the power needed for operating energy deposition devices is also a challenging aspect. Both fluidic and energy devices involve a larger number of parameters that control their operation. Fluidic device parameters include fluid thermodynamic properties, jet pressure and speed, and orifice design. Energy deposition devices involve even more tuning parameters that control their operation. The impact of adding these devices on subsystems onboard the vehicle forebody is an important aspect. While mechanical spike devices may interfere with onboard optical sensors, fluidic devices may occupy more internal space. Energy devices may have negative impact on onboard electronic devices.

In terms of efficiency, mechanical spike devices have "theoretically" infinite efficiency since they require no driving power to operate and the gained drag and aeroheating reductions are attained with no power cost. In contrast, cost effectiveness of fluidic and energy devices needs more improvement. The gained drag and aeroheating reduction upon using these devices should justify (with acceptable efficiency) the power needed to operate them. Excessive jet pressure may yield more drag (opposite thrust) rather than less drag. In addition, energy deposition devices may have negative impact on aeroheating to the vehicle forebody. As a consequence of their simplicity and efficiency, mechanical devices have found applications in real existing systems. Fluidic and energy devices are not implemented in any real system and their validity remains within the laboratory experimental domain.

In terms of flexibility and robustness of operation, energy deposition devices are advantageous over fluidic and mechanical spike devices since energy can be focused at any arbitrary location ahead of the vehicle. Hence, the shape of the effective body can be more easily tailored using energy devices. Energy devices can be theoretically used at any arbitrary values of flight speed and incidence angle and can be adapted easily to changes in operating

conditions. Fluidic devices yield less operation flexibility. The produced jet can be directed within a more limited range around the vehicle depending on the jet pressure and injection angle. The jet length and direction can be adapted to the vehicle flight speed and incidence angle. However, increasing the jet pressure yields a longer jet to a given maximum followed by a sudden drop in jet length. With mechanical spikes, the form of the effective body is constrained to the length of the spike; telescopic spikes of variable length can be a solution to cope with variable vehicle speed. Extendable spikes of fixed length are already implemented in real systems. Spike also operate best at zero or very small incidence angles; pivoting spikes can be used at higher incidence. Both variable-length and pivoting spikes have more complicated designs and sophisticated operation.

In terms of operation stability, the flow around the vehicle forebody can be unstable using either of the shock control devices which invokes operation instability. Mechanical spike devices encounter flow instability at certain combinations of spike length, forebody shape, and flight speed. The opposing fluidic jet generates flow instability if it is used in long penetration mode. Pulsating rather than continuous energy deposition devices are more efficient however, they trigger flow instability. Flow instability can yield irregularity in operation that may cause flight disturbances and uncertainties in flight path prediction.

The present survey addresses some existing gaps in knowledge for future researchers to work on. These gabs are illustrated throughout and the key ones are addressed here. Transients witnessed by all types of shock control devices during their operation invoke deeper analysis. These transients include turning on and off, protruding spikes, changing opposing jet pressure, and variation of flight conditions in real (maneuvering, accelerating, ascent, descent) flight cases. Comparative studies on the different and hybrid devices can also be conducted especially on their cost effectiveness and efficiency. Numerical simulation studies taking into consideration boundary layer transition and flow asymmetry are suggested. Developing mathematical models specific for energy deposition physics is also encouraged as well as coupling aerodynamics, flight mechanics, and structural mechanics (for spikes) in multi-disciplinary studies. More effort should be made to develop onboard fluidic and energy deposition devices that can function efficiently with minimum interference to other subsystems.

***Acknowledgements***

Funding from Egyptian Government to the first author for his visiting scholarship at the Department of Mechanical Engineering of the University of Sheffield.

## References

[1] Weiland C, Hirschel E. Selected Aerothermodynamic Design Problems of Hypersonic Flight Vehicles: AIAA, ISBN: 9783540899747; 2015.

[2] Bogdonoff SM, Vas IE. Preliminary Investigations of Spiked Bodies at Hypersonic Speeds. Journal of the Aerospace Sciences. 1959;26:65-74, https://arc.aiaa.org/doi/pdf/10.2514/8.7945.

[3] Menezes V, Saravanan S, Reddy KPJ. Shock tunnel study of spiked aerodynamic bodies flying at hypersonic Mach numbers. Shock Waves. 2002;12:197-204, https://doi.org/10.1007/s00193-002-0160-3.

[4] Shoemaker J. Aerodynamic Spike Flowfields Computed to Select Optimum Configuration at Mach 2.5 with Experimental Validation. 28th Aerospace Sciences Meeting. Reno, NV, USA, https://doi.org/10.2514/6.1990-4141990.

[5] Gauer M, Paull A. Numerical Investigation of a Spiked Blunt Nose Cone at Hypersonic Speeds. Journal of Spacecraft and Rockets. 2008;45:459-71, https://doi.org/10.2514/1.30590.

[6] Reding JP, Guenther RA, Richter BJ. Unsteady Aerodynamic Considerations in the Design of a Drag-Reduction Spike. Journal of Spacecraft and Rockets. 1977;14:54-60, https://doi.org/10.2514/3.57160.

[7] Early Look: This aircraft concept shows a hypersonic vehicle for passengers. https://wwwboeingcom/features/2018/06/hypersonic-concept-vehiclepage: Boeing.

[8] Lockheed Martin X-33. https://wwwnasagov/. p. https://www.nasa.gov/centers/armstrong/history/experimental_aircraft/X-33.html.
[9] Hypersonic Missions. p. https://www.grc.nasa.gov/WWW/BGH/hmission.html.
[10] Huebner LM, Anthony; Boudreaux, Ellis. Experimental results on the feasibility of an aerospike for hypersonic missiles. 33rd Aerospace Sciences Meeting and Exhibit. Reno, NV, USA, https://doi.org/10.2514/6.1995-7371995.
[11] Ahmed MYM, Qin N. Recent advances in the aerothermodynamics of spiked hypersonic vehicles. Progress in Aerospace Sciences. 2011;47:425-49, https://doi.org/10.1016/j.paerosci.2011.06.001.
[12] Huang W. A survey of drag and heat reduction in supersonic flows by a counterflowing jet and its combinations. Journal of Zhejiang University-Science A. 2015;16:551-61, https://doi.org/10.1631/jzus.A1500021.
[13] Wang ZG, Sun XW, Huang W, Li SB, Yan L. Experimental investigation on drag and heat flux reduction in supersonic/hypersonic flows: A survey. Acta Astronautica. 2016;129:95-110, https://doi.org/10.1016/j.actaastro.2016.09.004.
[14] Sun X, Huang W, Ou M, Zhang R, Li S. A survey on numerical simulations of drag and heat reduction mechanism in supersonic/hypersonic flows. Chinese Journal of Aeronautics. 2019;32:771-84, https://doi.org/10.1016/j.cja.2018.12.024.
[15] Huang W, Chen Z, Yan L, Yan Bb, Du Zb. Drag and heat flux reduction mechanism induced by the spike and its combinations in supersonic flows: A review. Progress in Aerospace Sciences. 2019;105:31-9, https://doi.org/10.1016/j.paerosci.2018.12.001.
[16] Karimi MS, Oboodi MJ. Investigation and recent developments in aerodynamic heating and drag reduction for hypersonic flows. Heat and Mass Transfer. 2019;55:547-69, https://doi.org/10.1007/s00231-018-2416-1.
[17] Album HH. Regarding the Utility of Spiked Blunt Bodies. Journal of Spacecraft. 1968;5:112-3, https://doi.org/10.2514/3.29195.
[18] Alexander SR. NACA RM L6K08a: Results of Tests to Determine the Effect of a Conical Windshield on the Drag of a Bluff Body at Supersonic Speeds. 1947, https://ntrs.nasa.gov/archive/nasa/casi.ntrs.nasa.gov/19930085627.pdf.
[19] Piland RO, Putland LW. NACA RM L54A27: Zero-Lift Drag of Several Conical and Blunt Nose Shapes Obtained in Free Flight at Mach number of 0.7 to 1.3. 1957, https://ntrs.nasa.gov/archive/nasa/casi.ntrs.nasa.gov/19930089303.pdf.
[20] McGhee RJ, Staylor WF. NASA TN D-5201: Aerodynamic Investigation of Sharp Cone-Cylinder Spikes on 120o Blunted Cones at Mach Numbers of 3, 4.5, and 6. 1969, https://ntrs.nasa.gov/archive/nasa/casi.ntrs.nasa.gov/19690019776.pdf.
[21] Howe D. Improved Sonic Boom Minimization with Extendable Nose Spike. 43rd AIAA Aerospace Sciences Meeting and Exhibit. Reno, NV, USA, https://doi.org/10.2514/6.2005-10142005.
[22] Mikhail AG. Spike-nosed projectiles: Computations and dual flow modes in supersonic flight. Journal of Spacecraft and Rockets. 1991;28:418-24, https://doi.org/10.2514/3.26261.
[23] Kobayashi H, Maru Y, Fukiba K. Experimental Study on Aerodynamic Characteristics of Telescopic Aerospikes with Multiple Disks. Journal of Spacecraft and Rockets. 2007;44:33-41, https://doi.org/10.2514/1.25250.
[24] Khlebnikov VS. Distribution of Heat Flux on the Surface of a Sphere with a Forward Separation Zone. Fluid Dynamics. 1986;21:654-8, https://doi.org/10.1007/BF01057155.
[25] Guenther RA, Reding JP. Fluctuating Pressure Environment of a Drag Reduction Spike. Journal of Spacecraft and Rockets. 1977;14:705-10, https://doi.org/10.2514/3.57253.
[26] Kalimuthu R, Mehta RC, Rathakrishnan E. Experimental Investigation on Spiked Body in Hypersonic Flow. The Aeronautical Journal. 2008;112:593- 8, https://doi.org/10.1017/S0001924000002554.
[27] Motoyama N, Mihara K, Miyajima R, Watanuki T, Kubota H. Thermal Protection and Drag Reduction with Use of Spike in Hypersonic Flow. A01-28042 AIAA/NAL-NASDA-ISAS 10th International Space Planes and Hypersonic Systems and Technologies Conference Kyoto, Japan, https://doi.org/10.2514/6.2001-182820001.
[28] Yadav R, Bodavula A, Joshi S. Numerical investigation of the effect of disk position on the aerodynamic heating and drag of a spiked blunt body in hypersonic flow. The Aeronautical Journal. 2018;122:1916-42, https://doi.org/10.017/aer.2018.109.

[29] Zhong K, Yan C, Chen Ss, Zhang Tx, Lou S. Aerodisk effects on drag reduction for hypersonic blunt body with an ellipsoid nose. Aerospace Science and Technology. 2019;86:599-612, https://doi.org/10.1016/j.ast.2019.01.027.
[30] Ahmed MYM, Qin N. Numerical Investigation of Aeroheating Characteristics of Spiked Blunt Bodies at Mach 6 Flight Conditions. The Aeronautical Journal. 2011;115:377-86, https://doi.org/10.1017/S0001924000005893.
[31] Ahmed MYM, Qin N. Drag Reduction Using Aerodisks for Hypersonic Hemispherical Bodies. Journal of Spacecraft and Rockets. 2010;47:62-80, https://doi.org/10.2514/1.46655.
[32] Yamauchi M, Fujii K, Higashino F. Numerical investigation of supersonic flows around a spiked blunt body. Journal of Spacecraft and Rockets. 1995;32:32-42, https://doi.org/10.2514/3.26571.
[33] Holden MS. Experimental studies of separated flows at hypersonic speeds. II - Two-dimensional wedge separated flow studies. AIAA Journal. 1966;4:790-9, https://doi.org/10.2514/3.3548.
[34] Qin Q, Xu J, Guo S. Fluid-thermal analysis of aerodynamic heating over spiked blunt body configurations. Acta Astronautica. 2017;132:230-42, https://doi.org/10.1016/j.actaastro.2016.12.037.
[35] Jones J. NACA RM L52E05a: Flow Separation from Rods Ahead of Blunt Noses at Mach Number 2.7. 1952, https://ntrs.nasa.gov/archive/nasa/casi.ntrs.nasa.gov/19930087040.pdf.
[36] Wood CJ. Hypersonic Flow over Spiked Cones. Journal of Fluid Mechanics. 1961;12:https://doi.org/10.1017/S0022112062000427.
[37] Kabelitz H. Zur Stabilität Geschlossener Greznschichtablösegebeite an Konischen Drehkörpern bei. 1971.
[38] Crawford DH. NASA TN D-118: Investigation of The Flow over a Spiked-Nose Hemisphere-Cylinder. 1959.
[39] Mehta RC. Numerical analysis of pressure oscillations over axisymmetric spiked blunt bodies at Mach 6.8. Shock Waves. 2002;11:431-40, https://doi.org/10.1007/s001930200127.
[40] Kenworthy M. A Study of Unsteady Axisymmetric Separation in High Speed Flows: Dept. of Aerospace and Ocean Engineering, Virginia Polytechnic Institute And State University; 1978.
[41] Calarese W, Hankey WL. Modes of shock-wave oscillations on spike-tipped bodies. AIAA Journal. 1985;23:185-92, https://doi.org/10.2514/3.8893.
[42] Ahmed MYM, Qin N. Investigation of flow asymmetry around axi-symmetric spiked blunt bodies in hypersonic speeds. The Aeronautical Journal. 2014;118:169-79, https://doi.org/10.1017/S0001924000009052.
[43] Xue Y, Wang L, Fu S. Detached-eddy simulation of supersonic flow past a spike-tipped blunt nose. Chinese Journal of Aeronautics. 2018;31:1815-21, https://doi.org/10.016/j.cja.2018.06.016.
[44] Hermach CA, Kraus S, Reller JO. NACA RM A56L05: Reduction in Temperature-Recovery Factor Associated with Pulsating Flows Generated by Spike-Nosed Cylinders at a Mach Number of 3.50. 1957.
[45] Panaras AG. Pulsating Flows about Axisymmetric Concave Bodies. AIAA Journal. 1981;19:804-6, https://doi.org/10.2514/3.7816.
[46] Menezes V, Saravanan S, Jagadeesh G, Reddy KPJ. Experimental Investigations of Hypersonic Flow over Highly Blunted Cones with Aerospikes. AIAA Journal. 2003;41:1955-66, https://doi.org/10.2514/2.1885.
[47] Kurbatskii KA, Montanari F. Application of Pressure-Based Coupled Solver to the Problem of Hypersonic Missiles with Aerospikes. 45th AIAA Aerospace Sciences Meeting and Exhibit. Reno, NV, USA, https://doi.org/10.2514/6.2007-4622007.
[48] Kalimuthu R, Mehta RC, Rathakrishnan E. Drag Reduction for Spike Attached to Blunt-Nosed Body at Mach 6. Journal of Spacecraft and Rockets.47:219-22, https://doi.org/10.2514/1.46023.
[49] Gnemmi P, Srulijes J, Roussel K, Runne K. Flowfield Around Spike-Tipped Bodies for High Attack Angles at Mach 4.5. Journal of Spacecraft and Rockets. 2003;40:622-31, https://doi.org/10.2514/2.6910.
[50] Milicev SS, Pavlovic MD. Influence of Spike Shape at Supersonic Flow Past Blunt-Nosed Bodies: Experimental Study. AIAA Journal. 2001;40:1018- 20, https://doi.org/10.2514/2.1745.
[51] Khurana S, Suzuki K. Application of Aerospikes for Lifting-Body Configuration in Hypersonic Flow at Mach 7. 43rd Fluid Dynamics Conference. San Diego, CA, USA, https://doi.org/10.2514/6.2013-31132013.
[52] Deng F, Xie F, Qin N, Huang W, Wang L, Chu H. Drag reduction investigation for hypersonic lifting-body vehicles with aerospike and long penetration mode counterflowing jet. Aerospace Science and Technology. 2018;76:361–73, https://doi.org/10.1016/j.ast.2018.01.039.
[53] Hutt GR, Howe AJ. Forward facing spike effects on bodies of different cross section in supersonic flow. Aeronautical Journal. 1989;93:229-34, https://doi.org/10.1017/S0001924000017085.

[54] Stalder JR, Nielsen HV. NACA TN 3287: Heat Transfer from a Hemisphere Cylinder Equipped with Flow Separation Spikes. 1954.
[55] Wagner RD, Pine WC, Henderson A. NASA TN D-891: Laminar Heat Transfer and Pressure Distribution Studies on a Series on Re-Entry Nose Shapes at a Mach Number of 19.4 in Helium. 1961.
[56] Karlovskii VN, Sakharov VI. Numerical Investigation of Supersonic Flow past Blunt Bodies with Protruding Spikes. Fluid Dynamics. 1986;21:437- 45, https://doi.org/10.1007/BF01409731.
[57] Zorea C, Rom J. Effect of a Spike on the Drag and on the Aerodynamic Stability of Blunt Bodies in Supersonic Flow. Journal of Spacecraft and Rockets. 1970;7:1017-9, https://doi.org/10.2514/3.30094.
[58] Huang W, Li Lq, Yan L, Zhang Tt. Drag and heat flux reduction mechanism of blunted cone with aerodisks. Acta Astronautica. 2017;138:168-75, https://doi.org/10.1016/j.actaastro.2017.05.040.
[59] Jones JJ. NACA RM L55E10: Experimental Drag Coefficients of Round Noses with Conical Windshields at Mach Number 2.72. 1955.
[60] Ahmed MYM, Qin N. Metamodels for aerothermodynamic design optimization of hypersonic spiked blunt bodies. Aerospace Science and Technology. 2010;14:364-76, https://doi.org/10.1016/j.ast.2010.03.003.
[61] Gerdroodbary MB, Hosseinalipour SM. Numerical simulation of hypersonic flow over highly blunted cones with spike. Acta Astronautica. 2010;67:180-93, https://doi.org/10.1016/j.actaastro.2010.01.026.
[62] Xue Y, Wang L, Fu S. Drag Reduction and Aerodynamic Shape Optimization for Spike-Tipped Supersonic Blunt Nose. Joural of Spacecraft and Rockets. 2018;55.
[63] Qin Q, Xu J. Role of aerodome in pulsation/oscillation control and aeroheating reduction. Acta Astronautica. 2019;162:481-96, https://doi.org/10.1016/j.actaastro.2019.05.030.
[64] Milićev SS, Pavlović MD, Ristić S, Vitić A. On the Influence of Spike Shape at Supersonic Flow past Blunt Bodies. Facta universitatis - series: Mechanics, Automatic Control and Robotics. 2002;3:371-82.
[65] Sahoo D, Das S, Kumar P, Prasad JK. Effect of spike on steady and unsteady flow over a blunt body at supersonic speed. Acta Astronautica. 2016;128:521-33, https://doi.org/10.1016/j.actaastro.2016.08.005.
[66] Sahoo D, Das S, Cohen J. Effect of Body Nose Fairing on the Unsteady Flow Characteristics over Spiked Flat Faced Cylinder at Supersonic Speed. AIAA Scitech 2019 Forum. San Diego, CA, USA, https://doi.org/10.2514/6.2019-23162019.
[67] Antonov AN, Gretsov VK. Unsteady separated supersonic flow over pointed and spiked bodies. Fluid Dynamics. 1974;9:578-82, https://doi.org/10.1007/BF01031316.
[68] Mohandas S, Siddharth RK, John B. Reduction of Wave Drag on Parameterized Blunt Bodies using Spikes with Varied Tip Geometries. Acta Astronautica. 2019;160:25-35, https://doi.org/10.1016/j.actaastro.2019.04.017.
[69] Ahmed MYM, Qin N. Surrogate-Based Multi-Objective Aerothermodynamic Design Optimization of Hypersonic Spiked Bodies. AIAA Journal. 2012;50:797-810, https://doi.org/10.2514/1.J051018.
[70] Moeckel WE. NACA RM E51I25: Flow Separation Ahead of a Blunt Axially Symmetric Body at Mach Numbers 1.76 to 2.10. 1951.
[71] Mair WA. Experiments on Separation of Boundary Layers on Probes in front of Blunt-Nosed Bodies in a Supersonic Air Stream. Philosophical Magazine. 1952;43:695- 716, https://doi.org/10.1080/14786440708520987
[72] Myshenkov VN. Numerical Investigation of Separated Flow in front of a Spiked Cylinder. Fluid Dynamics. 1981;16:938- 42, https://doi.org/10.1007/BF01089728.
[73] Paskonov VM, Cheraneva NA. Numerical investigation of laminar separation in the case of supersonic flow of viscous gas past spiked bodies. Fluid Dynamics. 1984;19:281-5, https://doi.org/10.1007/BF01091252.
[74] Antonov AN, Gretsov VK. Experimental investigation of the characteristics of unsteady-state breakaway zones arising in a supersonic flow at a needle with a screen. Fluid Dynamics. 1977;12:567-72, https://doi.org/10.1007/BF01089676.
[75] Antonov AN, Shalaev SP. Nonstationary Separation on Spiked Bodies. Fluid Dynamics. 1979;14:71-6, https://doi.org/10.1007/BF01050816.
[76] Antonov AN, Gretsov VK, Shalaev SP. Nonsteady supersonic flow over spiked bodies. Fluid Dynamics. 1976;11:746-51, https://doi.org/10.1007/BF01012969.

[77] Jagadeesh G, Viren M, Reddy K, Hashimoto T, Sun M, Takayama K. Hypersonic Buzz Phenomenon on the Spiked Blunt Cones. 41st Aerospace Sciences Meeting and Exhibit. Reno, NV, USA, https://doi.org/10.2514/6.2003-2842003.
[78] Kulkarni V, S. KP, J. RKP. Drag Reduction by a Forward Facing Aerospike for a Large Angle Blunt Cone in High Enthalpy Flows. Shock Waves. 2007:566- 70, https://doi.org/10.1007/978-3-540-85168-4_90.
[79] Mehta RC. Numerical Heat Transfer Study over Spiked Blunt Bodies at Mach 6.8. Journal of Spacecraft and Rockets. 2000;37:700- 3, https://doi.org/10.2514/2.3622.
[80] Mehta RC. Peak heating for reattachment of separated flow on a spiked blunt-body. Heat and Mass Transfer. 2000;36:277-83, https://doi.org/10.1007/s002310000091.
[81] Mehta R. Flow Field Computations Over Conical, Disc and Flat Spiked Body at Mach 6. 47th AIAA Aerospace Sciences Meeting including The New Horizons Forum and Aerospace Exposition. Orlando, FL, USA, https://doi.org/10.2514/6.2009-3252009.
[82] Kalimuthu R, Rathakrishnan E. Aerospike for Drag Reduction in Hypersonic Flow. 44th AIAA/ASME/SAE/ASEE Joint Propulsion Conference & Exhibit. Hartford, CT, USA, https://doi.org/10.2514/6.2008-47072008.
[83] Mehta R. Heat Transfer Analysis over Disc and Hemispherical Spike Attached to Blunt-Nosed Body at Mach 6. 17th AIAA International Space Planes and Hypersonic Systems and Technologies Conference. San Francisco, CA, USA, https://doi.org/10.2514/6.2011-22282011.
[84] Mehta RC. Numerical heat transfer study around a spiked blunt-nose body at Mach 6. Heat and Mass Transfer/Waerme- und Stoffuebertragung. 2013;49:485-96, https://doi.org/10.1007/s00231-012-1095-6.
[85] Kalimuthu R, Mehta RC, Rathakrishnan E. Investigation of aerodynamic coefficients at Mach 6 over conical, hemispherical and flat-face spiked body. The Aeronautical Journal. 2017;121:1711-32, https://doi.org/10.017/aer.2017.100.
[86] Mehta RC. Heat Transfer Analysis without and with Forward Facing Spike Attached to a Blunt Body at High Speed Flow. In: Volkov K, editor. Heat Transfer - Models, Methods and Applications: IntechOpen; 2018. p. 175-98, http://dx.doi.org/10.5772/intechopen.74522.
[87] Deng F, Jiao Z, Liang B, Xie F, Qin N. Spike Effects on Drag Reduction for Hypersonic Lifting Body. Journal of Spacecraft and Rockets. 2017;54:1185-95, https://doi.org/10.2514/1.A33865.
[88] Maull DJ. Hypersonic flow over axially symmetric spiked bodies. Journal of Fluid Mechanics. 1960;8:584-92, https://doi.org/10.1017/S0022112060000815.
[89] Panaras AG. High Speed Unsteady Separation about Concave Bodies- A Physical Expanation. Von Karman Institute for Fluid Dynamics 1977.
[90] Zapryagaev VI, G. MS. Features of Separated Supersonic Flow Pulsations Ahead of a Spike-Tipped Cylinder. Journal of Applied Mechanics and Technical Physics. 1991;32:913-9, https://doi.org/10.1007/BF00850639.
[91] Zapryagaev VI, Kavun IN. Experimental Study of the Reverse Flow in the Forward Separation Region in a Pulsating Flow around a Spiked Body. Journal of Applied Mechanics And Technical Physics. 2007;48:492–500, https://doi.org/10.1007/s10808-007-0062-3.
[92] Shang JS, Hankey WL. Flow Oscillations on Spiked Tipped Bodies. AIAA Journal. 1982;20:25-6, https://doi.org/10.2514/2.1769.
[93] Feszty D, Badcock KJ, Richards BE. Driving Mechanism of High-Speed Unsteady Spiked Body Flows, Part 1: Pulsation Mode. AIAA Journal. 2004;42:95- 106.
[94] Feszty D, Richards BE, Badcock KJ, Woodgate MA. Numerical simulation of a pulsating flow arising over an axisymmetric spiked blunt body at Mach 2.21 and Mach 6.00. Shock Waves. 2000;10:323-31, https://doi.org/10.1007/s001930000065.
[95] Hiraki K, Kleine H, Maruyama H, Hayashida T, Kitamura K, Yonai J, et al. Flow instability induced by spiked bodies. 28th International Congress on High-Speed Imaging and Photonics2009. p. 71260K, ISBN: 10.1117/12.823751.
[96] Beastall D, Turner J. RM No. 3007: The Effect of a Spike Protruding in Front Bluff Body at Supersonic Speeds. 1952.
[97] Feszty D, Badcock KJ, Richards BE. Driving Mechanism of High-Speed Unsteady Spiked Body Flows, Part 2: Oscillation Mode. AIAA Journal. 2004;42:107-13, https://doi.org/10.2514/1.9035.

[98] Feszty D, Badcock K, Richards B. Numerical Simulation of the Hysteresis Phenomenon in High-Speed Spiked Body Flows. 38th Aerospace Sciences Meeting and Exhibit. Reno, NV, USA, https://doi.org/10.2514/6.2000-1412000.
[99] Panaras AG, Drikakis D. High-speed unsteady flows around spiked-blunt bodies. Journal of Fluid Mechanics. 2009;632:69-96, https://doi.org/10.1017/S0022112009006235.
[100] Guy Y, Mclaughlin TE, Morrow JA. Blunt Body Wave Reduction by Means of a Standoff Spike. 39th Aerospace Sciences Meeting and Exhibit. Reno, NV, USA, https://doi.org/10.2514/6.2001-8882001.
[101] Khlebnikov VS. Effect of unsteady disturbances on the flow in a forward separation zone. Fluid Dynamics. 1992;27:294-7, https://doi.org/10.1007/BF01052100.
[102] Khlebnikov VS. The Influence of Unsteady Perturbations on the Flow in a Forward Separation Region Upstream of a Cone. Fluid Dynamics. 1966;31:274- 83, https://doi.org/10.1007/BF02029687.
[103] Khlebnikov VS. Effect of Periodic Disturbances on the Flow in a Nonsymmetric Separation Zone ahead of a Blunt Body. Fluid Dynamics. 1996;31:731 – 8, https://doi.org/10.1007/BF02078226.
[104] Gilinsky M, Blankson I, Sakharov V, Shvets A. Shock waves mitigation at blunt bodies using needles and shells against a supersonic flow. 37th AIAA/ASME/SAE/ASEE Joint Propulsion Conference & Exhibit. Salt Lake City,UT,USA., https://doi.org/10.2514/6.2001-32042001.
[105] Li Z, Sun C, Xinlin Xia, Li X. Numerical Simulation of Aerodynamic Heating over Solid Blunt Configuration with Porous Spike. Journal of Aerospace Engineering. 2018;31.
[106] Thurman WE. A Flow-Separation Spike for Hypersonic Control of a Hemisphere Cylinder. AIAA Journal. 1964;2:159- 61, https://doi.org/10.2514/3.255.
[107] Schülein E. Wave Drag Reduction Approach for Blunt Bodies at High Angles of Attack: Proof-of-Concept Experiments. 4th AIAA Flow Control Conference. Seattle, Washington, USA, https://doi.org/10.2514/6.2008-40002008.
[108] Schülein E. Wave drag reduction concept for blunt bodies at high angles of attack. Shock waves. 2009:1315-20, https://doi.org/10.007/978-3-540-85181-3_84.
[109] Schülein E. Flying Object for Transonic or Supersonic Velocities. 2010.
[110] Wysocki O, Schülein E, Schnepf C. Experimental Study on Wave Drag Reduction at Slender Bodies by a Self-aligning Aerospike. New Results in Numerical and Experimental Fluid Mechanics IX, 583 Notes on Numerical Fluid Mechanics and Multidisciplinary Design. 2014;124:583-90, https://doi.org/10.1007/978-3-319-03158-3_59.
[111] Schnepf C, Wysocki O, Schülein E. Wave drag reduction due to a self-aligning aerodisk. Progress in Flight Physics. 2015;7:475-88, https://doi.org/10.1051/eucass/201507475
[112] Kobayashi H, Maru Y, Hongoh M, Takeuchi S, Okai K, Kojima T. Study on variable-shape supersonic inlets and missiles with MRD device. Acta Astronautica. 2007;61:978-88, https://doi.org/10.1016/j.actaastro.2006.12.018.
[113] Srinath S, Reddy KPJ. Experimental Investigation of the Effects of Aerospike Geometry on Aerodynamic Drag and Heat Transfer Rates for a Blunt Body Configuration at Hypersonic Mach Numbers. International Journal of Hypersonics. 2010;1:93-114, https://doi.org/10.1260/759-3107.1.2.93.
[114] Yadav R, Guven U. Aerothermodynamics of a Hypersonic Projectile with a Double-disk Aerospike. Aeronautical Journal. 2013;117:913-28, https://doi.org/10.1017/S0001924000008587.
[115] Yadav R, Velidi G, Guven U. Aerothermodynamics of generic re-entry vehicle with a series of aerospikes at nose. Acta Astronautica. 2014;96:1-10, https://doi.org/.1016/j.actaastro.2013.11.015.
[116] Gopalakrishna N, Saravanan S. Investigation of the Heat Transfer in Hypersonic Flow on Modified Spike-Blunt Bodies. 31st International Symposium on Shock Waves 2, Applications2017. p. 1053–61, doi:10.07/978-3-319-91017-8_131
[117] Staylor WF. NASA TN D-5754: Flow-Field Investigation for Large-Angle Cones with Short Spikes at a Mach Number of 9.6. 1970.
[118] Jiang Z, Liu Y, Han G, Zhao W. Experimental demonstration of a new concept of drag reduction and thermal protection for hypersonic vehicles. Acta Mechanica Sinica/Lixue Xuebao. 2009;25:417-9, https://doi.org/10.1007/s10409-009-0252-8.

[119] Chinnappan AK, Malaikannan G, Kumar R. Insights into flow and heat transfer aspects of hypersonic rarefied flow over a blunt body with aerospike using direct simulation Monte-Carlo approach. Aerospace Science and Technology. 2017;66:119-28, https://doi.org/10.1016/j.ast.2017.02.024.
[120] Khurana S, Suzuki K. Assessment of Aerodynamic Effectiveness for Aerospike Application on Hypothesized Lifting Body Configuration in Hypersonic Flow. 31st AIAA Applied Aerodynamics Conference. San Diego, CA, USA, https://doi.org/10.2514/6.2013-25132013.
[121] Mikhail AG. Spike-Nosed Projectiles with Vortex Rings: Steady and Nonsteady Flow Simulations. Journal of Spacecraft and Rockets. 1996;33:8-14, https://doi.org/0.2514/3.55700.
[122] Hur K, Kim S, Lee D. Numerical analysis on supersonic, viscous flowfield around a spike-nosed projectile with fins. 21st Atmospheric Flight Mechanics Conference. San Diego,CA,USA., https://doi.org/10.2514/6.1996-34491996.
[123] Chapman DR, Kuehn DM, Larson HK. NACA TR 1356: Investigation of Separated Flows in Supersonic and Subsonic Streams with Emphasis on the Effect of Transition. NACA; 1957.
[124] Sims WH, Boylan DE, Hahn JS. Drag on Blunt Bodies with and without Spikes in Low-Density Hypersonic Flow. AIAA Journal. 1965;3:365- 6, https://doi.org/10.2514/3.863.
[125] Love ES. RM L52119a: The Effects of a Small Jet of Air Exhausting From the Nose of a Body of Revolution in Supersonic Flow. 1952.
[126] Wasko RA. NASA TN D-1535: Heat Transfer to a Sphere with a Retrorocket Exhausting into a Free Stream; Mach 2.0 and 0.8. 1962.
[127] Jarvinen PO, Adams RH. The Effects of Retrorockets on the Aerodynamic Characteristics of Conical Aeroshell Planetary Entry Vehicles. 8th Aerospace Sciences Meeting. New York, USA, https://doi.org/10.2514/6.1970-2191970.
[128] Mcghee RJ. NASA TN D-6002: Effects of a Retronozzle Located at the Apex of a140° Blint Cone at Mach Numbers of 3.00, 4.50, and 6.00. 1971.
[129] Stalder JR, Inouye M. RM A65B72a: A Method of Reducing Heat Transfer to Blunt Bodies by Air Injection. Washington1956.
[130] Kitamura T, Ohnishi N, Sawada K. Computational Analysis of Opposing Jet from Vertical-Lander Space Vehicle. 42nd AIAA Aerospace Science Meeting and Exhibits. Reno, NV, USA, https://doi.org/10.2514/6.2004-8712004.
[131] Bibi A, Maqsood A, Sherbaz S, Dala L. Drag reduction of supersonic blunt bodies using opposing jet and nozzle geometric variations. Aerospace Science and Technology. 2017;69:244-56, https://doi.org/10.1016/j.ast.2017.06.007.
[132] Daso EO, Beaulieu W, Hager JO. Prediction of Drag Reduction in Supersonic and Hypersonic Flows with Counterflow Jets. AIAA/AAAF 11th International Space Planes and Hypersonic Systems and Technologies Conference. Orleans, France, https://ntrs.nasa.gov/archive/nasa/casi.ntrs.nasa.gov/20030014748.pdf2002.
[133] Adamson Jr. TC. On the Structure of Jets from Highly Underexpanded Nozzles Into Still Air. Journal of the Aerospace Sciences. 1959;26:16-24, https://doi.org/10.2514/8.7912
[134] Sriram R, Jagadeesh G. Film cooling at hypersonic Mach numbers using forward facing array of micro-jets. International Journal of Heat and Mass Transfer. 2009;52:3654-64, https://doi.org/10.1016/j.ijheatmasstransfer.2009.02.035.
[135] Pamadi BN. Forebody Drag Reduction. AIAA Journal. 1981;19:1370-2, https://doi.org/10.2514/3.60070.
[136] Shang JS, Hayes J, Wurtzler K, Strang W. Jet-spike bifurcation in high-speed flows. AIAA Journal. 2001;39:1159-65, https://doi.org/10.2514/2.1430.
[137] Fujita M. Axisymmetric oscillations of an opposing jet from a hemispherical nose. AIAA Journal. 1995;33:1850-6, https://doi.org/10.2514/6.1994-659.
[138] Romeo JD, Sterrett JR. Flow field for sonic jet exhausting counter to a hypersonic mainstream. AIAA Journal. 1965;3:544-6, https://doi.org/10.2514/3.907.
[139] Nishida M, Teshima K, Ueno K, Tanaka S. Shock waves generated by an opposing jet. AIP Conference Proceedings 1990;208:114-9.
[140] Finley PJ. The flow of a jet from a body opposing a supersonic free stream. Journal of Fluid Mechanics. 1966;26:337-68, https://doi.org/10.1017/S0022112066001277.

[141] Whitefield DL, Smithson HK, Price LL. Plume boundary jump of an underexpanded jet exhausting counter to a freestream. AIAA Journal. 1973;11:1336-7, https://doi.org/10.2514/3.6918.
[142] Vasil'kov AP, Murzinov IN. Outflow of gas from a severely underexpanded nozzle in opposition to a hypersonic flow. Fluid Dynamics. 1975;8:428-33, https://doi.eog/10.1007/bf01019969.
[143] Venkatachari BS, Cheng G, Chang C-L, Zichettello B, Bilyeu DL. Long Penetration Mode Counterflowing Jets for Supersonic Slender Configurations — A Numerical Study. 31st AIAA Applied Aerodynamics Conference. San Diego, CA, USA, https://doi.org/10.2514/6.2013-26622013.
[144] Meyer B, Nelson HF, Riggins DW. Hypersonic Drag and Heat-Transfer Reduction Using a Forward-Facing Jet. Journal of Aircraft. 2001;38:680-6, https://doi.org/10.2514/2.819.
[145] Hayashi K, Aso S, Tani Y. Numerical Study of Thermal Protection System by Opposing Jet. 43rd AIAA Aerospace Sciences Meeting and Exhibit. Reno, NV, USA, https://doi.org/10.2514/6.2005-1882005.
[146] Hongqing L, Zhenqing W, Chengbin J, Cuie Z, Yongjun W. Numerical simulation for aerodynamic heating and opposing jet thermal protection. 2nd International Symposium on Systems and Control in Aerospace and Astronautics, ISSCAA 2008. Shenzhen, China, DOI: 10.1109/ISSCAA.2008.4776288 2008.
[147] Karpman IM. Outflow of an Unexpanded Jet into Counter Supersonic and Subsonic Flows. Fluid Dynamics. 1977;12:73-9, https://doi.org/10.1007/BF01074628.
[148] Debiève JF, Ardissone JP, Dussauge JP. Shock motion and state of turbulence in a pertubed supersonic flow around a sphere. Journal of Turbulence. 2003;4:DOI: 10.1088/468-5248/4/1/026
[149] Lohner R, Baum JD. On the Drag Efficiency of Counterjets in Low Supersonic Flow. 53rd AIAA Aerospace Sciences Meeting. Kissimmee, FL, USA, https://doi.org/10.2514/6.2015-00692015.
[150] Berdyugin AE, Fomin VM, Fomiehev VP. Body Drag Control in Supersonic Gas Flows by Injection of Liquid Jets. Journal of 4pplied Mechanics and Technical Physics. 1995;36:675–81, https://doi.org/10.1007/BF02369280.
[151] Zhou C, Ji W. A three-dimensional numerical investigation on drag reduction of a supersonic spherical body with an opposing jet. Proceedings of the Institution of Mechanical Engineers, Part G: Journal of Aerospace Engineering. 2014;228:163-77, https://doi.org/10.1177/0954410012468539
[152] Shang JS. Plasma injection for hypersonic blunt-body drag reduction. AIAA Journal. 2012;40:1178-86, https://doi.org/10.2514/2.1769.
[153] Lu HB, Liu WQ. Numerical investigation on properties of attack angle for an opposing jet thermal protection system. Chinese Physics B. 2012;21:https://doi.org/10.1088/674-56/21/8/084401.
[154] Li SB, Wang ZG, Huang W, Yan L. Analysis of flowfield characteristics for equal polygon opposing jet on different freeflow conditions. Acta Astronautica. 2017;133:50-62, https://doi.org/10.1016/j.actaastro.2017.01.011.
[155] Deng F, Xie F, Huang W, Dong H, Zhang D. Numerical exploration on jet oscillation mechanism of counterflowing jet ahead of a hypersonic lifting-body vehicle. Science China Technological Sciences. 2018;61:1056-71, https://doi.org/10.07/s11431-017-9135-0.
[156] Cheng G, Neroorkar K, Chen Y-S, Wang T-S, Daso E. Numerical Study of Flow Augmented Thermal Management for Entry and Re-entry Environments. 25th AIAA Applied Aerodynamics Conference. Miami, FL, USA, https://doi.org/10.2514/6.2007-45602012.
[157] Warren CHE. An experimental investigation of the effect of ejecting a coolant gas at the nose of a bluff body. Journal of Fluid Mechanics. 1960;8:400-17, https://doi.org/10.1017/S0022112060000694.
[158] Daso EO, Pritchett VE, Wang T-S, Ota DK, Blankson IM, Auslender AH. Dynamics of Shock Dispersion and Interactions in Supersonic Freestreams with Counterflowing Jets. AIAA Journal. 2009;47:1313-26, https://doi.org/10.2514/1.30084.
[159] Guo J, Lin G, Bu X, Bai L, Chao Y. Parametric study on the heat transfer of a blunt body with counterflowing jets in hypersonic flows. International Journal of Heat and Mass Transfer. 2018;121:84-96, https://doi.org/10.1016/j.ijheatmasstransfer.2017.12.115.
[160] Venukumar B, Reddy KPJ. Experimental investigation of drag reduction by forward facing high speed gas jet for a large angle blunt cone at Mach 8. Sadhana - Academy Proceedings in Engineering Sciences2007. p. 123-31, ISBN: 10.1007/s12046-007-0011-0.
[161] Gerdroodbary BM, Imani M, Ganji DD. Investigation of film cooling on nose cone by a forward facing array of micro-jets in Hypersonic flow. International Communications in Heat and Mass Transfer. 2015;64:42-9, https://doi.org/10.1016/j.icheatmasstransfer.2015.02.015.

[162] Klich GF, Leyhe EW. NASA TN D-2478: Experimental Results of Cooling A 12.5o Semivertex Angle Cone by Ejection of Hydrogen and Helium from its Apex at Mach 7. 1964.
[163] Gollnick AF. Blunt body experiments with central injection. AIAA Journal. 1966;4:374-6, https://doi.org/10.2514/3.3447.
[164] Sahoo N, Kulkarni V, Saravanan S, Jagadeesh G, Reddy KPJ. Film cooling effectiveness on a large angle blunt cone flying at hypersonic speed. Physics of Fluids. 2005;17:https://doi.org/10.1063/1.1862261
[165] Gerdroodbary BM, Bishehsari S, Hosseinalipour SM, Sedighi K. Transient analysis of counterflowing jet over highly blunt cone in hypersonic flow. Acta Astronautica. 2012;73:38-48, https://doi.org/10.1016/j.actaastro.2011.12.011.
[166] Medvedev AE. Reflection of an Oblique Shock Wave in a Reacting Gas with a Finite Relaxation-Zone Length. Journal of Applied Mechanics and Technical Physics. 2001;42:211-8, https://doi.org/10.1023/A:1018811516116.
[167] Barber EA. An Experimental Investigation of Stagnation Point Injection. AIAA Conference on Physics of Entry into Planetary Atmospheres. New Haven,CT,U.S.A., https://doi.org/10.2514/6.1963-4331963.
[168] Shen BX, Liu WQ, Yin L. Drag and heat reduction efficiency research on opposing jet in supersonic flows. Aerospace Science and Technology. 2018;77:696-703, https://doi.org/10.1016/j.ast.2018.03.051.
[169] Shen B, Liu W. Thermal protection performance of opposing jet generating with solid fuel. Acta Astronautica. 2018;144:90-6, https://doi.org/10.1016/j.actaastro.2017.12.024.
[170] Ganiev Y, Gordeev V, Krasilnikov A, Lagutin V, Otmennikov V, Panasenko A. Theoretical and experimental study of the possibility of reducing aerodynamic drag by employing plasma injection. 37th Aerospace Sciences Meeting and Exhibit. Reno, NV, USA, https://doi.org/10.2514/6.1999-6031999.
[171] Baron JR, Alzner E. An experimental investigation of a two-layer inviscid shock cap due to blunt-body nose injection. Journal of Fluid Mechanics. 1963;15:442-8, https://doi.org/10.1017/S0022112063000367.
[172] Lovick B, McDearmon RW. NASA TN D-1016: Jet Effects on Cylindrical Afterbodies Housing Sonic and Supersonic Nozzles which Exhaust against a Supersonic Stream at Angles of Attack from 90° to 180°. 1962.
[173] Rong YS, Liu WQ. Analysis of the Influence of Opposing Jet on Flow Field and Aerodynamic Heating at the Nose of Reentry Vehicle. Acta Aeronautica and Astronautica Sinica. 2010;31:1552–7.
[174] Yisheng R. Drag reduction research in supersonic flow with opposing jet. Acta Astronautica. 2013;91:1-7, https://doi.org/10.1016/j.actaastro.2013.04.015.
[175] Lopatoff M. RM L51E09: Wing-Flow Study of Pressure-Drag Reduction at Transonic Speed by Projecting a Jet of Air from the Nose of a Prolate Spheriod of Fineness Ratio 6. 1951.
[176] Romeo DJ, Sterrett JR. NASA TN D-1605: Exploratory investigation of the effect of a forward-facing jet on the bow shock of a blunt body in a Mach number 6 free stream. NASA; 1963.
[177] Cassanova RA, Wu YCL. Flow field of a sonic jet exhausting counter to a low-density supersonic airstream. Physics of Fluids. 1969;12:2511-4, https://doi.org/10.1063/1.1692388
[178] Schiff L. The Axisymmetric Jet Counterflow Problem. 9th Fluid and Plasma Dynamics Conference. San Diego,CA,USA., https://doi.org/10.2514/6.1976-3251976.
[179] Macaraeg M. Application of CFD to aerothermal heating problems. 24th Aerospace Sciences Meeting. Reno,NV, USA, https://doi.org/10.2514/6.1986-2321986.
[180] Fox J. Counterflow sonic nosejet into a supersonic stream. 4th Applied Aerodynamics Conference. San Diego, CA, USA, https://doi.org/10.2514/6.1986-1808 1986.
[181] Chen LW, Wang GL, Lu XY. Numerical investigation of a jet from a blunt body opposing a supersonic flow. Journal of Fluid Mechanics. 2011;684:85-110, https://doi.org/10.1017/jfm.2011.276.
[182] Fujita M. Three-dimensional Oscillations of a Supersonic Opposing Jet Flow around a Hemispherical Nose. Journal of Japan Society of Aeronautical Space Sciences. 2002;50:373-9, https://doi.org/10.2322/jjsass.50.373.
[183] Karashima K, Sato K. An experimental study of an opposing jet. Bulletin of the Institute of Space Aeronautical Sciences. 1975;11:53-64.
[184] Nomura H, Aso S, Nishida M. Numerical simulation of opposing sonic jets. Computers and Fluids. 1992;21:229-33, https://doi.org/10.1016/0045-7930(92)90022-N.

[185] Aso S, Hayashi K, Mizoguchi M. A Study on Aerodynamic Heating Reduction due to Opposing Jet in Hypersonic Flow. 40th AIAA Aerospace Sciences Meeting & Exhibit. Reno, NV, USA, https://doi.org/10.2514/6.2002-646 2002.
[186] Hayashi K, Aso S. Effect of Pressure Ratio on Aerodynamic Heating Reduction due to Opposing Jet. 33rd AIAA Fluid Dynamics Conference and Exhibit. Orlando, FL, USA, https://doi.org/10.2514/6.2003-40412003.
[187] Hayashi K, Aso S, Tani Y. Experimental Study on Thermal Protection System by Opposing Jet in Supersonic Flow. Journal of Spacecraft and Rockets. 2006;43:233-5, https://doi.org/10.2514/1.15332.
[188] Tamada I, Aso S, Tani Y. Reducing Aerodynamic Heating by the Opposing Jet in Supersonic and Hypersonic Flows. 48th AIAA Aerospace Sciences Meeting Including the New Horizons Forum and Aerospace Exposition. Orlando, FL, USA, https://doi.org/10.2514/6.2010-991 2010.
[189] Imoto T, Okabe H, Tani Y. Enhancement of Aerodynamic Heating Reduction in High Enthalpy Flows with Opposing Jet. 49th AIAA Aerospace Sciences Meeting including the New Horizons Forum and Aerospace Exposition. Orlando, FL, USA, https://doi.org/10.2514/6.2011-3462011.
[190] Venukumar B, Jagadeesh G, Reddy KPJ. Counterflow drag reduction by supersonic jet for a blunt body in hypersonic flow. Physics of Fluids. 2006;18:https://doi.org/10.1063/1.2401623
[191] Kulkarni V, Reddy KPJ. Enhancement in counterflow drag reduction by supersonic jet in high enthalpy flows. Physics of Fluids. 2008;20:https://doi.org/10.1063/1.2813042.
[192] Kulkarni V, Reddy KPJ. Effect of a Supersonic Counterflow Jet on Blunt Body Heat Transfer Rates for Oncoming High Enthalpy Flow. Journal of Engineering Physics and Thermophysics. 2009;82:1-5, https://doi.org/10.1007/s10891-009-0173-1.
[193] Chang C-L, Venkatachari BS, Cheng G. Effect of Counterflow Jet on a Supersonic Reentry Capsule. 42nd AIAA/ASME/SAE/ASEE Joint Propulsion Conference & Exhibit. Sacramento, CA, USA, https://doi.org/10.2514/6.2006-4776 2006.
[194] Venkatachari BS, Ito Y, Cheng G, Chang C-L. Numerical Investigation of the Interaction of Counterflowing Jets and Supersonic Capsule Flows. 42nd AIAA Thermophysics Conference. Honolulu, Hawaii, USA, https://doi.org/10.2514/6.2011-40302011.
[195] Venkatachari BS, Mullane M, Cheng G, Chang C-L. Numerical Study of Counterflowing Jet Effects on Supersonic Slender-Body Configurations. 33rd AIAA Applied Aerodynamics Conference. Dallas, TX, USA, https://doi.org/10.2514/6.2015-30102015.
[196] Fujita M, Karashima K. An Experimental and Computational Study on Self-excited Oscillations in Supersonic Opposing Jet Flow. Transactions of Japan Society of Aeronautical Space Sciences 1999;42:112-9.
[197] Li SB, Wang ZG, Huang W, Liu J. Drag and Heat Reduction Performance for an Equal Polygon Opposing Jet. Journal of Aerospace Engineering. 2016;30.
[198] Li SB, Wang ZG, Huang W, Liu J. Effect of the injector configuration for opposing jet on the drag and heat reduction. Aerospace Science and Technology. 2016;51:78-86, https://doi.org/10.1016/j.ast.2016.01.014.
[199] Farr R, Chang C-L, Jones JH, Dougherty NS. On the Comparison of the Long Penetration Mode (LPM) Supersonic Counterflowing Jet to the Supersonic Screech Jet. 21st AIAA/CEAS Aeroacoustics Conference. Dallas, TX, USA, https://doi.org/10.2514/6.2015-3126 2015.
[200] Li SB, Wang ZG, Barakos GN, Huang W, Steijl R. Research on the drag reduction performance induced by the counterflowing jet for waverider with variable blunt radii. Acta Astronautica. 2016;127:120-30, https://doi.org/10.1016/j.actaastro.2016.05.031.
[201] Li S, Huang W, Lei J, Wang Z. Drag and heat reduction mechanism of the porous opposing jet for variable blunt hypersonic vehicles. International Journal of Heat and Mass Transfer. 2018;126:1087-98, https://doi.org/10.16/j.ijheatmasstransfer.2018.06.054.
[202] Rui-rui Zhang, Min-zhou Dong, Wei Huang, Shi-bin Li, Zhao-bo Du, Liao J. Drag and heat flux reduction mechanism induced by the combinational forward-facing cavity and pulsed counterflowing jet configuration in supersonic flows. Acta Astronautica. 2019;160:63-75, https://doi.org/10.1016/j.actaastro.2019.04.026.
[203] Yisheng R, Yuechuan W, Renjun Z. Research on thermal protection by opposing jet and transpiration for high speed vehicle. Aerospace Science and Technology. 2016;48:322-7, https://doi.org/10.1016/j.ast.2015.11.014.

[204] Shen BX, Yin L, Zhang XL, Liu WQ. Investigation on cooling effect with a combinational opposing jet and platelet transpiration concept in hypersonic flow. Aerospace Science and Technology. 2019;85:399-408, https://doi.org/10.1016/j.ast.2018.11.021.
[205] Shen BX, Yin L, Liu HP, Liu W. Thermal protection characteristics for a combinational opposing jet and platelet transpiration cooling nose-tip. Acta Astronautica. 2019;155:143-52, https://doi.org/10.1016/j.actaastro.2018.11.052.
[206] Ce Z, Tomita R, Suzuki K, Watanabe Y. Effect of Opposing Multiphase Jet on Hypersonic Flow Around Blunt Body. IOP Conference Series: Materials Science and Engineering2017. p. doi: 10.1088/757-899X/249/1/012014.
[207] Zhang Rr, Huang W, Li Lq, Yan L, Moradi R. Drag and heat flux reduction induced by the pulsed counterflowing jet with different periods on a blunt body in supersonic flows. International Journal of Heat and Mass Transfer. 2018;127:503-12, https://doi.org/10.1016/j.ijheatmasstransfer.2018.08.066.
[208] Zhang Rr, Huang W, Yan L, Li Lq, Li Sb, Moradi R. Numerical investigation of drag and heat flux reduction mechanism of the pulsed counterflowing jet on a blunt body in supersonic flows. Acta Astronautica. 2018;146:123-33, https://doi.org/10.1016/j.actaastro.2018.02.040.
[209] Zhang Rr, Huang W, Yan L, Chen Z, Moradi R. Drag and heat flux reduction induced by the pulsed counterflowing jet with different waveforms on a blunt body in supersonic flows. Acta Astronautica. 2019;160:635-45, https://doi.org/10.1016/j.actaastro.2019.03.012.
[210] Gordeev VP, Krasil'nikov AV, Lagutin VI, Otmennikov VN. Experimental study of the possibility of reducing supersonic drag by employing plasma technology. Fluid Dynamics. 1996;31:313-7, https://doi.org/10.1007/BF02029693.
[211] Ganiev Y, Gordeev V, Krasilnikov A, Lagutin V, Otmennikov V. Experimental Study of the Possibility of Reducing Aerodynamic Drag by Employing Plasma Injection. Third International Conference on Experimental Fluid Mechanics. Moscow1997.
[212] Ganiev Y, Gordeev V, Krasilnikov A, Lagutin V, Otmennikov V, Panasenko A. Experimental and Theoretical Study of the Possibility of Reducing Aerodynamic Drag by Employing Plasma Injection. Second Workshop of Weakly Ionozed Gases. Norfolk, VA1998.
[213] Ganiev YC, Gordeev VP, Krasilnikov AV, Lagutin VI, N. OV, Panasenko AV. Aerodynamic Drag Reduction by Plasma and Hot-Gas Injection. Journal of Thermophysics and Heat Transfer. 2012;14:10-7, https://doi.org/.2514/2.6504.
[214] Babichev J, Krasilnikov A, Panasenko A, Sipachev G. Effect of plasma jet characteristics on supersonic cone-cylinder drag. 9th International Space Planes and Hypersonic Systems and Technologies Conference. Norfolk, VA, USA, https://doi.org/10.2514/6.1999-48811999.
[215] Shang JS, Hayes J, Menart J, Miller J. Blunt Body in Hypersonic Electromagnetic Flow Field. Journal of Aircraft. 2008;40:314-22, https://doi.org/10.2514/2.3095.
[216] Shang JS, Hayes J, Menart J. Hypersonic Flow over a Blunt Body with Plasma Injection. Journal of Spacecraft and Rockets. 2002;39:367-75, https://doi.org/10.2514/2.3835.
[217] Malmuth N, Fomin V, Maslov A, Fomichev V, Shashkin A, Korotaeva T, et al. Influence of a counterflow plasma jet on supersonic blunt body pressures. AIAA Journal. 1999;40:1170-7, https://doi.org/10.2514/2.1768
[218] Fomin VM, Maslov A, Malmuth ND, Fomichev VP, Shashkin AP, Korotaeva TA, et al. Influence of a counterflow plasma jet on supersonic blunt-body pressures. AIAA Journal. 2012;40:1170-7, https://doi.org/10.2514/6.1999-4883
[219] Bletzinger P, Ganguly BN, Van Wie D, Garscadden A. Plasmas in high speed aerodynamics. Journal of Physics D: Applied Physics. 2005;38:https://doi.org/10.1088/0022-3727/38/4/R01.
[220] Hartmann J. On a new method for the generation of sound-waves. Physical Review. 1922;20:719-27, https://doi.org/10.1103/PhysRev.20.719.
[221] Yuceil B, Dolling D, Wilson D. A preliminary investigation of the Helmholtz resonator concept for heat flux reduction. 28th Thermophysics Conference. Orlando, FL, USA, https://doi.org/10.2514/6.1993-27421993.
[222] Ladoon DW, Schneider SP, Schmisseur JD. Physics of Resonance in a Supersonic Forward-Facing Cavity. Journal of Spacecraft and Rockets. 1998;35:626-32, https://doi.org/10.2514/2.3395.

[223] Engblom WA, Goldstein DB. Nose-tip surface heat reduction mechanism. Journal of Thermophysics and Heat Transfer. 1996;10:598-606, https://doi.org/10.2514/3.835
[224] Silton S, Goldstein DB. Use of an axial nose-tip cavity for delaying ablation onset in hypersonic flow. Journal of Fluid Mechanics. 2005;528:297–321, https://doi.org/10.1017/S0022112004002460.
[225] Yadav R, Guven U. Aerothermodynamics of a hypersonic vehicle with a forward-facing parabolic cavity at nose. Proceedings of the Institution of Mechanical Engineers, Part G: Journal of Aerospace Engineering. 2014;228:1863-74, https://doi.org/10.177/0954410013498056
[226] Lu HB, Liu WQ. Forward-facing cavity and opposing jet combined thermal protection system. Thermophysics and Aeromechanics. 2012;19:561-9, https://doi.org/10.1134/S086986431204004X.
[227] Lu H, Liu W. Thermal protection efficiency of forward-facing cavity and opposing jet combinational configuration. Journal of Thermal Science. 2012;21:342-7, https://doi.org/10.1007/s11630-012-0553-2.
[228] Lu H, Liu W. Investigation of thermal protection system by forward-facing cavity and opposing jet combinatorial configuration. Chinese Journal of Aeronautics. 2013;26:287-93, https://doi.org/10.1016/j.cja.2013.02.005.
[229] Lu HB, Liu WQ. Research on thermal protection mechanism of forward-facing cavity and opposing jet combinatorial thermal protection system. Heat and Mass Transfer/Waerme- und Stoffuebertragung. 2014;50:449-56, https://doi.org/10.1007/s00231-013-1247-3.
[230] Sun Xw, Guo Zy, Huang W, Li Sb, Yan L. A study of performance parameters on drag and heat flux reduction efficiency of combinational novel cavity and opposing jet concept in hypersonic flows. Acta Astronautica. 2017;131:204-25, https://doi.org/10.1016/j.actaastro.2016.11.044.
[231] Sun XW, Guo ZY, Huang W, Li SB, Yan L. Drag and heat reduction mechanism induced by a combinational novel cavity and counterflowing jet concept in hypersonic flows. Acta Astronautica. 2016;126:109-19, https://doi.org/10.1016/j.actaastro.2016.04.022.
[232] Sun X-w, Huang W, Guo Z-y, Yan L. Multiobjective Design Optimization of Hypersonic Combinational Novel Cavity and Opposing Jet Concept Jornal of Spacecraft and Rockets. 2017;54:https://doi.org/10.2514/1.A33801.
[233] Huang W, Jiang YP, Yan L, Liu J. Heat flux reduction mechanism induced by a combinational opposing jet and cavity concept in supersonic flows. Acta Astronautica. 2016;121:164-71, https://doi.org/10.1016/j.actaastro.2016.01.008.
[234] Huang W, Yan L, Liu J, Jin L, Tan JG. Drag and heat reduction mechanism in the combinational opposing jet and acoustic cavity concept for hypersonic vehicles. Aerospace Science and Technology. 2015;42:407-14, https://doi.org/10.1016/j.ast.2015.01.029.
[235] Aruna S, Anjalidevi SP. Computational study on the influence of jet on reduction of drag over cone flare bodies in hypersonic turbulent flow. Procedia Engineering. 2012;38:3635-48, https://doi.org/10.1016/j.proeng.2012.06.420.
[236] Larina IN. Interaction of a Jet Exhausting from a Body with an Opposing Supersonic Stream of Rarefied Gas. Fluid Dynamics. 1983;18:607-11, https://doi.org/10.1007/BF01090629.
[237] Zheng Y, Ahmed N. A novel means of dissipation of shock wave induced heat in a high speed flow. 43rd Fluid Dynamics Conference. San Diego, CA, USA, https://doi.org/10.2514/6.2013-31142013.
[238] Josyula E, Pinney M, Blake WB. Applications of a Counterflow Drag Reduction Technique in High-Speed Systems. Journal of Spacecraft and Rockets. 2002;39:605-14, https://doi.org/10.2514/2.3850.
[239] Takaki R, Liou M-S. Parametric study of heat release preceding a blunt body in hypersonic flow. AIAA Journal. 2002;40:501-9, https://doi.org/10.2514/2.1674.
[240] Knight D, Kuchinskiy V, Kuranov A, Sheikin E. Survey of Aerodynamic Flow Control at High Speed Using Energy Deposition (Invited). 41st Aerospace Sciences Meeting and Exhibit. Reno, NV, USA, https://doi.org/10.2514/6.2003-5252002.
[241] Levin VA, Terent'eva LV. Supersonic flow over a cone with heat release in the neighborhood of the apex. Fluid Dynamics. 1993;28:244-7, https://doi.org/10.1007/BF01051214.
[242] Luk'yanov GA. Drag of an object in a supersonic flow with an isobaric region of energy release in front of the object. Technical Physics Letters. 1999;25:29-31, https://doi.org/10.1134/1.1262344.
[243] Borzov VY, Rybka IV, Yur'ev AS. Estimation of energy consumption for body drag reduction in a supersonic flow. Journal of Engineering Physics and Thermophysics. 1992;63:1171-5, https://doi.org/10.007/BF00853515.

[244] Krasnobaev KV, Syunyaev RA. Calculation of Flow of Stellar Wind Past an X-ray Source. Fluid Dynamics. 1983;18:584-9, https://doi.org/10.1007/BF01090625.
[245] Krasnobaev KV. Supersonic flow past weak sources of radiation. Fluid Dynamics. 1984;19:629-32, https://doi.org/10.1007/BF01091088.
[246] Marconi F. An investigation of tailored upstream heating for sonic boom and drag reduction. 36th AIAA Aerospace Sciences Meeting and Exhibit. Reno,NV, USA, https://doi.org/10.2514/6.1998-3331998.
[247] Myrabo L, Raizer Y. Laser-induced air spike for advanced transatmospheric vehicles. 25th Plasmadynamics and Lasers Conference. Colorado Springs,CA, USA, https://doi.org/10.2514/6.1994-24511994.
[248] Borzov VY, Mikhailov VM, Rybka IV, Savishchenko NP, Yur'ev AS. Experimental investigation of supersonic flow about an obstacle with power delivery into the undisturbed flow. Journal of Engineering Physics and Thermophysics. 1994;66:449-54, https://doi.org/10.1007/BF00851704.
[249] Bityurin V, Klimov A, Leonov S, Van Wie D, Brovkin V, Kolesnichenko Y, et al. Effect of Hetrogenous Discharge Plasma on Shock Wave Structure and Propagation. 9th International Space Planes and Hypersonic Systems and Technologies Conference. Norfolk,VA, USA, https://doi.org/10.2514/6.1999-494011999.
[250] Soloviev V, Krivtsov V, Konchakov A, Malmuth ND. Mechanism of Shock Wave Dispersion and Attenuation in Weakly Ionozed Cold Discharge Plasmas. 9th International Space Plasma and Hypersonic Systems and Technologies Conference. Norfolk,VA,USA., https://doi.org/10.2514/6.1999-490811999.
[251] Leonov S, Bityurin V, Kolesnichenko Y. Dynamic of a single-electrode HF plasma filament in supersonic airflow. 39th Aerospace Sciences Meeting and Exhibit. Reno,NV, USA, https://doi.org/10.2514/6.2001-4932001.
[252] Kremeyer K, Pakhomov AV. Lines of Energy Deposition for Supersonic⁄Hypersonic Temperature⁄Drag-Reduction and Vehicle Control. AIP Conference AIP Publishing; 2008. p. 353-66.
[253] Yuriev AS, Pirogov SY, Savischenko NP, Ryizhov ME. Numerical and Experimental Investigation of Pulse-Repetitive Energy Release Upstream Body under Supersonic Flow. 1st Flow Control Conference. St. Louis, Missouri, USA, https://doi.org/10.2514/6.2002-273002002.
[254] Satheesh K, Jagadeesh G. Experimental investigations on the effect of energy deposition in hypersonic blunt body flow field. Shock Waves. 2008;18:53-70, https://doi.org/10.1007/s00193-008-0140-3.
[255] Kuo SP, Kalkhoran IM, Bivolaru D, Orlick L. Observation of shock wave elimination by a plasma in a Mach-2.5 flow. Physics of Plasmas. 2000;7:1345-8, https://doi.org/10.063/1.873776
[256] Myrabo LN, Raizer YP, Shneider MN. Drag and total power reduction for artificial heat input in front of hypersonic blunt bodies. AIP Conference Proceedings. 2005;766:485-98, https://doi.org/10.1063/1.1925169
[257] Zaidi SH, Shneider MN, Miles RB. Shock-Wave Mitigation Through an off-Body Pulsed Energy Deposition. AIAA Journal. 2004;42:326-31, https://doi.org/10.2514/1.9097.
[258] Sangtabi AR, Ramiar A, Ranjbar AA, Abdollahzadeh M, Kianifar A. Influence of repetitive laser pulse energy depositions on supersonic flow over a sphere, cone and oblate spheroid. Aerospace Science and Technology. 2018;76:72-81, https://doi.org/10.1016/j.ast.2018.02.005.
[259] Merriman S, Ploenjes E, Palm P, Adamovich IV. Shock wave control by nonequilibrium plasmas in cold supersonic gas flows. AIAA Journal. 2001;39:1547-52, https://doi.org/10.2514/2.1479.
[260] Adelgren RG, Yan H, Elliott GS, Knight DD, Beutner TJ, Zheltovodov AA. Control of Edney IV Interaction by Pulsed Laser Energy Deposition. AIAA Journal. 2005;43:256-69, https://doi.org/10.2514/1.7036
[261] Satheesh K, Jagadeesh G. Effect of concentrated energy deposition on the aerodynamic drag of a blunt body in hypersonic flow. Physics of Fluids. 2007;19:https://doi.org/10.1063/1.2565663
[262] Riggins D, Nelson HF, Johnson E. Blunt-body wave drag reduction using focused energy deposition. AIAA Journal. 1999;37:460-7, https://doi.org/10.2514/2.756.
[263] Ganesh AM, John B. Concentrated energy addition for active drag reduction in hypersonic flow regime. Acta Astronautica. 2018;142:221-31, https://doi.org/10.1016/j.actaastro.2017.11.003.
[264] Schülein E. Simplified Model for Flow-Heating Effect on Wave Drag and Its Validation. AIAA Journal. 2016;54:1030-9, https://doi.org/10.2514/1.J054604.
[265] Schülein E, Zheltovodov AA, Pimonov EA, Loginov MS. Experimental and Numerical Investigation of Electric−Arc Airspikes For Blunt and Sharp Bodies at Mach 5. International Conference on Methods of Aerophysical Research, ICMAR. http://ftp.itam.nsc.ru/tmp/Test/2/Schulen2.pdf2008.

[266] Erdem E, Yang L, Kontis K. Drag Reduction Studies by Steady Energy Deposition at Mach 5. 49th AIAA Aerospace Sciences Meeting including the New Horizons Forum and Aerospace Exposition. Orlando, FL, USA, https://doi.org/10.2514/6.2011-1027 2011.
[267] Oliveira AC, Minucci MAS, Toro PGP, Chanes JB, Myrabo LN, Pakhomov AV. Schlieren Visualization of the Energy Addition by Multi Laser Pulse in Hypersonic Flow. AIP Conference Proceedings: AIP Publishing; 2008. p. 390-400, ISBN: 10.1063/1.2931909.
[268] Ohnishi N, Tate M, Ogino Y. Computational study of shock wave control by pulse energy deposition. Shock Waves. 2012;22:521-31, https://doi.org/10.1007/s00193-012-0407-6.
[269] Meyer R, Palm P, Plonjes E, Rich J, Adamovich I. The effect of a nonequilibrium RF discharge plasma on a conical shock wave in a M = 2.5 flow. 32nd AIAA Plasmadynamics and Lasers Conference and 4th Weakly Ionized Gases Workshop. Anaheim,CA, USA, https://doi.org/10.2514/6.2001-30592001.
[270] Kuo SP, Bivolaru D. Plasma effect on shock waves in a supersonic flow. Physics of Plasmas. 2001;8:3258-64, https://doi.org/10.1063/1.1376422
[271] Misiewicz C, Myrabo LN, Shneider MN, Raizer YP. Combined experimental and numerical investigation of electric-arc airspikes for blunt body at Mach 3. AIP Conference Proceedings. 2005;766:528-41, https://doi.org/10.1063/1.1925172
[272] Kandala R, Candler GV. Numerical Studies of Laser-Induced Energy Deposition for Supersonic Flow Control. AIAA Journal. 2004;42:2266-75, https://doi.org/10.514/1.6817.
[273] Bivolaru D, Kuo SP. Aerodynamic Modification of Supersonic Flow Around Truncated Cone Using a Pulsed Electrical Discharges. AIAA Journal. 2005;43:1482-9, https://doi.org/10.2514/1.7361.
[274] Erdem E, Kontis K, Yang L. Steady energy deposition at Mach 5 for drag reduction. Shock Waves. 2013;23:285-98, https://doi.org/10.1007/s00193-012-0405-8.
[275] Desai S, Kulkarni V, Gadgil H, John B. Aerothermodynamic considerations for energy deposition based drag reduction technique. Applied Thermal Engineering. 2017;122:451-60, https://doi.org/10.1016/j.applthermaleng.2017.04.114.
[276] Das D, Desai S, Kulkarni V, Gadgil H. Performance assessment of energy deposition based drag reduction technique for Earth and Mars flight conditions. Acta Astronautica. 2019;159:418-28, https://doi.org/10.1016/j.actaastro.2019.01.049.
[277] Kremeyer K, Sebastian KA, Shu C-W. Computational Study of Shock Mitigation and Drag Reduction by Pulsed Energy Lines. AIAA Journal. 2006;44:1720-31, https://doi.org/10.2514/1.17854.
[278] Riggins DW, Nelson HF. Hypersonic flow control using upstream focused energy deposition. AIAA Journal. 2000;38:723-5, https://doi.org/10.2514/2.1020.
[279] Arafailov SI. Effect of Energy Release in the Shock Layer on Supersonic Flight. Fluid Dynamics. 1987;22: 645–8, https://doi.org/10.1007/BF01051435.
[280] Georgievskii PY, Levin VA. Control of the Flow Past Bodies Using Localized Energy Addition to the Supersonic Oncoming Flow. Fluid Dynamics. 2003;38:794-805, https://doi.org/10.1023/B:FLUI.0000007841.91654.10.
[281] Azarova OA, Knight DD. An approach of drag force decrease for combined cylinder AD bodies under the action of microwave and laser energy deposition. Aerospace Science and Technology. 2017;64:154-60, https://doi.org/10.1016/j.ast.2017.01.025.
[282] Hartley CS, Portwood TW, Filippelli MV, Myrabo LN, Nagamatsu HT, Shneider MN, et al. Experimental and computational investigation of drag reduction by electric-arc airspikes at Mach 10. AIP Conference Proceedings. 2005;766:499-513, https://doi.org/10.1063/1.1925170
[283] Iwakawa A, Shoda T, Majima R, Pham SH, Sasoh A. Mach Number Effect on Supersonic Drag Reduction using Repetitive Laser Energy Depositions over a Blunt Body. Transactions of the Japan Society for Aeronautical and Space Sciences. 2017;60:303-11.
[284] Knight D. Survey of Aerodynamic Drag Reduction at High Speed by Energy Deposition. Journal of Propulsion and Power. 2008;24:1153, 67, DOI: 10.2514/1.24595.
[285] Sperber D, Eckel HA, Steimer S, Fasoulas S. Objectives of Laser-Induced Energy Deposition for Active Flow Control. Contributions to Plasma Physics. 2012;52:636-43, https://doi.org/10.1002/ctpp.201210060|.
[286] Fang J, Hong Y, Li Q, Wen M, Liu Z. The influence of flight altitude on supersonic drag reduction with laser energy depositions. AIP Conference Proceedings. 2011;1402:430-6, https://doi.org/10.1063/1.3657051

[287] Kim J-H, Matsuda A, Sakai T, Sasoh A. Wave Drag Reduction with Acting Spike Induced by Laser-Pulse Energy Depositions. AIAA Journal. 2011;49:2076-8, https://doi.org/10.514/1.j051145.
[288] Guvernyuk SV, Samoilov AB. Control of supersonic flow around bodies by means of a pulsed heat source. Technical Physics Letters. 1997;23:333-6, https://doi.org/10.1134/1.1261673.
[289] Tret'yakov PK, Yakovlev VI. Formation of quasisteady supersonic flow with a pulse-periodic plasma heat source. Technical Physics Letters. 1998;24:626-7, https://doi.org/10.1134/1.1262222.
[290] Borzov VY, Rybka IV, Yur'ev AS. Effect of Local Energy Supply to a Hypersonic Flow on the Drag of Bodies with Different Nose Bluntness. Journal of Engineering Physics and Thermophysics. 1994;67:997-1002, https://doi.org/10.7/BF00852714.
[291] Vidmar RJ. On the Use of Atmospheric Pressure Plasmas as Electromagnetic Reflectors and Absorbers. IEEE Transactions on Plasma Science. 1990;18:733-41, https://doi.org/10.1109/27.57528.
[292] Soloviev V, Krivtsov V, Konchakov A, Malmuth N. Simulation of supersonic body drag reduction produced by forebody filamentary plasmas. 32nd AIAA Plasmadynamics and Lasers Conference. Anaheim,CA,USA., https://doi.org/10.2514/6.2001-27272001.
[293] Sasoh A, Sekiya Y, Sakai T, Kim J-H, Matsuda A. Supersonic Drag Reduction with Repetitive Laser Pulses Through a Blunt Body. AIAA Journal. 2010;48:2811-7, https://doi.org/10.514/1.J050174.
[294] Joarder R, Padhi UP, Singh AP, Tummalapalli H. Two-dimensional numerical simulations on laser energy depositions in a supersonic flow over a semi-circular body. International Journal of Heat and Mass Transfer. 2017;105:723-40, https://doi.org/10.1016/j.ijheatmasstransfer.2016.10.025.
[295] Schülein E, Zheltovodov A, Pimonov E, Loginov M. Experimental and Numerical Modeling of the Bow Shock Interaction with Pulse-Heated Air Bubbles. International Journal of Aerospace Innovations. 2010;2:165-88, https://doi.org/10.1260/757-2258.2.3.165.
[296] Schülein E, Zheltovodov A. Effects of steady flow heating by arc discharge upstream of non-slender bodies. Shock Waves. 2011;21:383-96, https://doi.org/10.1007/s00193-011-0307-1.
[297] Bracken R, Myrabo L, Nagamatsu H, Meloney E, Shneider M. Experimental investigation of an electric arc air-spike with and without blunt body in hypersonic flow. 39th Aerospace Sciences Meeting and Exhibit. Reno,NV, USA, https://doi.org/10.2514/6.2001-7962001.
[298] Schülein E, Zheltovodov A. Effects of Localized Flow Heating by DC-Arc Discharge Ahead of Non-Slender Bodies. 16th AIAA/DLR/DGLR International Space Planes and Hypersonic Systems and Technologies Conference. Bremen, Germany, https://doi.org/10.2514/6.2009-734620 09.
[299] Bivolaru D, Kuo SP. Observation of supersonic shock wave mitigation by a plasma aero-spike. Physics of Plasmas. 2002;9:721-3, https://doi.org/10.1063/1.1433662.
[300] Sasoh A, Kim JH, Yamashita K, Sakai T, Matsuda A. Efficient supersonic drag reduction using repetitive laser pulses of up to 80 kHz. AIP Conference Proceedings2011. p. 424-9, ISBN: 10.1063/1.3657050.
[301] Suchomel CF, Van Wie D. Energy Based Performance Parameters for Hypersonic Flight Vehicles. 13th International Space Planes and Hypersonics Systems and Technologies2005.
[302] Suchomel C. F. , Van Wie D.M. , G. B. Energy Based Plasma Performance Specifications For Flight Vehicles. 37th AIAA Plasmadynamics and Lasers Conference2006.
[303] Suchomel C. F., Van Wie D.M., D. T. Assessment of Energetic Flow Control Techniques Using an Energy-Based Methodology. 7th AIAA Aviation Technology, Integration and Operations Conference2007.
[304] Liu Y, Jiang Z. Concept of Non-Ablative Thermal Protection System for Hypersonic Vehicles. AIAA Journal. 2013;51:584-90, https://doi.org/10.2514/1.J051875.
[305] Hahn M. Pressure distribution and mass injection effects in the transitional separated flow over a spiked body at supersonic speed. Journal of Fluid Mechanics. 1966;24:209-23, https://doi.org/10.1017/S0022112066000600.
[306] Jiang Z, Liu Y, Han G. Conceptual study on non-ablative TPS for hypersonic vehicles. 17th AIAA International Space Planes and Hypersonic Systems and Technologies Conference. San Francisco, CA, USA, https://doi.org/10.2514/6.2011-23722012.
[307] Han G, Jiang Z. Hypersonic Flow Field Reconfiguration and Drag Reduction of Blunt Body with Spikes and Sideward Jets. International Journal of Aerospace Engineering. 2018;2018:1-16, https://doi.org/0.1155/2018/7432961.

[308] Zhu L, Chen X, Li Y, Musa O, Zhou C. Investigation of drag and heat reduction induced by a novel combinational lateral jet and spike concept in supersonic flows based on conjugate heat transfer approach. Acta Astronautica. 2018;142:300-13, https://doi.org/10.1016/j.actaastro.2017.11.001.
[309] Morimoto N, Yoon JY, Aso S, Tani Y. Reduction of Aerodynamic Heating with Opposing Jet through Extended Nozzle in High Enthalpy Flow. 29th Congress of the Aeronautical Sciences. St. Petersberg, Russia2014.
[310] Morimoto N, Yoon JY, Aso S, Tani Y. Reduction of Aerodynamic Heating with Opposing Jet through Extended Nozzle in High Enthalpy Flow. 52nd Aerospace Sciences Meeting. National Harbor, Maryland, USA, https://doi.org/10.2514/6.2014-07052014.
[311] Morimoto N, Yamashita J, Aso S, Tani Y. An Expedient for Alleviating Aerodynamic Heating and Drag on Capsule Forward Heat Shield. 53rd AIAA Aerospace Sciences Meeting. Kissimmee, FL, USA, https://doi.org/10.2514/6.2015-20802015.
[312] Qu F, Sun D, Bai J, Zuo G, Yan C. Numerical investigation of blunt body's heating load reduction with combination of spike and opposing jet. International Journal of Heat and Mass Transfer. 2018;127:7-15, https://doi.org/0.1016/j.ijheatmasstransfer.2018.06.154.
[313] Pish F, Moradi R, Edalatpour A, Barzegar Gerdroodbary M. The effect of coolant injection from the tip of spike on aerodynamic heating of nose cone at supersonic flow. Acta Astronautica. 2019;154:52-60, https://doi.org/10.1016/j.actaastro.2018.10.021.
[314] Huang W, Liu J, Xia Z-x. Drag reduction mechanism induced by a combinational opposing jet and spike concept in supersonic flows. Acta Astronautica. 2015;115:24-31, https://doi.org/10.1016/j.actaastro.2015.04.025.
[315] Eghlima Z, Mansour K. Drag reduction for the combination of spike and counterflow jet on blunt body at high Mach number flow. Acta Astronautica. 2017;133:103-10, https://doi.org/10.1016/j.actaastro.2017.01.008.
[316] Eghlima Z, Mansour K, Fardipour K. Heat transfer reduction using combination of spike and counterflow jet on blunt body at high Mach number flow. Acta Astronautica. 2018;143:92-104, https://doi.org/10.1016/j.actaastro.2017.11.012.
[317] Ou M, Yan L, Huang W, Li Sb, Li Lq. Detailed parametric investigations on drag and heat flux reduction induced by a combinational spike and opposing jet concept in hypersonic flows. International Journal of Heat and Mass Transfer. 2018;126:10-31, https://doi.org/10.1016/j.ijheatmasstransfer.2018.05.013.
[318] Ou M, Yan L, Huang W, Zhang Tt. Design exploration of combinational spike and opposing jet concept in hypersonic flows based on CFD calculation and surrogate model. Acta Astronautica. 2019;155:287-301, https://doi.org/10.1016/j.actaastro.2018.12.012.
[319] Qin Q, Xu J, Guo S. Reduction of Aeroheating and Drag Using Lateral/Oblique/Opposing Jet on Aerodome. Journal of Spacecraft and Rockets. 2018;55:523-7, https://doi.org/10.2514/1.A34041.
[320] Moradi R, Mosavat M, Barzegar Gerdroodbary M., Abdollahi A., Amini Y. The influence of coolant jet direction on heat reduction on the nose cone with Aerodome at supersonic flow. Acta Astronautica. 2018;151:487-93, https://doi.org/10.1016/j.actaastro.2018.06.026.
[321] Gerdroodbary MB, Goudarzi AM, Imani M, Sedighi K, Ganji DD. Influence of Opposing Jet on an Aerodisk Nose Cone at Hypersonic Flow. ASME 2014 12th Biennial Conference on Engineering Systems Design and Analysis. Copenhagen, Denmark, ISBN: 978-0-7918-4583-72014. p. V001T13A7.
[322] Gerdroodbary BM, Imani M, Ganji DD. Heat reduction using conterflowing jet for a nose cone with aerodisk in hypersonic flow. Aerospace Science and Technology. 2014;39:652-65, https://doi.org/10.1016/j.ast.2014.07.005.
[323] Gerdroodbary BM. Numerical analysis on cooling performance of counterflowing jet over aerodisked blunt body. Shock Waves. 2014;24:537-43, https://doi.org/10.1007/s00193-014-0517-4.
[324] Huang J, Yao WX, Shan XY. Numerical investigation on drag and heat reduction mechanism of combined spike and rear opposing jet configuration. Acta Astronautica. 2019;155:179-90, https://doi.org/10.1016/j.actaastro.2018.11.039.
[325] Huang J, Yao WX. A novel non-ablative thermal protection system with combined spike and opposing jet concept. Acta Astronautica. 2019;159:41-8, https://doi.org/10.1016/j.actaastro.2019.02.005.
[326] Qin Q, Xu J. Numerical evaluation of aerodome and cooling jet for aeroheating reduction. Aerospace Science and Technology. 2019;86:520-33, https://doi.org/10.1016/j.ast.2019.01.046.

[327] Qin Q, Xu J. Aeroheating reduction for blunt body using aerodome jet. Acta Astronautica. 2019;159:17-26, https://doi.org/10.1016/j.actaastro.2019.03.042.
[328] Zhu L, Li Y, Gong L, Chen X, Xu J. Coupled investigation on drag reduction and thermal protection mechanism induced by a novel combinational spike and multi-jet strategy in hypersonic flows. International Journal of Heat and Mass Transfer. 2019;131:944-64, https://doi.org/10.1016/j.ijheatmasstransfer.2018.11.119.
[329] Zhang J, Ma H, Qin Y. Research on the Parameters Optimization of Combination of Spike and Forward-facing Jet. 34th AIAA Applied Aerodynamics Conference. Washington, D.C., USA, https://doi.org/10.2514/6.2016-4040 2016.
[330] Fomin VM, Tretyakov PK, Taran J-P. Flow control using various plasma and aerodynamic approaches (Short review). Aerospace Science and Technology. 2004;8:411-21, https://doi.org/10.1016/j.ast.2004.01.005.
[331] Redding JP, Jecmen DM. An Advanced Aerospike to Minimize. Lockheed Horizons Magazine1984. p. 46-54.
[332] Reding JP, Jecmen DM. Effects of external burning on spike-induced separated flow. Journal of Spacecraft and Rockets. 1983;20:452-3, https://doi.org/10.2514/3.25628.
[333] Maurer F, Brungs W. Influencing the Drag and the Bow Wave by a Heat Addition in the Stagnation Point Domain of Blunt Bodies in Supersonic Flow. VI International Congress of Flight Sciences (ICAS). Munich, Germany1968.
[334] Srinivasan G, Chamberlain R. Drag Reduction of Spiked Missile by Heat Addition. AIAA Atmospheric Flight Mechanics Conference and Exhibit. Providence, Rhode Island, USA, https://doi.org/10.2514/6.2004-4714 2004.
[335] Golovitchev VT, P.; Raffoul, C. Evaluation of Drag Reduction of Blunt Bodies at Supersonic Speeds by Counter-flow Combustion. 32nd AIAA Fluid Dynamics Conference and Exhibit. St. Louis, Missouri, USA, https://doi.org/10.2514/6.2002-3296 2002.
[336] Iwakawa AH, Naoki; Osuka, Takeshi; Majima, Ryosuke; Sakai, Takeharu; Sasoh, Akihiro. Supersonic Drag Reduction Performance of Blunt-Body with Conical Spike using with Energy Depositions. 44th AIAA Plasmadynamics and Lasers Conference. San Diego, CA, USA, https://doi.org/10.2514/6.2013-3127 2013.
[337] Trident I C-4 FBM / SLBM. https://fasorg/nuke/guide/usa/slbm/c-4htm. p. https://fas.org/nuke/guide/usa/slbm/c-4.htm.
[338] Trident II D-5 Fleet Ballistic Missile. https://fasorg/nuke/guide/usa/slbm/d-5htm. p. https://fas.org/nuke/guide/usa/slbm/d-5.htm.
[339] IGLA 9K38 / SA-18 / GROUSE Surface-to-Air Missile. p. Igla Missiles.
[340] Launch Escape Subsystem. p. Launch Escape Subsystem.
[341] Quiet Spike. https://wwwnasagov/centers/dryden/multimedia/imagegallery/Quiet_Spike/Quiet_Spike_proj_deschtml.
[342] Trident. https://wwwdefenseindustrydailycom/?s=trident.
[343] Hitt D. Saturn V: The Rocket Comes to the Rocket City. https://blogsnasagov/Rocketology/tag/saturn-v/.
[344] TM 43-0001-28: Army Ammunition Data Sheets for Artillery Ammunition Guns, Howitzers, Mortars, Recoilless Rifles, Grenade Launchers and Artillery Fuzes. In: Army Dot, editor.
[345] NASA F-15B #836 in flight with Quiet Spike attached. https://wwwdfrcnasagov/Gallery/Photo/Quiet_Spike/HTML/ED06-0184-23html.
[346] Shang JS, Hankey WL, Smith RE. Flow Oscillations of Spike-Tipped Bodies. 18th Aerospace Sciences Meeting. Pasadena, California, USA, https://doi.org/10.2514/6.1980-621980.
[347] White J. Application of Navier-Stokes flowfield analysis to the aerothermodynamic design of an aerospike-configured missile. Aerospace Design Conference. Irvine, CA, USA, https://doi.org/10.2514/6.1993-9681993.
[348] Srulijes J, Gnemmi P, Seiler F, Runne K. Shock tunnel high-speed photography and CFD calculations on spike-tipped bodies. 25th International Congress on High-Speed Photography and Photonics. Saint-Louis Codex, France, https://doi.org/10.1117/12.516788 2003.
[349] Asif M, Zahir S, Kamran N, Khan M. Computational Investigations Aerodynamic Forces at Supersonic / Hypersonic Flow past a Blunt Body with various Forward Facing Spikes. 22nd Applied Aerodynamics Conference and Exhibit. Provence, Rhode Island, USA, https://doi.org/10.2514/6.2004-5189 2004.
[350] Roveda R. Benchmark CFD Study of Spiked Blunt Body Configurations. 47th AIAA Aerospace Sciences Meeting including The New Horizons Forum and Aerospace Exposition. Orlando, FL, USA, https://doi.org/10.2514/6.2009-367: American Institute of Aeronautics and Astronautics (AIAA); 2009.

[351] D'Humières G, Stollery JL. Drag reduction on a spiked body at hypersonic speed. Aeronautical Journal. 2010;114:113-20, https://doi.org/10.1017/S0001924000003584.
[352] Khurana S, Suzuki K. Towards Heat Transfer Control by Aerospikes for Lifting-Body Configuration in Hypersonic Flow at Mach 7. 44th AIAA Thermophysics Conference. San Diego, CA, USA, https://doi.org/10.2514/6.2013-28982013.
[353] Mansour K, Khorsandi M. The drag reduction in spherical spiked blunt body. Acta Astronautica. 2014;99:92-8, https://doi.org/10.1016/j.actaastro.2014.02.009.
[354] Khurana S, Suzuki K. Aerothermodynamics of Lifting-Body Configuration in Hypersonic Flow with Aerodisk at Nose. 52nd Aerospace Sciences Meeting. Maryland, USA, https://doi.org/10.2514/6.2014-12472014.
[355] Ma Y, Liu X, Ou P. Numerical Investigation of Hypersonic Unsteady Flow Around a Spiked Blunt-body. Procedia Engineering. 2015;126:163-8, https://doi.org/10.1016/j.proeng.2015.11.204.
[356] Sebastian JJ, James SE, Suryan A. Computational Study of Hypersonic Flow Past Spiked Blunt Body Using RANS and DSMC Method. Procedia Technology. 2016;25:892-9, https://doi.org/10.1016/j.protcy.2016.08.174.
[357] Guo S, Xu J, Qin Q, Gu R. Fluid–Thermal Interaction Investigation of Spiked Blunt Bodies at Hypersonic Flight Condition. Journal of Spacecraft and Rockets. 2016;35:https://doi.org/10.2514/1.A33370.
[358] Sebastian JJ, Suryan A, Kim HD. Numerical Analysis of Hypersonic Flow Past Blunt Bodies with Aerospikes. Journal of Spacecraft and Rockets. 2016;35:https://doi.org/10.2514/1.A33414.
[359] Narayan A, Narayanan S, Kumar R, Singh T, Kumar CS, Jagadeesh G. Control of Aerodynamic Drag and Heating of Nose Cones Through Taper Spikes. Journal of Spacecraft and Rockets. 2019;article in advance:1-12, https://doi.org/0.2514/1.A34250.
[360] Das S, Kumar P, Prasad JK. Hypersonic flow over hemispherical blunt body with spikes. Scientia Iranica Transactions B: Mechanical Engineering. 2019;26:358-66, doi: 10.24200/sci.2018.0339.
[361] Wang CY. Contours for stagnation-point mass injection in hypersonic flow. AIAA Journal. 1964;2:178-9, https://doi.org/10.2514/3.267.
[362] Wang CY. Mass injection contours for a hypersonic leading edge at an angle of attack. AIAA Journal. 1965;3:184-5, https://doi.org/10.2514/3.829.
[363] Fleeman EN, R. Aerodynamic forces and moments on a slender body with a jet plume for angles of attack up to 180 degrees. 12th Aerospace Sciences Meeting. Washington,DC,USA, https://doi.org/10.2514/6.1974-1101974.
[364] Hayashi K, Aso S, Tani Y. Numerical Study on Aerodynamic Heating Reduction by Opposing Jet. Memoirs of the Faculty of Engineering, Kyushu University. 2006;66:40-54, http://kenkyo.eng.kyushu-u.ac.jp/memoirs-eng/bulletin/66/1/paper4.pdf.
[365] Chen L-W, Xu C-Y, Lu X-Y. Large-Eddy Simulation of Opposing-Jet-Perturbed Supersonic Flows Past a Hemispherical Nose. Modern Physics Letters B. 2010;24:1287-90, https://doi.org/10.142/S021798491002344X.
[366] Huang W, Zhang RR, Yan L, Ou M, Moradi R. Numerical experiment on the flow field properties of a blunted body with a counterflowing jet in supersonic flows. Acta Astronautica. 2018;147:231-40, https://doi.org/10.1016/j.actaastro.2018.04.018.
[367] Huang J, Yao WX, Jiang ZP. Penetration mode effect on thermal protection system by opposing jet. Acta Astronautica. 2019;160:206-15, https://doi.org/10.1016/j.actaastro.2019.03.023.
[368] Klimov A, Leonov S, Pashina A, Skvortsov V, Cain T, Timofeev B. Influence of a corona discharge on the supersonic drag of an axisymmetric body. 9th International Space Planes and Hypersonic Systems and Technologies Conference. Norfolk,VA, USA, https://doi.org/10.2514/6.1999-485619999.
[369] Soloviev VR, Krivtsov VM, Konchakov AM, Malmuth ND. Supersonic Body Drag Reduction during Forebody Filamentary Discharge Temporal Evolution. 2nd WSMPA. http://mhd.ing.unibo.it/Wsmpa/WSMPA%202000/DIVISIONE%20PDF/SESSION%20III/14.pdf2000.
[370] Palm P, Meyer R, Pl-ograve E, njes, Rich JW, Adamovich IV. Nonequilibrium Radio Frequency Discharge Plasma Effect on Conical Shock Wave: M = 2.5 Flow. AIAA Journal. 2008;41:465-9, https://doi.org/10.2514/2.1968.
[371] Soloviev VR, Krivtsov VM, Konchakov AM, Malmuth ND. Drag Reduction by Plasma Filaments over Supersonic Forebodies. AIAA Journal. 2003;41:2403-9, https://doi.org/10.514/2.6839.

[372] Kuo SP, Kuo SS. A physical mechanism of nonthermal plasma effect on shock wave. Physics of Plasmas. 2005;12:1-5, https://doi.org/10.1063/1.1829295.
[373] Joarder R. On the mechanism of wave drag reduction by concentrated laser energy deposition in supersonic flows over a blunt body. Shock Waves. 2019;29:487-97, https://doi.org/10.1007/s00193-018-0868-3.
[374] Zhang J, Ma H, Qin Y. Experimental Investigation on Flow Characteristic of Combination of Forward-facing Jet and Spike. 21st AIAA International Space Planes and Hypersonics Technologies Conference. Xiamen, China, https://doi.org/10.2514/6.2017-24022017.

## Appendix A-1: Summary of the previous studies on mechanical spike devices

| Ref. | Type of study | Freestream conditions | | Geometry | | | Focus of study | | | | | | Special features |
|---|---|---|---|---|---|---|---|---|---|---|---|---|---|
| | | Mach | Alpha | Forebody | spike tip/ aerodisk | L/D | S | D | L | P | A | U | |
| [18] | **F** | 0.95:1.37 | 0 | BO/SO | CA | 1.5 | | ▲ | | | | | First study ever |
| [70] | **E** | 1.76: 1.93 | 0 | H | PT | 1:12 | | ▲ | | | | | |
| [71] | **E** | 1.96 | 0 | FC/H | PT | Up to 6 | ▲ | ▲ | | | | ▲ | First record of pulsation |
| [35] | **E** | 2.72 | 0 | SK | PT | Up to 4.5 | ▲ | | | | | | |
| [96] | **E** | 1.5:1.8 | 0 | FC | PT | Up to 4.7 | ▲ | | | | | ▲ | First record of hysteresis and oscillation |
| [19] | **F** | 0.7:1.3 | 0 | H | PT | Up to 2 | | ▲ | | | | | The term "spike" is introduced |
| [54] | **E** | 0.12: 5.04 | 0 | H | FT/CA | 0.5:2 | | | | | ▲ | | First aeroheating study |
| [59] | **E** | 2.72 | 0 | H/BK | CA | Up to 2 | | ▲ | | | | | Impact of spike aerodisk length |
| [44] | **E** | 3.5 | 0 | FC | PT | Up to 2 | | | | | ▲ | ▲ | |
| [2] | **E** | 14 | 0 | FC/H | PT | Up to 8 | | ▲ | | | ▲ | ▲ | |
| [38] | **E** | 6.8 | 0 | H | PT | Up to 4 | | ▲ | | | ▲ | | |
| [88] | **E** | 6.8 | 0 | FC | PT | Up to 3 | ▲ | | | | | ▲ | Impact of shoulder roundness |
| [36] | **E** | 10 | 0 | SK | PT | Up to 5 | ▲ | | | | | ▲ | declare flow patterns |
| [55] | **E** | 19.4 | 0 | BO/H | PT | Up to 5 | | ▲ | | | ▲ | | |
| [106] | **E** | 11.76 | 0: 7 | H | PT | 4 | | ▲ | | | | | Spike is deflect w.r.t. model axis |
| [124] | **E** | 10.1 | 0: 25 | FC/BK | PT | Up to 5 | | ▲ | | | | | Very low Reynolds number |
| [33] | **E** | 10, 15 | 0 | H/FC/SK | PT | Up to 4 | ▲ | | | | ▲ | ▲ | Declare more flow patterns |
| [20] | **E** | 3, 4, 6 | 2 , 5 | BK | CA | 0.055: 0.083 | ▲ | | | | | ▲ | Impact of very short spikes |
| [117] | **E** | 9.6 | 0 | BK,SK | CA | Up to 0.13 | ▲ | | | | ▲ | ▲ | |
| [57] | **E** | 1.5,2.25 | >0 | FC, H | PT | 0.5:2 | ▲ | ▲ | | | | | |
| [37] | **E** | NA | | | | | | | | | | | "pulsation" and "oscillation" terms |
| [67] | **E** | 6 | 0 | FC | PT | Up to 3 | ▲ | ▲ | | | ▲ | ▲ | Spike lengths for each flow modes |
| [76] | **E** | 6 | 0 | FC | PT | Up to 3 | ▲ | | | | | ▲ | Explain the pulsation mode |
| [6] | **E** | Up to 3.5 | > 0 | BO | BA | Telescoping | ▲ | ▲ | | | | ▲ | Aerodisk superiority, spike bending |
| [25] | **E** | Up to 4 | 0,4,8 | BO | BA | 0.8 | ▲ | | | | | ▲ | |
| [74] | **E** | 2: 6 | 0 | SK | PT | Up to 5 | ▲ | | | | | ▲ | Amp. and freq. of unsteadiness |
| [89] | **E** | - | 0 | FC | PT | - | ▲ | | | | | ▲ | Explain pulsation |
| [40] | **E** | NA | | | | | ▲ | | | | | ▲ | Explain the oscillation mode |
| [75] | **E** | 2: 6 | 0 | SK | PT | Up to 5 | ▲ | | | | | ▲ | |
| [346] | **NE** | 3 | 0 | TK | RT | 0.75 | ▲ | | | | | ▲ | First numerical study of pulsation |
| [45] | **E** | - | 0 | FC | PT | - | ▲ | | | | | ▲ | |
| [72] | **N** | 0.5: 3 | 0 | FC | PT | Up to 3.25 | ▲ | ▲ | | | | | First comprehensive numerical study |
| [92] | **NE** | 3 | 0 | TK | RT | 0.75 | ▲ | | | | | ▲ | |
| [332] | **E** | 2.2 | 0 | BO | FA | 1 and 1.875 | ▲ | ▲ | | | | | Injection/ burning gas jet at aerodisk |
| [73] | **N** | 2: 6 | 0 | FC/SK | PT | Up to 1 | | ▲ | | | ▲ | | Low Reynolds number |
| [41] | **E** | 3 | 0 | TK | RT | 0.75 | ▲ | | | | | ▲ | Extensible spike |
| [24] | **E** | 3 | 0 | H | CA/PA | 0.283: 1.78 | | | | | ▲ | | |
| [56] | **N** | 3: 8 | 0 | TK | RT | Up to 1 | ▲ | | | | | | |
| [53] | **E** | 1.64 | 0: 15 | BK | FT | Up to 1.6 | ▲ | ▲ | ▲ | | | | Lifting bodies |
| [4] | **NE** | 2.5 | 0 | BK/H | BA | 2: 9 | ▲ | ▲ | | | | | |
| [22] | **NE** | 1.72 | 0 | FC | FT | 1.08 and 1.47 | ▲ | ▲ | | | | | |
| [90] | **E** | 2 and 3 | 0 | FC | PT | Up to 1.5 | ▲ | | | | | ▲ | |

| Ref. | Type of study | Freestream conditions | | Geometry | | | Focus of study | | | | | | Special features |
|---|---|---|---|---|---|---|---|---|---|---|---|---|---|
| | | Mach | Alpha | Forebody | spike tip/ aerodisk | L/D | S | D | L | P | A | U | |
| [101] | **E** | 3 | 0, 10 | FC/SK/H | WA | Up to 1.68 | | ▲ | | | ▲ | | Rotating aerodisk |
| [347] | **NE** | 4 | 0 | H/HC | FT | 0.875 and 1.3 | | ▲ | | | ▲ | | |
| [10] | **E** | 6.06 | 0: 40 | HC | FA | 3 | | ▲ | | | ▲ | | |
| [32] | **NE,V[38]** | 2.01, 4.15, 6.8 | 0,10 | H | PT | 0.5, 1 and 2 | ▲ | ▲ | | | | ▲ | |
| [121] | **NE** | 1.72 | 0 | FC | FT | 1.08 and 1.47 | ▲ | ▲ | | | | | |
| [122] | **NE** | 3 | 0, 2 | H/FC | FT | 1.42 | ▲ | | | | | | |
| [102] | **E** | 3 | 0, 10 | FC/SK/H | WA | Up to 1.68 | | ▲ | | | ▲ | | Rotating aerodisk |
| [103] | **E** | 3 | 0, 10 | FC/SK/H | WA | Up to 1.68 | | ▲ | | | ▲ | | Rotating aerodisk |
| [79] | **NV[32, 38]** | Numerical reproduction of [32, 38] | | | | | ▲ | ▲ | | | ▲ | | |
| [80] | **NV[32, 38]** | Numerical reproduction of [32, 38] | | | | | ▲ | | | | ▲ | | |
| [94] | **NV[40]** | 6 | 0 | FC | PT | 1 | ▲ | | | | | ▲ | |
| [98] | **NV[40]** | 2.21 | 0 | FC | PT | 1.25: 2.4 | ▲ | | | | | ▲ | Fine hysteresis simulation |
| [27] | **E** | 7 | 0: 8 | H | FT/RT/HA/FA | 0.5 and 1 | | ▲ | | ▲ | ▲ | | Drag decomposition, pitching |
| [50] | **E** | 1.89 | -4:10 | H | FT /RT/ PT | 1 | | ▲ | ▲ | | | | Impact of spike tip shape |
| [100] | **E** | 0.92, 1.62 | 0 | H | CA | 0.773 | | ▲ | | | | | Aerodisk on struts, no stem |
| [348] | **EN** | 3 | 0 | FC | FT | 0.5,1,1.5 | | ▲ | ▲ | | | | Five spikes vs. one spike |
| [64] | **E** | 1.89 | -4:10 | H | FT/RT/PT | 1 | | ▲ | ▲ | | | | |
| [39] | **NV[38]** | Numerical reproduction of [38] | | | | | ▲ | | | | | ▲ | |
| [3] | **EN** | 5.75 | 0:12 | BK | FA | 1 | | ▲ | | | | | |
| [348] | **EN** | 4.5 | 0: 24 | H | FA/HA/BCA | 1 | ▲ | ▲ | | | | | |
| [77] | **EN** | 5.75 | 0 | BK | FA | 1 | ▲ | | | | | ▲ | |
| [46] | **EN** | 5.75 | 0:12 | BK | FT/ HA/ FA | Up to 1 | | ▲ | | | ▲ | | |
| [49] | **EN** | 4.5 | 0: 24 | H | FA/HA/BCA | 1 | ▲ | ▲ | | | | | |
| [349] | **NV[38, 50]** | 4:8 | 0:12 | H | PT | 0.5,1 | ▲ | ▲ | ▲ | ▲ | | | |
| [334] | **EN** | 2.2 | 0 | BO | FA | 1 and 1.875 | ▲ | ▲ | | | | | |
| [93] | **NV[40]** | 2.21 | 0 | FC | PT | 1 | ▲ | | | | | ▲ | Fine simulation of pulsation |
| [97] | **NV[40]** | 6 | 0 | FC | PT | 2 | ▲ | | | | | ▲ | Fine simulation of oscillation |
| [47] | **NV[10, 49]** | 6.06 | 0: 40 | HC | FA | 3 | | ▲ | | | ▲ | | |
| [78] | **EN** | 8 | 0 | BK | FA | 1 | | ▲ | | | | | |
| [91] | **E** | 6.08 | 0 | FC | PT | Up to 1.5 | ▲ | | | | | ▲ | |
| [112] | **EN** | 1.5:3 | 0:12 | TK | CA | 3.25 | ▲ | ▲ | | | | | Multi-row-disk concept |
| [23] | **E** | 1.5:3 | 0:12 | TK | CA | 3.25 | ▲ | ▲ | | | | | Telescopic aerodisk |
| [107] | **E** | 2,3,5 | 0:30 | H | FT | Up to 3.3 | ▲ | ▲ | ▲ | | | | Pivoting spike, proof of concept |
| [95] | **E** | 3 | 0 | FC | PT, RT | 0.24 :1.43 | ▲ | | | | | ▲ | Fine Sheleiren for pulsation |
| [82] | **E** | 6 | >0 | H | RT | 1.5, 2 | ▲ | ▲ | ▲ | | | | |
| [26] | **E** | 6 | 0: 8 | H | HA/FA | 1.5 and 2 | | ▲ | ▲ | ▲ | | | |
| [5] | **NV[38]** | 5, 7, 10 | 0 | BK | RT/HA | 1: 4 | ▲ | ▲ | | | ▲ | | |
| [108] | **E** | 2, 3, 5 | 0: 30 | H | PT | - | | ▲ | | | ▲ | | "Pivoting spike" concept confirmed |
| [118] | **E** | 6 | 0, 4 | H | RT | 1 | ▲ | ▲ | | | | | Injection/ burning gas jet at aerodisk |
| [81] | **NV[26]** | Numerical reproduction of [26] | | | | | | | | | | | |
| [350] | **NV** | Numerical reproduction of [10, 47, 49] | | | | | ▲ | | | | | | Compare commercial CFD codes |
| [99] | **NV** | Numerical reproduction of [38, 40, 41, 89] | | | | | ▲ | | | | | | |
| [351] | **E** | 8.2 | 0 | H/SK | PT | Up to 2.125 | ▲ | ▲ | | | | | |

| Ref. | Type of study | Freestream conditions | | Geometry | | | Focus of study | | | | | | Special features |
|---|---|---|---|---|---|---|---|---|---|---|---|---|---|
| | | Mach | Alpha | Forebody | spike tip/ aerodisk | L/D | S | D | L | P | A | U | |
| [113] | **E** | 5.75, 7.9 | 0:10 | BK | PT | | ▲ | ▲ | | | ▲ | | Telescopic spike concept |
| [61] | **NV[38]** | 5.75 | 0:12 | BK | FT/FA/HA | 0.3:1.5 | ▲ | ▲ | | | ▲ | | |
| [109] | **Patent** | | | | | | | | | | | | Pivoting spikes techniques |
| [60] | **NV[38]** | 6 | 0 | H | HA | | ▲ | ▲ | | ▲ | ▲ | | |
| [31] | **NV[38]** | 6 | 0 | H | HA | 1.5:2.5 | ▲ | ▲ | | ▲ | | ▲ | Generalized effective body |
| [83] | **NV[38]** | 6 | 0 | H | | | ▲ | | | | ▲ | | |
| [11] | | | | | | | | | | | | | Literature review up to 2010 |
| [30] | **NV[38]** | 6 | 0 | H | HA | 1.5:2.5 | ▲ | | | | ▲ | ▲ | |
| [69] | **NV[38]** | 6 | 0 | BK | BK | | ▲ | ▲ | | ▲ | ▲ | ▲ | Multi-objective optimization, forebody included |
| [84] | **NV[26]** | 6 | 0 | H | FA/HA | 0.5 | | | | | ▲ | | |
| [115] | **NV[38]** | 6.2 | 0 | H | HA | 1,1.25,1.5 | ▲ | ▲ | | | ▲ | | Intermediate aerodisk. |
| [51] | **E** | 7 | | | | | | ▲ | ▲ | | | | Lifting body |
| [352] | **E** | 7 | | | | | | | | | ▲ | | Lifting body |
| [120] | **E** | 7 | | | | | | ▲ | ▲ | | ▲ | | A delta lifting body |
| [110] | **E** | 1.4, 2.2 | 0: 20 | H | FA,no stem | | ▲ | ▲ | | | | | Self-aligning aerodisk |
| [353] | **NV[82]** | 6 | 0 | H | RT | 1.5 | ▲ | ▲ | | | | | |
| [354] | **E** | 7 | | | | | | ▲ | ▲ | | ▲ | | Lifting body |
| [42] | **NV[38]** | 6 | 0 | H | HA | 0.5, 1.5 | ▲ | ▲ | | | | ▲ | assessing axisymmetry |
| [355] | **N** | 5 | 0 | FC | PT | 1 | ▲ | | | | | ▲ | |
| [111] | **NV[107]** | 1.4:2.2 | 0:20 | H | FA,no stem | 1.5,2 | ▲ | ▲ | | | | | Pitching body, self-aligning aerodisk |
| [65] | **EN** | 2 | 0 | H | PT/RT/FA | 0.75,1,1.5 | | ▲ | | | | ▲ | Rounding tip reduces fluctuations |
| [356] | **NV[82]** | 6 | 0 | H | RT | 1.5,2 | ▲ | | | | | | Use of DSMC |
| [357] | **N** | 5 | 0 | H | | | | | | | ▲ | | Structural study of spiked body |
| [358] | **N** | 6 | 0:8 | H | | 1.5,2 | | ▲ | | | | | |
| [119] | **N** | 5.75 | 0 | BK | HA | 0.5:2 | | ▲ | | | ▲ | | Semi-rarefied air |
| [116] | **NE** | 5.68 | 0 | H | HA | 1 | ▲ | | | | ▲ | | Double disks |
| [58] | **N** | 5 | 0 | H | FT/FA | 0.5:1 | ▲ | | | | ▲ | | |
| [85] | **E** | 6 | 0:8 | H | PT/FT/RT | 0.5:2.0 | ▲ | ▲ | ▲ | | | | |
| [87] | **NV[26]** | 8 | 0:12 | BK | HA, FA | 1:3 | ▲ | ▲ | ▲ | ▲ | | | Lifting body, mounting angles |
| [34] | **N** | 5 | 0 | H | PT/FT/RT/HA | 1 | ▲ | | | | ▲ | | Aero-thermo-structural study |
| [105] | **NV[38]** | 5 | 0 | H | RT | 0.5:2 | | ▲ | | ▲ | ▲ | | Porous spike |
| [43] | **NV[49]** | 3 | 0 | H | FA | 1 | ▲ | | | | | ▲ | |
| [86] | **NE** | 2:6 | 0 | BK, H | PT, RT, HA, FA | 0.5:2 | ▲ | | | ▲ | ▲ | | |
| [52] | **NV[26]** | 8 | 0:12 | H | FA | 2 | ▲ | ▲ | ▲ | | | | Spike vs. jet, lifting body |
| [28] | **NV[38]** | 6.2 | 0 | H | HA | 1,1.25,1.5 | ▲ | ▲ | | | ▲ | | Three aerodisks in a row |
| [62] | **N** | 4.5 | 0 | H | HA | | | ▲ | | | | | Design optimization |
| [29] | **NV[32, 38]** | 5 | 0 | | FA | 0.4 :2.5 | ▲ | ▲ | | | | | lifting body, ellipsoid nose |
| [66] | **ENV[347]** | 2 | 0 | FC, H | PT/HA | 1 | ▲ | ▲ | | | | ▲ | |
| [68] | **N** | 2 | 0 | BK | PT/RT/HA | 1 | | ▲ | | | | | |
| [359] | **EN** | 5.8 | 0 | BK, O | FT | 1 | ▲ | | | | ▲ | | Stepped taper spike |
| [63] | **NV[40]** | 6 | 0 | FC | PT/HA | 1, 2 | ▲ | ▲ | | | | ▲ | |
| [360] | **NV[38]** | 6 | 0 | H | PT,HA | 0.75,1,1.5 | ▲ | ▲ | | ▲ | | | |

| Key for: type of study | Key for: forebody geometry | Key for: spike tip/ aerodisk geometry | Key for: focus of study |
|---|---|---|---|
| **E**= experimental study,<br>**EN**= experimental study with numerical validation,<br>**F**= firing test,<br>**N**= numerical study with no experimental validation<br>**NE**= numerical study, validation with own experimental results<br>**NV[10]**= numerical study, validation with experiment of [10]<br>NA= The reference was not available during the study | **BK**= blunt cone,<br>**BO**= blunt ogive<br>**FC**= flat-faced cylinder,<br>**H**= hemisphere<br>**HC**= hemisphere-capped cylinder<br>**SK**= sharp cone,<br>**SO**= sharp ogive<br>**TK**= truncated cone | **BA**= blunt aerodisk, **CA**= conical aerodisk<br>**FA**= flat aerodisk, **FT**= flat tip<br>**HA**= hemispherical aerodisk,<br>**PA**= pyramid aerodisk, **PT**= pointed tip<br>**RT**= rounded tip, **WA**= wedge aerodisk<br>**L/D**= ratio of spike length to forebody caliber | **A**= aeroheating<br>**D**= drag,<br>**L**= lift<br>**P**= surface pressure<br>**S**= flowfield structure<br>**U**= flow unsteadiness |

## Appendix A-2: Summary of the previous studies on fluidic (opposing jet) devices

| Ref. | Type of study | Freestream conditions | | Forebody geometry | Jet features | Focus of study | | | | | | Special features |
|---|---|---|---|---|---|---|---|---|---|---|---|---|
| | | Mach | Alpha | | | S | D | L | P | A | U | |
| [125] | **E** | 1.62 | 0 | E | PR=1.01 | | ▲ | | | | | First study ever |
| [129] | **E** | 2.7 | 0 | H | F= 0:0.015 | | | | | ▲ | | First study on aeroheating |
| [157] | **E** | 5.8 | 0,4,8 | BK | N2: 0.8, He: 0.6 | | ▲ | | | ▲ | | Introducing mass and momentum flow coefficients |
| [171] | **E** | 4.8 | 0 | H | | ▲ | | | | | | |
| [172] | **E** | 2.9 | 0 | FC | M 1,3 | ▲ | | | | | | |
| [126] | **E** | 2 | 0:20 | H | oxidant-fuel mixture | ▲ | | | ▲ | | | |
| [176] | **E** | NA | 0 | | | | | | | | | |
| [167] | **E** | 6, 8 | 0 | H | N2, He, H2 | ▲ | | | | ▲ | | New parameter: relative mass flow |
| [162] | **E** | 7 | 0 | TK | H2, He | ▲ | | | | | ▲ | First record of unsteadiness |
| [361] | **T** | | 0 | | | ▲ | | | | | | |
| [138] | **E** | 6, 8.5 | 0 | FC | | ▲ | | | | | | Fine flowfield anatomy |
| [362] | **T** | | 0 | | | ▲ | | | | | | Effective body contours |
| [140] | **E** | 2.5 | 0 | H, BC | PR=1:12.5, Mach 1 2.6 | ▲ | | | ▲ | | | Fine illustrations for flowfield structure |
| [163] | **E** | 7.46 | 0 | H | He, air | | | | | ▲ | | |
| [177] | **ET** | 3 | 0 | FC | | ▲ | | | | | | |
| [127] | **E** | 0.4: 2 | 0: 18 | BK | M 4.3, F=0: 30, one, three nozzles | ▲ | ▲ | | ▲ | | | LPM and SPM terminologies introduced |
| [128] | **E** | 3, 4.5, 6 | 0, 2, 5 | BK | | | ▲ | | ▲ | | | First analysis of a real reentry model |
| [141] | **ET** | 7.9 | 0 | FC | | ▲ | | | | | | |
| [142] | **T** | | 0 | | | ▲ | | | | | | |
| [183] | **E** | NA | 0 | | | | | | | | | |
| [147] | **E** | 2.9 | 0 | FC | M 1, 3, PR=1.3-136 | ▲ | | | | | | |
| [178] | **NV[363]** | | 0 | | | ▲ | | | | | | First numerical study ever |
| [236] | **T** | | 0 | H | | | | | | ▲ | | Rarefied medium conditions |
| [135] | **T** | Based on data of [157] and [140] | | | | | ▲ | | | | | Introducing momentum coefficient |
| [179] | **N** | 6.7 | 0 | BK | | | | | ▲ | ▲ | | |
| [180] | **N** | 2.5, 6 | 0 | H | | ▲ | | | ▲ | | | |
| [139] | **E** | 3 | 0 | FC | PR=1.02: 30.7 | ▲ | | | | | | |
| [184] | **NV[139]** | 3 | 0 | FC | PR=5, 15.4 | ▲ | | | | | | |
| [137] | **NV[183]** | 2.5 | 0 | H | PR=1.63:3.26 | ▲ | | | | | | Clear explanation of the oscillation cycle |
| [150] | **E** | 2: 4 | 0 | BK | Various liquid jets | ▲ | ▲ | | | | | Use of liquid jets |
| [196] | **E** | NA | 0 | | | | | | | | | |
| [144] | **NV[140]** | 6.5 | 0 | 2D body | M 2: 3 | | ▲ | | | ▲ | | |

| Ref. | Type of study | Freestream conditions | | Forebody geometry | Jet features | Focus of study | | | | | | Special features |
|---|---|---|---|---|---|---|---|---|---|---|---|---|
| | | Mach | Alpha | | | S | D | L | P | A | U | |
| [136] | **N** | 5.8 | 0 | H | M 1, 2.84, PR=4.35:30.9 | ▲ | ▲ | | | | | |
| [132] | **EN** | 2 | 0 | TK | M 1: 4 | ▲ | | | | | | |
| [185] | **EN** | 4 | 0 | H | Nitrogen, Mach 1, | ▲ | | | ▲ | ▲ | | |
| [238] | | | 0 | | | | | | | | | Practical implementation issues |
| [182] | **E** | NA | 0 | | | ▲ | | | | | ▲ | |
| [148] | **E** | 2.29 | 0 | H | angle 0,10,20, Mach 1,2, PR=0: 90 | ▲ | | | ▲ | | ▲ | |
| [186] | **E** | 4 | 0 | H | M 1, PR=0.2:0.8, Nitrogen | ▲ | | | | ▲ | | |
| [164] | **EN** | 5.75 | 0 | BK | PR=2.78, 5.17 | | ▲ | | | ▲ | | |
| [145] | **EN** | 4 | 0 | H | M 1, PR=0.2:0.8, Nitrogen | ▲ | | | | ▲ | | |
| [190] | **E** | 8 | 0 | BK | | | ▲ | | | | | |
| [364] | **NV[145]** | 4, 8 | 0 | H | M 1: 5, PR=0.025: 0.8 | | ▲ | | | ▲ | | |
| [187] | **E** | 4 | 0 | H | M 1, PR=0.2:0.8, Nitrogen | ▲ | | | | ▲ | | |
| [193] | **EN** | 3.48 | 0 | BK | PR=1.05:13.5 | ▲ | | | | | | Re-entry capsule model |
| [160] | **E** | 8 | 0 | BK | N2, He | | ▲ | | | | | |
| [156] | **NV[132]** | 3.48, 4 | 0 | BK | M 1, 2.44, 2.94, PR=1.05:13.5 | ▲ | ▲ | ▲ | | ▲ | | Re-entry capsule, impact on lift |
| [191] | **E** | 8 | 0 | BK | PR=7,15,22 | | ▲ | | | | | |
| [146] | **NV[185]** | 3.98 | 0 | H | N2, PR=2.88,4.3,5.7 | | | | | ▲ | | |
| [134] | **E** | 5.9 | 0 | BK | Microjets array; N2, He, PR=0.1:1.45 | | | | | ▲ | | |
| [192] | **E** | 8 | 0 | BK | PR= 7.45: 37.27 | | | | | ▲ | | |
| [158] | **EN** | 3.48, 4. | -9: 5 | BK | M 1, 2.44, 2.94, PR=1.05:13.5 | | | | | ▲ | | Comprehensive study and a fine review |
| [188] | **NV[187]** | 3.98, 8 | 0 | BO | | | | | | ▲ | | Extended nozzle |
| [365] | **NV[140, 183]** | 2.5 | 0 | H | PR=1.6, 3.3 | ▲ | ▲ | | ▲ | ▲ | | |
| [173] | **NA** | | 0 | | | | | | | | | Introducing jet intensity parameter |
| [181] | **NV[140, 183]** | 2.5 | 0 | H | PR=1.6, 3.3 | ▲ | ▲ | | | ▲ | ▲ | Assessing the axisymmetry assumption |
| [189] | **E** | 6.6 | 0 | H | Nitrogen, Helium, PR=0: 0.04 | | | | | ▲ | | |
| [194] | **NV[158]** | Numerical reproduction of [158] | | | | ▲ | | | | ▲ | ▲ | Fine numerical illustrations |
| [153] | **NV[187]** | 3.98 | 0:10 | H | PR=2.88 | | ▲ | ▲ | | ▲ | | |
| [235] | **NV[190]** | 6.5 | 0 | BK | | | ▲ | | | | | |
| [165] | **NV[164]** | 5.75 | 0 | BK | CO2, He, PR= 2.875, 4.6 | ▲ | | | | ▲ | ▲ | Jet transients |
| [174] | **NV[132]** | 3.98 | 0 | H | PR=2.88, 4.32, 5.76, | | ▲ | | | | | Correlating drag and intensity parameter [173] |
| [143] | **N** | 1.6 | 0 | K, KB | M 2.94 | | | | | | | Supersonic aircraft, impact on boom signature |
| [151] | **NV[140]** | 2.5 | 0: 10 | H | PR=1.05:24 | | ▲ | | | | | |
| [161] | **NV[134]** | 5.9 | 0 | BK | Microjets, N2, He, PR=0.1:1.45 | | | | | ▲ | | impact of microjets |
| [195] | **N** | 1.6 | 0 | K, BK | M 2.94 | | | | | | | |
| [149] | **N** | 2.5 | 0 | BK | | ▲ | ▲ | | | | | |
| [199] | **E** | Various | 0 | BK | Various | ▲ | | | | | ▲ | Aeroacoustics of LPM |
| [198] | **NV[145]** | 3.98 | 0 | H | PR=2.88 | | ▲ | | | ▲ | | Impact of jet hole shape |
| [200] | **NV[145]** | 6 | 0 | | Aperture jet, PR=1.35 | | ▲ | ▲ | | | | Wave rider model, jet aperture |
| [203] | **NV[187]** | 3.98 | 0 | H | N2, Mj= 1, PR=0:0.005 | ▲ | | | | ▲ | | Jet augmented with platelet transpiration cooling |
| [197] | **NV[187]** | 3.98 | 0 | H | Polygons, PR=2.88 | ▲ | ▲ | | | ▲ | | impact of hole shape |
| [154] | **NV[186]** | 3.98 | 0: 15 | H | Star, PR=2.88, Delta 0, 5 | | ▲ | ▲ | | ▲ | | Impact of jet angle |
| [206] | **E** | 7 | 0 | BK | Air and water jet, PR=6.9 | ▲ | | | | | | Air-water jets comparison |
| [131] | **NV[145, 158]** | 3.98 | 0 | H | PR=0.4 : 0.8 | ▲ | ▲ | | | | | Impact of nozzle design |

| Ref. | Type of study | Freestream conditions | | Forebody geometry | Jet features | Focus of study | | | | | | Special features |
|---|---|---|---|---|---|---|---|---|---|---|---|---|
| | | Mach | Alpha | | | S | D | L | P | A | U | |
| [159] | **NV[187]** | 6 | 0 | H | PR= 0.198 | | | | | ▲ | | Sensitivity analysis of parameters on heating |
| [201] | **NV[145]** | 6 | 0 | | Multiple jets | ▲ | ▲ | | | ▲ | | Wave rider model |
| [209] | **NV[187]** | 3.98 | 0 | H | Pulsed jet | ▲ | ▲ | | | ▲ | | role of pulsed jet settings |
| [169] | **N** | 7.96 | 0 | BK | PR=0.07,0.14,0.21 | | | | | ▲ | | Using a gas generator as a jet source |
| [155] | **NV[158]** | 8 | 4: 12 | | PR=1: 15.6, Mach2 | | ▲ | ▲ | | | ▲ | Lifting body model |
| [168] | **NV[145]** | 6 | 0 | H | PR=0.075:0.25 | | ▲ | | | ▲ | | Introducing jet efficiency parameter |
| [208] | **NV[187]** | 3.98 | 0 | H | Pulsed jet | | ▲ | | | ▲ | | Sinusoidal pulsed jet |
| [366] | **NV[187]** | 3.98 | 0 | H | PR=0.6 : 1 | ▲ | | | ▲ | ▲ | | |
| [209] | **NV[187]** | 3.98 | 0 | H | Pulsed jet | ▲ | | | | ▲ | | Impact of pulsed jet wave form |
| [367] | **NV[187]** | 6 | 0 | H | M 1.5, PR=0.05:0.4 | | ▲ | | | ▲ | | Aero-thermo-structural study |
| [204] | **NV[187]** | 3.98 | 0 | H | M 1, PR 0.1 | ▲ | | | | ▲ | | Augmented transpiration cooling |
| [205] | **NV[187]** | 6 | 0 | H | M 1, PR 0.1:0.115 | ▲ | | | | ▲ | | Augmented transpiration cooling |
| [202] | **NV[187]** | 6 | 0 | | M 1, PR 8:11 | ▲ | ▲ | | | ▲ | | Leading edge of a hypersonic vehilce |

| Key for: type of study | Key for: forebody geometry | Key for: jet features | Key for: focus of study |
|---|---|---|---|
| **E**= experimental study,<br>**EN**= experimental study with numerical validation,<br>**T**= theoretical,<br>**N**= numerical study with no experimental validation<br>**NE**= numerical study, validation with own experimental results<br>**NV[10]**= numerical study, validation with experiment of [10]<br>NA= The reference was not available during the study | **BK**= blunt cone,<br>**FC**= flat-faced cylinder,<br>**H**= hemisphere<br>**TK**= truncated cone<br>**E**= ellipsoid | **M=** jet exit Mach number<br>**PR**= pressure ratio,<br>**F**= thrust ratio<br>**He, CO2, air, N2, ..** = jet gas type | **A**= aeroheating<br>**D**= drag,<br>**L**= lift<br>**P**= surface pressure<br>**S**= flowfield structure<br>**U**= flow unsteadiness |

## Appendix A-3: Summary of the previous studies on energy deposition devices

| Ref. | Type of study | Freestream Mach | Forebody geometry | Energy deposition technique | Focus of study | | | | Special features |
|---|---|---|---|---|---|---|---|---|---|
| | | | | | S | D | L | A | |
| [279] | **T** | 10 | BK | G | | ▲ | ▲ | | First study of energy devices |
| [243] | **N** | 17 | Ellip. | G | ▲ | ▲ | | | concentrated vs. distributed energy source |
| [241] | **N** | 3: 8 | PK | G | | ▲ | | | |
| [290] | **N** | 10 | Ellip. | G | | ▲ | | | Role of forebody geometry |
| [248] | **E** | 1.95 | H | PL | ▲ | | | | |
| [247] | **T** | 0: 20 | NA | C/PL | ▲ | | | | |
| [288] | **N** | 3 | H | PL | | ▲ | | | **impact of frequency** |
| [289] | **E** | 2 | NA | PL | ▲ | | | | |
| [246] | **N** | 1.4 | Airfoil | G | ▲ | ▲ | ▲ | ▲ | |
| [368] | **E** | 2 | PL, K | Cold, AC | ▲ | ▲ | | | **Spike-like needle acts as the single electrode** |
| [262] | **N** | 6.5, 10 | H | G | ▲ | ▲ | | ▲ | |
| [242] | **N** | 10 | Wedge | G | | ▲ | | | |
| [249] | **E** | 8 | NA | Cold, AC | ▲ | | | | |
| [250] | **T** | | | Cold, AC | ▲ | | | | |
| [278] | **N** | 1.5: 6.5 | H | G | ▲ | ▲ | ▲ | | |
| [255] | **E** | 2.5 | TK | AC | ▲ | | | | |
| [369] | **N** | 2:6 | K | PAC | | ▲ | | | Filamentary plasma |
| [292] | **N** | 2:6 | K | PAC | ▲ | | | | |
| [269] | **E** | 2.5 | K | Cold, DC, AC | ▲ | | | | |
| [251] | **E** | 1.7:1.8 | H | AC | ▲ | | | | |
| [270] | **E** | 2.5 | TK | AC | ▲ | | | | |
| [299] | **E** | 2.5 | TK | AC | ▲ | | | | |
| [259] | **E** | 2 | Wedge | Cold, DC | ▲ | | | | |
| [297] | **EN** | 10 | Blunt spheroid | AC | ▲ | | | | |
| [239] | **N** | 14 | H | G | | ▲ | | ▲ | |
| [240] | **EN** | 1.5: 4 | H | G | ▲ | | | | |
| [253] | **EN** | 1.5: 2.5 | H | PL | ▲ | ▲ | | | |
| [370] | **E** | 2.5 | Cone | Cold plasma | ▲ | | | | |
| [280] | **N** | 2, 3 | H, PO, K | G | | ▲ | | | |
| [371] | **N** | 2:6 | K | PAC | ▲ | | | | |
| [257] | **EN** | 2.4 | Wedge | PL | ▲ | | | | |
| [272] | **N** | 3.45 | H | Single pulse L | | ▲ | | ▲ | |
| [273] | **E** | 2.5 | TK | AC | ▲ | | | | Spike-like needle acts as one electrode |
| [271] | **EN** | 3 | BK | AC | | ▲ | | | |
| [256] | **EN** | 10 | Spheroid | AC | ▲ | | | | |
| [282] | **EN** | 10 | Spheroid | AC | | ▲ | | | |
| [372] | **N** | 2.5 | Wedge | AC | ▲ | | | | |
| [260] | **E** | 3.45 | H | PL | ▲ | | | | Very fine anatomy of the flowfield |
| [301] | **T** | | | | | | | | Overall system performance assessment |
| [277] | **N** | 2:8 | K | G | | ▲ | | | |
| [302] | **T** | | | | | | | | Overall system performance assessment |

| Ref. | Type of study | Freestream Mach | Forebody geometry | Energy deposition technique | Focus of study | | | | Special features |
|---|---|---|---|---|---|---|---|---|---|
| | | | | | S | D | L | A | |
| [261] | **E** | 6, 9 | BK | DC | | ▲ | | ▲ | |
| [303] | **T** | | | | | | | | Overall system performance assessment |
| [267] | **E** | 7 | H | PL | ▲ | | | | Evolution of energy bubble |
| [252] | **EN** | 2:8 | K | Cold plasma, L | | ▲ | | ▲ | |
| [265] | **EN** | 5 | H, K | DC | | ▲ | | | |
| [254] | **EN** | 6, 9, 12 | BK | DC | | ▲ | | ▲ | |
| [284] | | | | | | | | | Short selective survey |
| [298] | **E** | 5 | H, K | DC | ▲ | ▲ | | | Fine flowfield anatomy |
| [293] | **EN** | 1.92 | FC | PL | | ▲ | | | |
| [295] | **EN** | 2 | H | PL | ▲ | | | | |
| [266] | **EN** | 5 | TK, K | DC | ▲ | ▲ | | | Oscillatory flow structure |
| [300] | **EN** | 1.92 | FC | PL | | ▲ | | | |
| [287] | **EN** | 1.92 | FC | PL | | ▲ | | | |
| [286] | **N** | 6.5 | H | CL | | ▲ | | | Effect of altitude |
| [296] | **E N** | 5 | H, K | DC | | ▲ | | | |
| [268] | **N** | 5 | H | PL, cold | ▲ | ▲ | | ▲ | |
| [285] | **E** | 2.1, 2.7 | H | PL | ▲ | | | | |
| [274] | **EN** | 5 | TK | DC | ▲ | ▲ | | | |
| [264] | **T** | | | G | | ▲ | | | Drag prediction technique |
| [294] | **N** | 3.45 | H | Single laser pulse | | ▲ | | | |
| [275] | **N** | 8 | H | G | | ▲ | | | |
| [283] | **EN** | 1.92, 3.2 | FC | PL | | ▲ | | | |
| [281] | **N** | 2.1, 3.45 | H, BK | G | | ▲ | | | |
| [258] | **N** | 2, 3.45, 5 | H, K, oblate | PL | | ▲ | | | Impact of Mach, frequency, number of pulses, location |
| [263] | **N** | 8 | H | G | ▲ | ▲ | | | |
| [373] | **N** | 3.45 | H | Single laser pulse | | ▲ | | | |
| [276] | **N** | 4, 5, 7 | H | G | | ▲ | | | |

| Key for: type of study | Key for: forebody geometry | Key for: energy deposition dechnique | Key for: focus of study |
|---|---|---|---|
| **E**= experimental study,<br>**EN**= experimental study with numerical validation,<br>**T**= theoretical,<br>**N**= numerical study with no experimental validation<br>**NE**= numerical study, validation with own experimental results<br><br>NA= The reference was not available during the study | **K=**<br>**BK**= blunt cone,<br>**BO**= blunt ogive<br>**FC**= flat-faced cylinder,<br>**H**= hemisphere<br>**HC**= hemisphere-capped cylinder<br>**SK**= sharp cone,<br>**SO**= sharp ogive<br>**TK**= truncated cone | **G**= generic energy source,<br>**PL**= pulsed laser<br>**CL**= continuous laser<br>**AC**= alternating electric current<br>**PAC**= pulsed alternating electric current<br>**DC**= direct current | **A**= aeroheating<br>**D**= drag,<br>**L**= lift<br>**S**= flowfield structure |

## Appendix A-4: Summary of the previous studies on hybrid spike-fluidic devices

| Ref. | Type of study | Freestream Conditions | | Geometry | | | | Focus of study | | | | | | Special features |
|---|---|---|---|---|---|---|---|---|---|---|---|---|---|---|
| | | Mach | alpha | Body | Jet | Spike tip/ aerodisk | L/D | S | D | L | P | A | U | |
| [305] | **E** | 3.3 | 0 | H | L, SR, R | FT | 1.5, 2 | ▲ | | | ▲ | | | First study ever |
| [118] | **E** | 6 | 0, 4 | H | L, PR=0.3 | RT | 1 | ▲ | | | | | | Physics defined |
| [306] | **EN** | 6 | 0, 4 | H | L, PR=0.3 | RT | 1 | ▲ | | | ▲ | | ▲ | |
| [304] | **EN** | 6 | 0, 4 | H | L, PR=0.3 | RT | 1 | ▲ | | | | ▲ | | |
| [321] | **N** | 5.75 | 0 | BK | SR, He, CO2, PR=0.05:0.9 | HA | 1 | | | | ▲ | ▲ | ▲ | |
| [322] | **N** | 5.75 | 0 | BK | SR, He, CO2, PR=0.05:0.9 | HA | 0.5, 1 | ▲ | | | ▲ | ▲ | ▲ | |
| [323] | **N** | 5.75 | 0 | BK | SR, He, CO2, PR=0.05:0.9 | HA | 0.5, 1 | ▲ | | | ▲ | ▲ | ▲ | |
| [309] | **EN** | 6.6 | 0 | H | ST, PR=0.03:0.06 | FT | 0.25 | | ▲ | | ▲ | ▲ | ▲ | Following[188], extending the nozzle |
| [310] | **EN** | 6.6 | 0 | H | ST, PR=0.03:0.06 | FT | 0.25 | ▲ | | | | ▲ | | |
| [314] | **N** | 4 | 0 | H | ST, PR=0.4:0.8, | FT | 0: 2 | | ▲ | | | | | |
| [311] | **N** | 6.6 | 0 | BK | | FT | | | ▲ | | | ▲ | | |
| [329] | **N** | 2.5 | 0 | H | ST, PR=1:31 | FT | 0: 4 | | ▲ | | | | | MO design optimization |
| [374] | **E** | 2.4, 4 | 0 | H | ST, PR=5, 8 | FT | 0.4: 2 | | ▲ | | ▲ | | ▲ | Fine flowfield anatomy |
| [315] | **NV[48, 186]** | 6 | 0 | H | ST, PR=0.3:0.8 | FT | 1.5:7.5 | ▲ | ▲ | | | | | |
| [307] | **NV[374]** | 5:10 | 0 | H | L, PR=0.3 | RT | 0.5: 1 | | ▲ | | | | | |
| [308] | **NV[186]** | 3.98 | 0 | H | L, ST, PR=0.4:0.8 | FT, RT | 0.5: 1.5 | ▲ | ▲ | | ▲ | | ▲ | Impact of lateral jet location |
| [316] | **NV[48, 186]** | 6 | 0 | H | ST, PR=0.3:0.8 | FT | 1.5: 7.5 | ▲ | | | ▲ | ▲ | ▲ | |
| [317] | **NV[186]** | 5.75 | 0 | BK | ST, PR=0.4:0.8 | FA | 1: 2 | ▲ | ▲ | | | ▲ | | |
| [312] | **N** | 6.6 | 0 | H | ST, PR=0.03:0.12 | FT | 0.25 | | ▲ | | ▲ | ▲ | ▲ | |
| [319] | **NV[374]** | 5 | 0 | H | L, AT, AB, PR=14: 36 | FA | 1 | ▲ | ▲ | | | ▲ | | |
| [320] | **N** | 5 | 0 | H | L,AT,AB, PR=0.3,He, CO2 | HA | 1 | ▲ | | | | ▲ | | |
| [313] | **N** | 4 | 0 | H | ST, He, CO2, PR=5:60 | FT | 0.4:2.5 | | ▲ | | ▲ | ▲ | ▲ | |
| [324] | **N** | 5 | 0 | H | SR, PR=0.1:0.5, N2, CO2 | FT | 1: 3 | ▲ | ▲ | | | ▲ | | |
| [325] | **N** | 6 | 0 | H | SR, PR=0.05:0.3 | FT | 1: 3 | | | | ▲ | | ▲ | |
| [328] | **NV[186]** | 5 | 0 | H | ST, L | FT | 0.5: 2 | ▲ | ▲ | | ▲ | ▲ | ▲ | **multi-jet strategy,** Aero-thermo-structural study |
| [318] | **N** | 5.75 | 0 | BK | AT, PR=0.2:0.6 | FT | 0.5:1.5 | ▲ | ▲ | | | ▲ | | Multi-objective design optimization |
| [326] | **NV[187, 374]** | 5, 7 | 0 | H | AB, PR=0.06 : 0.1, | HA | 1.5 | | ▲ | | ▲ | ▲ | ▲ | Double aerodisks |
| [327] | **NV[187]** | 4, 6 | 0 | H | AB, PR=0.2 :1, N2 | HA | 0.2: 1 | ▲ | | | ▲ | ▲ | ▲ | |

| Key for: type of study | Key for: forebody geometry | Key for: spike tip/ aerodisk geometry | Key for: jet features | Key for: focus of study |
|---|---|---|---|---|
| **E**= experimental study,<br>**N**= numerical study with no experimental validation<br>**EN**= experimental study with numerical validation,<br>**NE**= numerical study, validation with own experimental results<br>**NV[10]**= numerical study, validation with experiment of [10]<br>**NA**= The reference was not available during the study | **BK**= blunt cone,<br>**H**= hemisphere | **FA**= flat aerodisk,<br>**FT**= flat tip<br>**HA**= hemispherical aerodisk,<br>**RT**= rounded tip<br>**L/D**= ratio of spike length to forebody caliber | **PR**= pressure ratio<br>**L**= lateral jet<br>**SR**= spike root jet<br>**ST**= spike tip jet<br>**AT**= aerodisk tip<br>**AB**= aerodisk base<br>**He, CO2**,..: jet gas type | **A**= aeroheating<br>**D**= drag,<br>**L**= lift<br>**P**= surface pressure<br>**S**= flowfield structure<br>**U**= flow unsteadiness |